



Norwegian University of Life Sciences  
Faculty of Environmental Sciences and Technology  
Department of Mathematical Sciences and Technology

Master Thesis 2014  
30 credits

# Developing an In-Vitro Dynamic Model of the Stomach and Small Intestine for Milk Products – First Prototype

May Helen Tysse



## Preface

This thesis is written by May Helen Tysse as a finishing touch on the five year long technology study; Mechanics and Process Technology at the Norwegian University of Life Sciences. The thesis is 30 credits, and is a combination of the two directions within the mechanics programme: product development and process technology.

This thesis was a part of a project initiated by a group of researchers at the Norwegian University of Life Sciences where they are developing an *in-vitro* dynamic model of the stomach and the small intestine for milk products with rheological monitoring. This thesis was carried out in order to start the first phases of designing and building this dynamic model.

First, I would like to thank my supervisor, associate professor Carlos Salas-Bringas, who has been an active participant throughout the period, and without there would be no thesis.

Furthermore, I would like to thank my co-supervisor professor Reidar Barfod Schüller, for all help and guidance at the laboratory.

I would also like to thank the entire team down at IKBM for good input and new ideas. One special thanks to Irene Comi and Ellen Kathrine Ulleberg for all your help with laboratory tests, answering questions at odd hours, and encouragement.

Finally, one huge thanks to all my friends and flatmates at TF209. You have made the days in the study hall fun and interesting.

Ås, 15.12.2014

---

May Helen Tysse

## Abstract

The aim of this study has been to design and develop the first prototype, of a dynamic *in-vitro* model of the digestive system through the stomach and the small intestine. This has been part of a project initiated by a group of researchers from NMBU, which will use this model to replicate the physical and mechanical processes of digesting milk through the human gastrointestinal tract.

Several conditions was set for the design of the *in-vitro* model, in order to make it able to keep the physical and chemical environment as similar to the *in-vivo* system as possible. In addition to these conditions, the initial limitation of the limited volume, set the framework for the development process.

In the approach to design this model, the fluid flow through vital parts of the system, like through the small intestine, was analysed. To achieve this, the CFD analysis tool “Flow Simulations” by the 3D CAD software SolidWorks, was actively used throughout the design and prototyping processes.

The finished apparatus, consists of several components, each with its own purpose. First, the rheometer (Physica UDS200, Germany) function as the “heart” of the operation. It continuously monitors the rheological characteristics of the digestive fluid, in addition to serving as the main container where the different circuits is attached, and to keep one of the physical conditions (the temperature) constant. The different fluid circuits in the system is first the stomach circuit, which consists of milk, saliva and gastric juices in its volume of approximately 15 ml. The second circuit, which is the one circulating the small intestine, consist of the stomach volume added to duodenal juices, which doubles the volume. The third circuit is the buffer volume, where the components from the digested milk should diffuse to, through the membrane. A peristaltic pump (Reclo ICC) controls the circulation of fluid through the entire system, in addition to contributing to the content’s mixing. The chemical condition (the pH-value) is monitored and controlled through a titrator (Compact Titrator G20) apparatus, which is attached to the system.

The small intestine device has been one of the primary focuses in this thesis. This device should function as a dialyzer, where different components in the milk is subtracted from the digestive fluid flowing inside the membrane. For this first prototype, an artificial membrane with an ordinary inner diameter was chosen. However, a goal for the further development is to be able to use an intestine from for example a fish to get a more realistic simulation. The finished small intestine device (excluded the membrane) was made successfully by glassblowers from UiO. However, the function of the device mentioned above, has not been successfully developed. Several test were done to test the system’s capability to create diffusion through the membrane, which were unsuccessful. This is a crucial function of the dynamic model, which should be prioritized in further development of this system.

The overall dynamic model’s first prototype has been design and developed, keeping the initial conditions intact. A mathematical model to estimate the simplified fluid environment locally at different running conditions, is also presented in this thesis.

## Sammendrag

Målet med dette studiet har vært å designe samt å utvikle den første prototypen av en dynamisk *in-vitro* modell av fordøyelsessystemet gjennom magen og tynntarmen. Dette har vært en del av et større prosjekt som en gruppe forskere ved Norges miljø- og biovitenskapelige universitet har initiert, hvor de skal bruke modellen for å kopiere de fysiske og mekaniske prosessene ved melk som blir fordøyd i det menneskelige fordøyelse systemet.

Flere betingelser satte rammevilkår for designet av *in-vitro* modellen, for å gjøre den i stand til å holde de fysiske og kjemiske forholdene så like som det virkelige systemet som mulig. I tillegg til disse betingelsene, så satte den initiale begrensingen om det begrensede volumet i systemet, rammer for utviklingsprosessen av modellen.

Som en inngangsvinkel til design-prosessen, ble fluid sirkulering gjennom vitale deler av systemet, som gjennom tynntarmen, analysert. For å kunne gjøre dette, ble CFD-analyse verktøyet «Flow Simulation» i DAK-programmet SolidWorks, aktivt brukt gjennom hele design samt prototype virksomheten.

Det ferdige apparatet består av flere komponenter, hver enkelt med sin egen funksjon. Reometeret (Physica UDS200, Tyskland) funksjonerer som «hjertet» i systemet. Det måler de reologiske egenskapene til fluidet kontinuerlig, samtidig som det fungerer som en hoved beholder som de ulike kretsene er knyttet til, samt den holder den ene fysiske betingelsen (temperaturen) konstant. De ulike kretsene består først av mage-kretsen som består av melk, spytt og magesaft. Deretter blir tynntarm-kretsen tilkoblet som består av fluidet fra mage-kretsen samt tynntarm-saft, noe som dobler volumet. Den tredje kretsen gjelder buffer fluidet, hvor komponenter fra den fordøyede melken skal diffundere til, gjennom membranen i tynntarmen. En peristaltisk pumpe (Reclo ICC) kontrollerer denne sirkuleringen i hele systemet, i tillegg til at den bidrar med å blande innholdet i fluidet. Den kjemiske betingelsen (pH-verdien) er målt samt kontrollert av et titrator-apparat (Compact Titrator G20), som er tilkoblet systemet.

Tynntarm-enheten har vært et av hovedfokusene gjennom denne mastergradsoppgaven. Enheten burde fungere som en dialysator, hvor ulike komponenter fra melk kan fjernes fra det fordøyde fluidet som sirkulerer på innsiden av membranen. Når det gjelder denne første prototypen, har en kunstig membran med en vanlig indre diameter blitt valgt. Et ønske er likevel at gjennom videre utvikling, skal det utvikles en måte hvor tynntarm fra f.eks. fisk kan bruke, for å kunne gi en mer realistisk simulering. Den ferdige tynntarm-enheten, foruten membranen, ble laget av glassblåsere fra Universitetet i Oslo, som ønsket. Likevel har tynntarm-enheten vist seg, gjennom ulike tester, å ikke fungere som ønsket. Flere tester ble gjort for å teste systemets evne til å skape diffundering gjennom membranen, hvor alle var mislykket. Dette er en kritisk funksjon ved systemet, som burde bli prioritert i videre utvikling.

Den første prototypen av denne dynamiske modellen, er designet samt utviklet slik at de initiale betingelsene holdes intakt. En matematisk modell som estimerer et forenklet bilde av fluid forholdene lokalt i systemet, ved ulike kjørebetingelser, er også presentert i denne oppgaven.

# List of Contents

Preface.....	III
Abstract .....	IV
Sammendrag .....	V
List of Figures.....	IX
List of Tables.....	XIII
List of Equations .....	XV
List of Symbols.....	XVI
Abbreviations .....	XVII
1 Introduction .....	1
1.1 Motivation .....	1
1.1.1 Previous Similar Work .....	1
1.2 Objectives and Limitations .....	1
1.2.1 Main Objective .....	1
1.2.2 Secondary Objectives .....	1
1.2.3 Initial Limitation .....	2
1.3 Choice of Method .....	2
1.3.1 Simulations .....	2
1.3.2 Physical Tests.....	2
1.4 Structure of the Thesis .....	3
2 Theory .....	4
2.1 Fluid Flow.....	4
2.1.1 General Hydraulic Principle Applied on Flow in a Pipe .....	4
2.1.2 Rheology.....	5
2.2 Diffusion of Soluble Products through a Membrane .....	15
2.2.1 Diffusion in Liquids .....	16
2.2.2 Dimensionless Numbers $Sc$ and $Sh$ and $Gz'$ .....	16
2.2.3 Types of Membranes in the Relevant Size Region .....	18
2.3 The Dynamics and Biomechanics of the Digestive System .....	21
2.3.1 Movements of the Intestinal Walls .....	22
2.3.2 The Small Intestine .....	23
2.3.3 Transport Across the Intestinal Wall.....	27
3 Components of the System.....	27

3.1	The Apparatus and overall Design Requirements .....	27
3.1.1	Designs from Previous Work .....	27
3.1.2	Function.....	28
3.1.3	Design Requirements .....	28
3.2	The Artificial Model of the Human Digestive System.....	29
3.2.1	The Peristaltic Pump.....	29
3.2.2	The Tubes .....	31
3.2.3	The Small Intestine .....	32
3.2.4	The Artificial Membrane .....	34
3.2.5	The Rheometer.....	35
3.2.6	The Heating Container .....	36
3.2.7	The Titrator.....	37
3.3	Building the Apparatus .....	38
3.3.1	Step-by-Step Digestive Fluids.....	38
3.3.2	The Total Apparatus .....	40
4	Experimental Work .....	41
4.1	Testing of Equipment.....	41
4.1.1	Selection of Tubing Sizes .....	41
4.2	The Stomach .....	42
4.2.1	The Lid .....	42
4.3	The Small Intestine .....	45
4.3.1	Preliminary Studies – Flow Simulations .....	45
4.3.2	Functionality Test of the Small Intestine Device.....	50
4.3.3	Optimization.....	52
4.3.4	Permeability Test.....	58
4.4	Fluid Calculations.....	61
4.4.1	Reynolds Number .....	61
4.4.2	Schmidt, Sherwood and Graetz Number in the Digestive Composition .....	62
4.4.3	Volume Calculations.....	63
4.4.4	Roughness Calculations.....	64
4.5	Equations Used to Describe the Possible Flow Conditions in the System .....	65
5	Discussion and Conclusion .....	67
5.1	Functionality of the Apparatus and its Limitations .....	67

5.1.1	Results from Experimental Work .....	67
5.2	Ideas for Further Optimization .....	70
5.2.1	Ideas for New Optimized Designs .....	70
5.2.2	Permeability test .....	70
5.2.3	Factors of the human digestive system which can, with some modifications, be simulated.....	70
6	Conclusion.....	71
6.1	Further Work .....	71
7	References .....	72
Appendix A	.....	74
Appendix B	.....	77
.....	.....	77
Appendix C.....	.....	78
.....	.....	78
Appendix D .....	.....	79
Appendix E.....	.....	80
Appendix F.....	.....	84
Appendix G .....	.....	86
Appendix H .....	.....	87
Appendix I.....	.....	88
Appendix J .....	.....	89
Appendix K.....	.....	91
Appendix L.....	.....	92
Appendix M .....	.....	93
Appendix N .....	.....	94
Appendix O .....	.....	95
Appendix P.....	.....	96



## List of Figures

Figure 1: The principal of continuity where the fluids density remains unchanged (incompressible fluid).....	4
Figure 2: Shear deformation of a rectangular bar. (Steffe, 1996) .....	5
Figure 3: Shear stress/shear rate relationships in liquids ("Unit Operations," 2014). The n-value is the fluids flow behaviour index. ....	6
Figure 4: Viscosity measurements from in-vitro digestion of homogenized full fat milk with and without addition of human gastric (HGJ) and duodenal (HDJ) enzymes (Devle et al. 2012).....	8
Figure 5: Laminar velocity profiles for power law fluids with different values of the flow behaviour index (n) (Steffe, 1996). ....	9
Figure 6: The development of the velocity profile in a circular pipe. $V = V(r,z)$ and thus the flow is two-dimensional downstream when the velocity profile fully develops and remains unchanged in the flow direction (Çengel et al., 2011). ....	9
Figure 7: The development of the boundary layer for flow over a flat plate, and the different flow regimes (Çengel et al., 2011). ....	9
Figure 8: Right: Laminar, transitional and turbulent flows (Çengel et al., 2011). ....	10
Figure 9: Shear diagram vs. velocity profile of a laminar flow where $dv/dz$ present the velocity gradient, also known as the shear rate (Sleigh and Noakes, 2009). ....	10
Figure 10: Diagram of the pressure distribution in a pipe, where the pressure drop is linear (Salas-Bringas et al. 2009). ....	11
Figure 11: The shear rate in a power law fluid, where the flow is laminar, at different values of n (Schüller 2014). The fluid is flowing in a pipe with an inner diameter of 0.03 m and a mean velocity at 0.00016667 m/s. As the n-value increases toward 1 (Newtonian fluid), the shear rate becomes linear. See chapter 0 for calculations of the velocity and diameter. ....	12
Figure 12: Reynolds stress. A fluid in turbulent flow is moving in the positive x direction, and surface S is parallel to the flow (McCabe et al., 2005). The mean velocity of the flow is u. When an eddy moves towards the wall, its flow rate $v'$ has a negative value, and away from the wall, its flow rate is positive. ....	13
Figure 13: Entry length for different diameters, n values and Reynolds numbers for inelastic power law fluids (Salas-Bringas et al. 2009). ....	15
Figure 14: Left: Sketch of the principle of dialysis (diffusion) vs. ultrafiltration (Lekang 2013). Right: The concentration gradient across a membrane, from left to right (Cussler 2009). ....	19
Figure 15: The components of the human digestive system (Martini & Nath 2009). ....	21
Figure 16: Lagrangian description of flow induced by longitudinal contractions (Macagno & Christensen, 1980). ....	22
Figure 17: Left: Peristalsis movements. Right on top: Segmentation movements in contrast to the related peristalsis movements (Ganong & Barrett, 2005). Right on bottom: Frequency distribution of intercontractile times in the human duodenum (Macagno & Christensen, 1980). ....	23
Figure 18: <b>The intestinal wall.</b> (a) A single plicae circulares and multiple villi. (b) The organization of the intestinal wall. (c) Internal structure in a single villus, showing the capillary and lymphatic supplies. (d) A villus in sectional view. (Martini & Nath 2009). ....	24
Figure 19: Types of roughness, with different diameters and roughness parameters. $k/D$ is the relative roughness (McCabe et al. 2005). ....	25

Figure 20. Left: The striated border of two neighboring epithelial cells in the depths of a fold in the surface of a villus, picture taken through an electron microscopy (Palay & Karlin 1959). Bottom right: Distribution of microvilli on the villus surface in the intestinal wall (Palay & Karlin 1959). Top right: A sketch demonstrating microvilli vs. villi (Nutter's Exus)..	26
Figure 21: A process diagram of the full configuration of the dynamic in-vitro model that was the base for this project (Salas-Bringas et al. 2014).	27
Figure 22: Recló ICC.	30
Figure 23: MCP Standard pump with an easy-load pump-head.	30
Figure 24: The LP-BT100-2J, a classical peristaltic pump.	30
Figure 25: The LP-BT100-IL.	30
Figure 26: Example of tubes in different sizes in the same series (VWR 2014). They all have three stoppers (right picture) so that they fit in the cassette (middle picture).	31
Figure 27: Tube-A-Lyzer with one champer.	32
Figure 28: Hallow Fiber Dialysis Module.	32
Figure 29: A simple sketch done by Adams & Chittenden Scientific Glass, in the price-inquiry process.	33
Figure 30: Manufactured glassware made of Stein Høydahl at UiO, from the designs from this thesis.	33
Figure 31: Left: Short outer buffer tube with inserted inner membrane-tube. Middle: Long outer buffer tube. Right: Inner membrane tube, there is to identical in the system.	34
Figure 32: Anton Paar Physica UDS 200, the rheometer of choice.	35
Figure 33: Left: The probe sketched in SW (scanned in a 3D-scanner). Right: The EMKA600 model in its container.	35
Figure 34: The rheometer cup used in this apparatus.	36
Figure 35: The heating container from Grant UK, used in this project. The peristaltic pump is placed beside the heating controller, saving room and volume of the entire apparatus.	36
Figure 36: The Compact Titrator G20 on the left, with the titration sensor DGi102-Mini, used in this apparatus.	37
Figure 37: The steps through the simulated digestive process. After step 3, the fluid starts to circulate in the stomach circuit, emptying a part of the cup. After step 4 the fluid starts to circulate the small intestine circuit, emptying a part of the cup again. The orange cylinder with the red tip represents the titrator sensor, where the red tip has to be immersed in the fluid to be able to measure the pH value. This is the reason that step 1 and 2 is mixed and measured first outside the cup. The last picture on the right is the rheometer with the cup full.	39
Figure 38: A sketch done in SW of the whole apparatus, with all the components described in chapter 1. Light brown circuit represents the stomach circuit. Dark red represents the small intestine circuit, with the light red as the buffer circuit.	40
Figure 39: The method used for the selection of tubing size.	41
Figure 40: Development of the lids in the prototyping process. 1-3 presents the three of the best prototypes. Every example consists of four parts: two upper and two bottom lids. 1c, 2c and 3c presents the lids combined with the rheometer cup.	43
Figure 41: The hose clamp around the first printed prototype. A screwdriver with a flat head is used to tighten the hose clamp.	44

Figure 42: The titrator sensor placed in one of the parts of prototype 9 of the lid. Prototype 9 is similar to prototype 10, which is presented in Figure 40. ....	44
Figure 43: Simple sketch of eddies that should be avoided in the active membrane part of the small intestine device (McCabe et al. 2005). ....	45
Figure 44: Simple sketches of two different solutions to overcome the turbulence. The sketch to the left is a cone-solution, chosen for this thesis. The sketch in the middle and the right demonstrates the flow separated by pipes to minimize the turbulence. ....	45
Figure 45: Lines used for plotting the result from the flow simulations in XY-plots, and the gap between them. ....	47
Figure 46: Sketch done in SW of the inner small intestine part used for flow simulations. Flow simulations were done at different angles (Table 23). ....	47
Figure 47: XY-Plot of the best solution found with the simulations, where the expansion angle is $15^\circ$ and the inlet volume flow is 0.2 ml/s. The liquid was water in the simulations, which is Newtonian. The lines from the top to bottom goes from 0 mm and to 80 mm distance from the inlet of the wider cylinder. Line4 (30 mm distance) marks where the flow becomes laminar (the entry length). These dimensions resulted in the shortest entry length among the scenarios in this particular test. The unsymmetrical curved lines (0-20 mm lines) is due to the turbulent flow. ....	48
Figure 48: A flow trajectories plot of the simulation giving the best conditions for laminar flow in the membrane region (Table 23). The flow through the tube has an inlet velocity of 0.2 ml/s and an expansion angle of 15 degrees. This plot demonstrates the cross between turbulent and laminar flow in the tube. The flow projectors are 250 lines with arrows, and the sketch is of the inner small intestine tube. ....	48
Figure 49: Sketch of the wanted dimensions for the small intestine tube, sent to Høydahl at UiO. ....	49
Figure 50: Left: Due to the thickness of the O-ring, it will cut of the buffer liquids flow outside the membrane. Middle: small rubber bands on the wide tip. Right: Small rubber bands on the narrow tip. ....	51
Figure 51: Idea for solution of the problem with the slippery membrane. ....	52
Figure 52: Simple sketch showing the air bobble in the membrane. ....	52
Figure 53: The new devices printed are painted in turquoise, with a simple sketch of the small intestine device in black. The outlet end is elevated with 15 degrees, avoiding the air bobble developing. The narrow gap (see where the arrows are pointing) is added to the design for the use of a rubber band to keep the devices attached to each other. ....	53
Figure 54: A static pressure cut plot of flow simulation where the inlet volume flow (right inlet) was 0.2ml/s. The pressure scale starts at blue (low) and continues to red (high). The plot shows that the pressure is highest at the bottom, and angled related to the angle ( $15^\circ$ ) the inner small intestine device is elevated. ....	54
Figure 55: Particle study shows the distribution when 250 water-particles is flowing from the inlet (right end). The dimensions of the small intestine is in this picture adjusted, to fit the distribution better. This is a proposal for future improvements to the design; the sketch is presented in Appendix I. ....	54
Figure 56: A flow trajectories plot of the simulation done in SW with an inlet volumetric flow at 0.1178 ml/s, and an expansion at $15^\circ$ . The plot demonstrates the transition between	

turbulent and laminar flow, showing less turbulence than the previous simulation (Figure 48).  
The flow projectors are 250 lines with arrows. .... 56  
Figure 57: XY-Plot of second simulation, where the expansion angle is  $15^{\circ}$  and the inlet volume  
flow is 0.1178 ml/s. The liquid was water in the simulations, which is Newtonian. The lines  
from the top to bottom goes from 0 mm and to 80 mm distance from the inlet of the wider  
cylinder. Line2 (10 mm distance) marks where the flow becomes laminar (the entry length).  
The unsymmetrical curved lines (0mm line – line1) is due to the turbulent flow..... 57  
Figure 58: Left: Evan's Blue colorant. Right: Myoglobin colorant..... 58  
Figure 59: Above: The dynamic permeability test through the membrane where the colorant  
Evan's Blue was used. Bottom left: The static permeability test with Evan's Blue. Bottom right:  
Leakage after two hours of dynamic flow..... 60  
Figure 60: Dimensions [mm] probe propeller..... 78  
Figure 61: Dimensions [mm] rheometer cup..... 79  
Figure 62: Dimensions [mm] lid, prototype nr 10..... 80  
Figure 63: Placement of the holes in the lid. .... 80  
Figure 64: Angle dimensions of the holes in the lid. .... 81  
Figure 65: Dimensions [mm] lid. .... 82  
Figure 66: Dimensions [mm] top lid..... 83  
Figure 67: Dimensions [mm] short holder. .... 84  
Figure 68: Dimensions [mm] long holder..... 85  
Figure 69: Dimensions rheometer UDS200 (Germany). .... 87  
Figure 70: Dimensions [mm] of future idea for design of the small intestine device. .... 88  
Figure 71: the membrane easily folds when the pressure changes both inside and outside the  
membrane. .... 90  
Figure 72: Friction factor plot for circular pipes (McCabe et al. 2005). .... 91  
Figure 73: Friction factor plot for circular pipes (McCabe et al. 2005). .... 95  
Figure 74: A simple sketch of an idea for a new probe propeller..... 96

## List of Tables

Table 1: Rheological characteristics of fluids (McCabe et al., 2005).....	6
Table 2: The major substrate groups in milk, and their transport across the intestinal mucosa (Martini & Nath 2009). .....	27
Table 3: A summary of factors considered when choosing the components of the system and their significance. ....	28
Table 4: Functions of the human stomach and small intestine that are modelled and not modelled in the apparatus. ....	29
Table 5: Requirement considered choosing a pump for this project. ....	29
Table 6: Specifications for option 1.....	30
Table 7: Specifications for option 3.....	30
Table 8: Specifications for option 4. *The information is not available. ....	30
Table 9: Specifications for option 5. *The information is not available. ....	30
Table 10: Requirement of the tubes. ....	31
Table 11: Requirements for the small intestine device. ....	32
Table 12: Specifications for option 1.....	32
Table 13: Specifications for option 2.....	32
Table 14: Specifications for option 3.....	33
Table 15: Specifications for option 4.....	33
Table 16: Requirements of the membrane. *Internal diameter. ....	34
Table 17: Requirements for the rheometer. ....	35
Table 18: Requirements for the heating container.....	36
Table 19: The composition of the digestive fluid in the apparatus, divided in four steps. *Acid or base needed to calibrate the pH level to $\text{pH} < 2$ is included in this volume. ....	38
Table 20: Suppliers list.....	40
Table 21: Results of the test with the coagulated milk pumped through the different tubes. The pump used for this test was a one-channel peristaltic pump, burrowed at IKBM.....	42
Table 22: General settings and initial conditions set in SW for the flow simulation with inlet volumetric flow 0.2 ml/s. Every setting is set at default.....	46
Table 23: Results from the flow simulations. Highlighted in yellow is the solution with the best result.*See Figure 46. **Represents the entry length.....	47
Table 24: The flow velocity ( $u_2$ ) in the artificial membrane is calculated to be 0.00159 m/s, in an ideal pipe flow. The flow velocity at the inlet is the same as in the previous flow simulations (0.2 ml/s). ....	50
Table 25: General settings and initial conditions set in SW for the flow simulation with inlet volumetric flow 0.2 ml/s. Every setting, except the gravity, is the default setting. The gravity setting is set so the elevation is in a $15^\circ$ angle as in the apparatus.....	53
Table 26: The parameters used to calculate the new inlet velocity ( $u_3$ ) in the narrow tube (right end in Figure 34), for a more realistic flow velocity through the membrane. The volumetric flow rate is based on information given in chapter 2.3. ....	55
Table 27: General settings and initial conditions set in SW for the flow simulation with inlet volumetric flow 0.1178 ml/s. Every setting, except the gravity, is the default setting. The gravity setting is set so the elevation is in a $15^\circ$ angle as in the apparatus.....	56

Table 28: Sizes of the two colorants used in this test. The membrane cut-off size was 3.5 kDa. ....	58
Table 29: Purposes of the different tests was to measure and visualize there three different events, based on these aaumptions. ....	58
Table 30: The time interval between every sample sent for spectroscopy. ....	59
Table 31: The time interval between the samples in the static permeability test. ....	59
Table 32: Parameters used to calculate the Reynolds number (Fellows 2009).....	61
Table 33: Volumes collected from drawing in SW. ....	63
Table 34: Volume of the fluid circulating in the stomach circuit. *This is after subtracting the volume left in the cup in-between the blades of the propeller that is not possible for the peristaltic pump so suck out. The volume available for circulation is less than the volume that is needed to circulate. ....	64
Table 35: Volume of the fluid circulating in the small intestine circuit. ....	64
Table 36: Mathematical models: Equations, which is possible to use, using data obtained from the system, to describe flow conditions both in the rheometer cup and in the artificial membrane. Regarding other equations described in this thesis not mentioned here, the current system does not provide enough information to use.....	65
Table 37: Properties of some fluids (Fellows, 2009). ....	92
Table 38: Consistency coefficients and flow behaviour indices for power law fluids (Smith 2011).....	93
Table 39: Villus dimensions, density, and area as a function of intestinal position in mice on a meat diet (Diamond et al. 1984). ....	94

## List of Equations

Equation 1: Continuity equation (Çengel et al., 2011).	4
Equation 2: Continuity equation of an incompressible fluid.	4
Equation 3: The fluid velocity in a pipe.	4
Equation 4: Angle ( $\gamma$ ) of shear (Steffe, 1996).	5
Equation 5: Viscosity in a Newtonian fluid (shear stress/shear rate).	5
Equation 6: Ostwald-de Waele equation. Shear stress for power law fluids.	7
Equation 7: Shear stress at the pipe wall (Salas-Bringas et al. 2009).	11
Equation 8: The shear rate of a power fluid, relevant in laminar flow (Smith 2011).	11
Equation 9: Reynolds number for a Newtonian fluid.	12
Equation 10: The Reynolds number for a non-Newtonian liquid.	13
Equation 11: The Reynolds critical number, which under indicates laminar flow.	13
Equation 12: Turbulent viscosity, called the Reynolds stress (McCabe et al. 2005).	14
Equation 13: The eddy viscosity (McCabe et al. 2005).	14
Equation 14: The total shear stress in a turbulent fluid is the sum of the viscous stress and the turbulent stress (McCabe et al. 2005).	14
Equation 15: The entry length ( $L_e$ ) of a non-Newtonian in-elastic power fluid.	14
Equation 16: Fick's first law of diffusion (McCabe et al. 2005).	16
Equation 17: Stokes-Einsteins equation (McCabe et al. 2005).	16
Equation 18: Schmidt number (McCabe et al. 2005).	17
Equation 19: Sherwood number relevant for fluid flow over a flat plate (McCabe et al. 2005)	17
Equation 20: Sherwood number relevant for laminar fluid flow inside a pipe (McCabe et al. 2005).	17
Equation 21: Graetz number (McCabe et al. 2005).	17
Equation 22: Sherwood number relevant for a turbulent fluid flow (McCabe et al. 2005).	17
Equation 23: The volumetric filtration flux through a membrane with gel formation (Shuler & Kargi 1992).	18
Equation 24: The mass transfer coefficient (Shuler & Kargi 1992).	18
Equation 25: The Hagen-Poiseuille equation for pressure drop in cross-flow filtration (Shuler & Kargi 1992).	19
Equation 26: Hagen-Poiseuille equation, which fits when the model is a cylindrical pore micro- or ultrafiltration (Lekang 2013).	20
Equation 27: The membrane's porosity (Lekang 2013).	20

## List of Symbols

Name	Symbol	Unit
Dynamic viscosity	$\mu$	mPa·s, mkg/m·s, cP
Kinematic viscosity	$\nu$	m <sup>2</sup> /s
Density	$\rho$	kg/m <sup>3</sup>
The total shear stress	$\tau$	Pa
Shear stress in viscoelastic fluids	$\tau_v$	Pa
Reynolds stress	$\tau_t$	Pa
Shear rate	$\gamma, du/dy$	s <sup>-1</sup>
Velocity	$u$	m/s
Average velocity	$\bar{V}$	m/s
Mean velocity	$u$	m/s
Diameter	$D$	mm
Radius	$r$	mm
Molecular radius	$r_0$	cm
Reynolds number	$Re$	-
Sherwood number	$Sh$	-
Schmidt number	$Sc$	-
Graetz number	$Gz'$	-
Molecular Weight	$MW$	g/mol, Da
Flow behaviour index	$n$	-
Consistency coefficient	$K$	Pa·s <sup>n</sup>
Volume	$V$	m <sup>3</sup> , ml
Area	$A$	m <sup>2</sup>
Volumetric flux	$Q$	m <sup>3</sup> /s
Length	$L$	mm, cm, m
Variation, film thickness	$\delta$	-, m
Force	$F$	N, kg·m/s <sup>2</sup>
Temperature	$T$	K, °C
Molar flux	$J$	mol/m <sup>2</sup> ·s
Volumetric filtration flux/Permeate flux	$J_v$	m <sup>3</sup> /m <sup>2</sup> ·s, L/m <sup>2</sup> ·h
Molar density	$\rho_M$	mol/l
Volumetric diffusivity	$D_v$	m <sup>2</sup> /s
Mass transfer coefficient	$k_c$	-
Mass flow rate	$\dot{m}$	kg/s
Eddy viscosity	$E_v$	mPa·s, mkg/m·s, cP
Pressure difference over membrane, across pipe	$\Delta P_m, \Delta P$	-
Flow rate	$v'$	m <sup>3</sup> /s
Entry length	$L_e$	m
Friction factor	$f$	-
Roughness parameter	$k$	m
Concentration	$C$	mol/m <sup>3</sup>



## Abbreviations

Expression	Explanation
IMT	Institute of Mathematical Sciences and Technology
IKBM	Institute of Chemistry, Biotechnology and Food Sciences
NMBU	Norwegian University of Life Sciences
UiO	University of Oslo
SW	SolidWorks
CAD	Computer-aided Design
CFD	Computer Fluid Dynamics
i.d.	The inner diameter [mm]
HCl	Hydrochloric acid
NaOH	Sodium hydroxide
MW	Molecular weight
HGJ	Human gastric juices
HDJ	Human duodenal juices



# 1 Introduction

## 1.1 Motivation

This thesis is a part of an ongoing project organized by a group of researchers from the Institute of Mathematical Sciences and Technology (IMT) and the Institute of Chemistry, Biotechnology and Food Science (IKBM), at the Norwegian University of Life Sciences (NMBU). The aim of their project is to develop an *in-vitro* dynamic model of the stomach and small intestine for milk products with rheological monitoring (Salas-Bringas et al. 2014).

Using an *in-vitro* method to study and simulate the *in-vivo* process of digestion in the gastrointestinal tract has advantages and disadvantages. *In-vivo* studies of the digestion process have great ethical and economic challenges. Using an *in-vitro* model to simulate the *in-vivo* system will eliminate the ethical challenges, and limit the costs extensively.

In order to develop such a dynamic model, a quantity of research and prototyping is expected. Prior to this thesis, a group of scientists<sup>1</sup> from NMBU, responsible for the project, had already published an article in the Annual Transactions of the Nordic Rheology Society. The article discussed a preliminary study they carried out to give an overview of the main factors relevant for the elaboration of a dynamic *in-vitro* model of the human stomach and small intestine (Salas-Bringas et al. 2014). This made a foundation for designing and developing the first prototyping stages of this model, which is the purpose of this thesis.

### 1.1.1 Previous Similar Work

A static model of the digestive process in the gastrointestinal tract is not a new technique, and is a common method to use for research in this area. However, a dynamic model is less common, and gives a more realistic simulation. There are some examples on developed dynamic models of this process; one of these is Ajay Tharakan. He did a doctorate thesis on modelling of the physical and chemical processes in the small intestine (Tharakan 2008). Tharakan's thesis is used extensively in this thesis, due to its similarities.

## 1.2 Objectives and Limitations

The objectives are divided in a main and several secondary objectives.

### 1.2.1 Main Objective

Design and development of a dynamic *in-vitro* model of the stomach and small intestine.

### 1.2.2 Secondary Objectives

- ❖ Design of the system indicating working conditions (velocities, volume, shear rate and temperature) and limitations (e.g. peristaltic and segmental movements in the small intestine, active carriers across the intestinal wall).
- ❖ Preliminary tests of the built system indicating the parameters that are possible to obtain, to describe the physical and chemical environments (velocities, temperature and pH).

---

<sup>1</sup> This group consists of Carlos Salas-Bringas, Elling-Olav Rukke, Tove Devold, Gerd Vegarud, Carl Fredrik Naess-Andersen, Reidar Barfod Schuller, Ellen Kathrine Ulleberg and Irene Comi. The group is from IKBM, except from Salas-Bringas.

- ❖ Description and development of data handling-system (logging data and calculations) from the model to describe the possible flow conditions in the system, and how a user get data and measurements needed for equations in this description.

### 1.2.3 Initial Limitation

The one initial limitation is the limited volume of the system. 75% of the fluid circulating in the system will be a combination of gastric and duodenal juices. The limited access to this fluid, directly affects the size of the apparatus. The maximum volume of the entire fluid circulating is therefore set at 40 ml.

## 1.3 Choice of Method

To analyse and evaluate the challenges of designing this system, different methods is used.

### 1.3.1 Simulations

A 3D CAD (Computer-Aided Design) software with a CFD (Computational Fluid Dynamics) analysis tool, is able to do simulations of the real process in a system. There are several advantages of using this method in the first phases of a design project, where the most important are eliminating economical cost and avoiding the time-consuming activity of physical tests.

Time is the only limit to how many different design-solutions that can be done to the same part, in a 3D CAD software. Using the CFD tool, one can test all of these solutions; test their functionality and find their weaknesses, etc. The best part is that all this can be done with no additional economic cost.

SolidWorks is a 3D CAD software, where CFD analysis is an included package. Its flow simulation tool offers a wide range of physical models and fluid flow capabilities to get a better insight into product behaviour. The application is used actively in this thesis is internal laminar and turbulent flows of an incompressible fluid.

### 1.3.2 Physical Tests

Before the apparatus is finished and functioning as intended, most details of every device is tested and improved. Physical tests are done on details that are difficult to simulate. These tests are used actively in this thesis, both in choosing devices (preliminary tests) and in testing the functionality of the devices when building the apparatus. The different tests are describe more detailed in chapter 1.

#### 1.3.2.1 Prototyping

The focus of this thesis is on the devices of the small intestine and the stomach. To find the best solutions in both of the cases, several designs are made, some with greater success than others. This kind of prototyping is very time-consuming, but is an important part of the development process. One example that stands out as the most time-consuming, but highly necessary, is the prototyping of the lid for the stomach system. See chapter 4.2.1.2 for details on this particular process.

## 1.4 Structure of the Thesis

### ❖ *Chapter 1: Introduction*

- Introduces the reader to the thesis. Describes the motivation behind the thesis, its main and sub-objectives, and the choice of method.

### ❖ *Chapter 2: Theory*

- Introduces the field of rheology.
- A short description of the concept diffusion through a dense or a porous membrane.
- Introduces the dimensionless numbers:  $Sc$ ,  $Sh$  and  $Gz'$  and how they apply to this system.
- Introduces the reader to the rheological properties of milk.
- Gives the reader an overview of the dynamics of the digestive system, and its biomechanics.
- Gives a detailed description of the small intestine, and transport across the intestinal membrane.

### ❖ *Chapter 3: Components of the system*

- Describes the apparatus and the design requirements.
- Describes all of the sub-components, with different examples.
- Suppliers list.

### ❖ *Chapter 4: Experimental work*

- The aim of every test.
- The process and result of every test.
- Prototyping activity and finished design.

### ❖ *Chapter 5: Discussion*

- Comments on the result.
- Discussion of limitations and future options.

### ❖ *Chapter 6: Conclusion*

- Concludes the thesis.
- Further work.

## 2 Theory

### 2.1 Fluid Flow

#### 2.1.1 General Hydraulic Principle Applied on Flow in a Pipe

##### 2.1.1.1 Continuity Equation

The principal of continuity says that mass cannot be created, nor can it disappear (Çengel et al. 2011). This means that the amount of energy and mass that enters a system, is the same amount that exits it. In this thesis, the principle is considered in the case of calculating the flow through the small intestine. Equation 1 below expresses the principle of continuity.

Equation 1: Continuity equation (Çengel et al., 2011).

$$A_1\rho_1u_1 = A_2\rho_2u_2 = Q$$

Where  $\rho$  is the fluids density

$A$  is the pipes cross sectional area [m<sup>2</sup>]

$u$  is the fluids velocity [m/s]

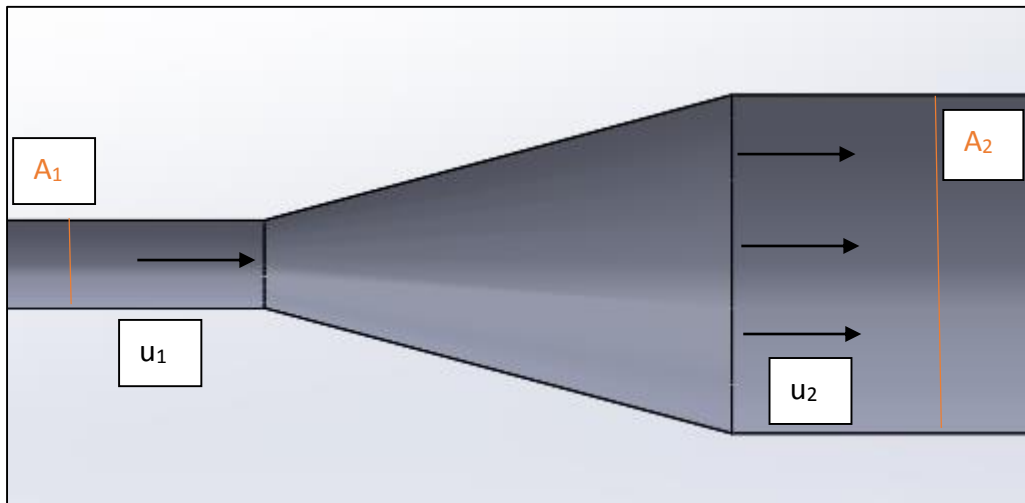


Figure 1: The principal of continuity where the fluids density remains unchanged (incompressible fluid).

The equation above simply says that the volume flow ( $Q$ ) is constant in the whole system. In this case, the fluid is incompressible, and the density of the fluid remains the same throughout the pipe. Eliminating the density parameters, a new equation appears (Equation 2).

Equation 2: Continuity equation of an incompressible fluid.

$$A_1u_1 = A_2u_2 = Q$$

Where  $Q$  is the volume flow [m<sup>3</sup>/s]

Knowing the volume flow and the cross sectional areas, one can calculate the velocity (Equation 3).

Equation 3: The fluid velocity in a pipe.

$$u = \frac{Q}{A}$$

### 2.1.2 Rheology

“Rheology is the science of the deformation and flow of matters. There are three ways to deform a substance; shear, extension, and bulk compression” (Steffe 1996). Shear deformation is the most relevant type of deformation in this case. The idea is illustrated in Figure 2 where the plate at the bottom is stationary and the upper plate is linearly displaced by an amount equal to  $\delta L$ . Picturing that a fluid is several plates/layers adjacent to each other, the size of each plate is not relevant. Equation 4 calculates the angle ( $\gamma$ ) of shear. The force ( $F$ ) to get this displacement over an area ( $A$ ) is called shear stress ( $\tau$ ) and is described later in chapter 2.1.2.4.

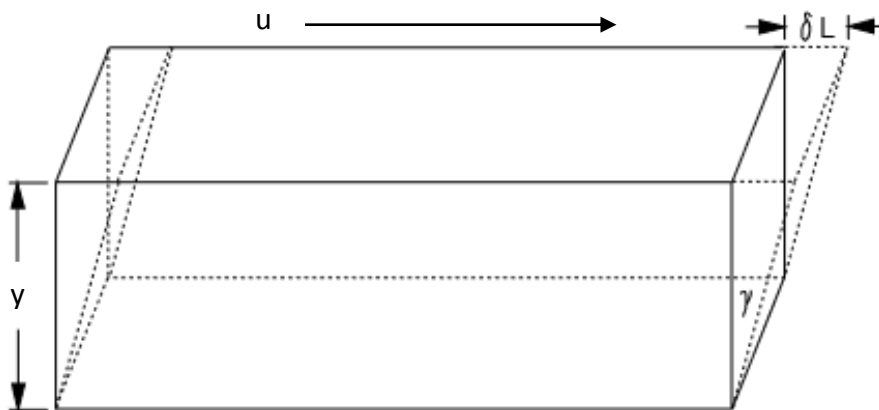


Figure 2: Shear deformation of a rectangular bar. (Steffe, 1996)

Equation 4: Angle ( $\gamma$ ) of shear (Steffe, 1996).

$$\tan \gamma = \frac{\delta L}{y}$$

#### 2.1.2.1 Rheological Properties of Fluids

Dynamic viscosity is a liquid's internal resistance to flow, where shear stress is the force that moves the liquid, and shear rate is the velocity gradient (Figure 2). In the most general cases, the viscosity increases with molecular weight (MW) and decreases rapidly with increasing temperature. The viscosity of liquids vary enormously, where the most viscous materials are non-Newtonian and possess no single viscosity independent of shear rate (McCabe et al., 2005).

Equation 5: Viscosity in a Newtonian fluid (shear stress/shear rate).

$$\mu = \frac{F/A}{du/dy}$$

Where  $F$  is the force applied [ $\text{kg}\cdot\text{m}/\text{s}^2$ ]

$A$  is the area over which force is applied [ $\text{m}^2$ ]

$dy$  is the distance between planes in the liquid [ $\text{m}$ ]

$du$  is the velocity of the planes relative to one another [ $\text{m}/\text{s}$ ]

$\mu$  is the dynamic viscosity [ $\text{kg}/\text{m}\cdot\text{s}$ ]

Liquids divide into two main groups regarding these rheological properties, Newtonian and non-Newtonian. Most simple liquids and gases, like water, are Newtonian and have a linear relationship between shear stress and shear rate. This means that, at a constant temperature, the viscosity will not change. All other liquids are categorized as non-Newtonian. These can be broadly classified into different types (Figure 3) depending on their behaviour (Fellows 2009).

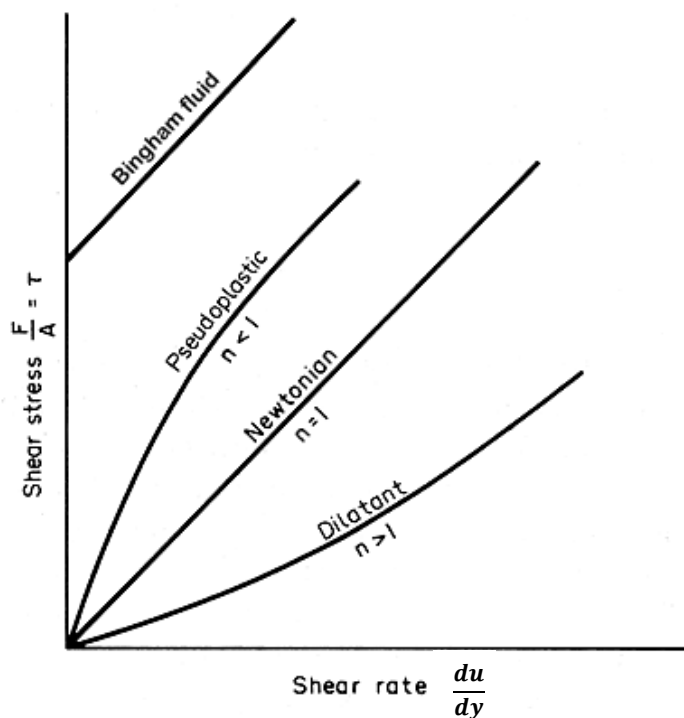


Figure 3: Shear stress/shear rate relationships in liquids ("Unit Operations," 2014). The  $n$ -value is the fluids flow behaviour index.

Table 1: Rheological characteristics of fluids (McCabe et al., 2005).

Designation	Viscosity effect when increasing shear rate	Examples
Bingham plastic	None	Sewage sludge
Pseudoplastic	Thins	Polymer solutions, mayonnaise
Newtonian	None	Gases, most simple liquids
Dilatant	Thickens	Corn flour-sugar solutions, wet beach sand



As presented in Table 1, it is the effect of shear rate on the fluids viscosity, which characterize the different fluids. Over some range of shear rates, dilatant and pseudoplastic fluids often follow a power law, the Ostwald-de Waele equation (Equation 1), and are known as power law fluids (McCabe et al. 2005). This power law is an empirical model, deduced from examination of experimental data (Rao 2014).

Equation 6: Ostwald-de Waele equation. Shear stress for power law fluids.

$$\tau_v = K \left( \frac{du}{dz} \right)^n$$

Where  $\tau_v$  is the shear stress in viscoelastic fluids [Pa]

$K$  is the flow consistency coefficient<sup>2</sup> [Pa·s<sup>n</sup>]

$n$  is the flow behaviour index

$\frac{du}{dz}$  is the shear rate [s<sup>-1</sup>]

#### 2.1.2.1.1 Rheological Properties of Milk

Milk is the fluid intended to be digested by the apparatus. In order to design and build the best possible model simulating the process of digesting milk, the milk's properties is considered. The chemical composition of milk, gives the fluid's rheological properties.

Milk is composed of a complex mixture of lipids, proteins, carbohydrates, vitamins and minerals (Damodaran et al. 2008). A relatively simple definition of milk is a mixture (emulsion) of fat in water, immersed in dissolved sugar and salt. 3.5% of the cow milk content is protein, where casein constitute approximately 80%. Four main types constitute the casein;  $\alpha_{s1-}$ ,  $\alpha_{s1-}$ ,  $\beta$ - and  $\kappa$ -caseins (Lucey 2002). Due to the phosphorylation and amphiphilic structure of the casein, the proteins interacts with each other and calcium phosphate to form spherical micelles. The stability of the micelles is due to the layer of  $\kappa$ -caseins that behaves as a polyampholyte brush. This makes casein, a protein usually insoluble in water, soluble (Damodaran et al. 2008).

As a shear thinning liquid, the milk's fluid behaviour is affected when the pH is changed. Lowering the pH close to the caseins isoelectric point, 4.6, the  $\kappa$ -caseins brush (with its negative charge) shrinks and finally collapses (de Kruif 1997). The caseins becomes insoluble, the milk coagulates and the viscosity increases.

As the milk passes through the digestive system, the pH will change. It will start at neutral and then decrease to pH < 2 as the HGJ and hydrochloric acid (HCl) is added. It will then increase again, when the HDJ and the sodium hydroxide (NaOH) is added.

<sup>2</sup> Some examples of K-values is presented in Appendix .

The viscosity range is continuously measured and documented by a rotational rheometer (Physica UDS200, Germany). Devle (Figure 4) has documented the changes of the viscosity during the digestive process of homogenized full fat milk, in previous research.

Normal milk behaves like a Newtonian fluid. However, its viscosity is affected by temperature, pH, content of fat and protein. So in this case when the viscosity changes due to the pH changes, milk is characterized as a pseudoplastic fluid.

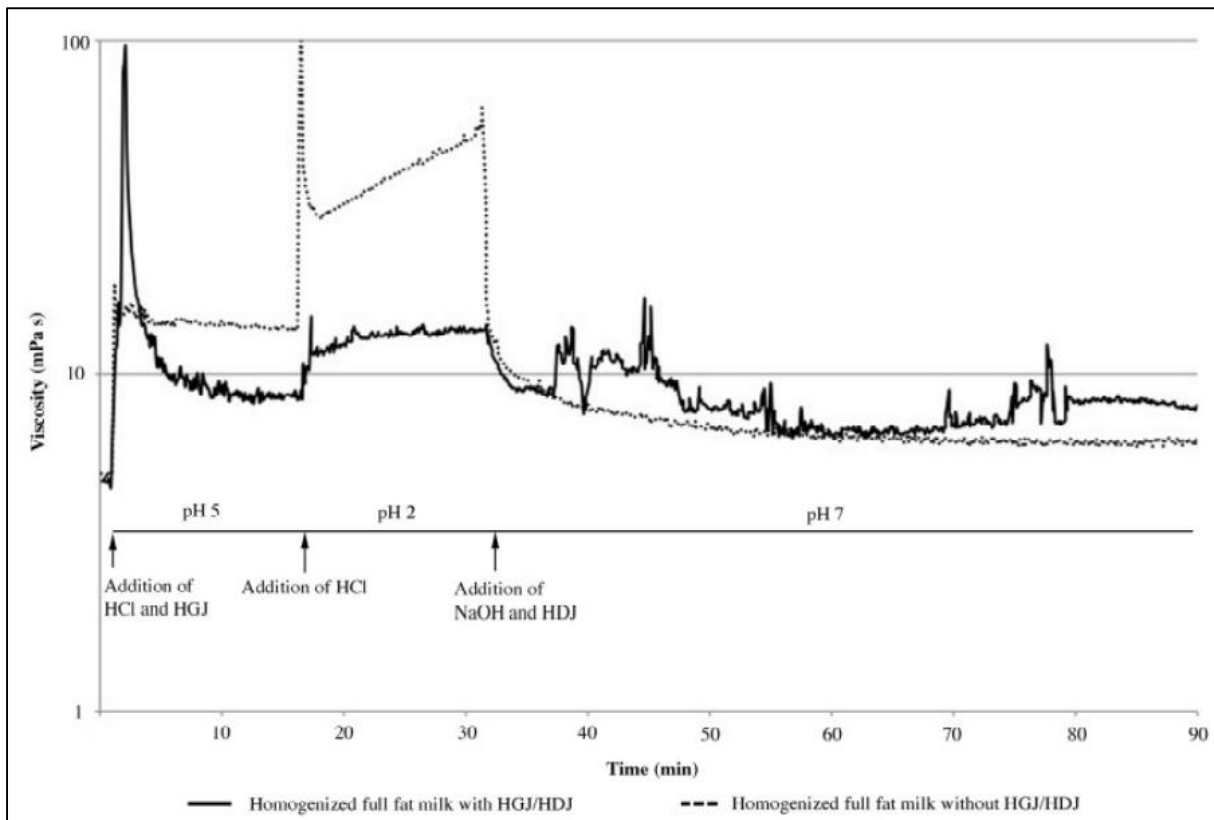


Figure 4: Viscosity measurements from in-vitro digestion of homogenized full fat milk with and without addition of human gastric (HGJ) and duodenal (HDJ) enzymes (Devle et al. 2012).

### 2.1.2.2 Velocity Boundary Layer

*“A fundamental principle of fluid mechanics, first stated by Prandtl in 1904, is that except for fluids moving at low velocities or possessing high viscosities, the effect of the solid boundary on the flow is confined to a layer of the fluid immediately adjacent to the solid wall. This is called the boundary layer, and shear and shear forces are confined to this part of the fluid. Outside the boundary layer, potential flow survives.” (McCabe et al. 2005).*

Considering fluid flow over a flat plate, one can simplify the fluid flow behaviour in a pipe. As over a flat plate (Figure 7), a velocity profile and a boundary layer develops in a pipe. In the example presented in Figure 6, fluid approaches the plate in the x-direction, with a uniform velocity  $v$ . Then along the plate, the velocity changes and a velocity profiles develops (Figure 5).

Adjacent to the plate, the fluids velocity is zero (assuming no-slip boundary condition<sup>3</sup>). Then the velocity increases with the distance from the plate (towards the centre of the pipe), until it is fully developed.

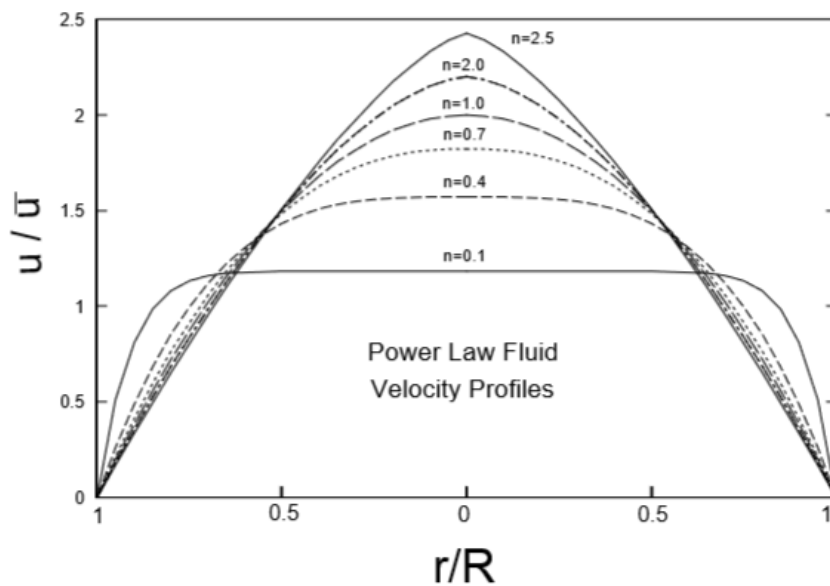


Figure 5: Laminar velocity profiles for power law fluids with different values of the flow behaviour index ( $n$ ) (Steffe, 1996).

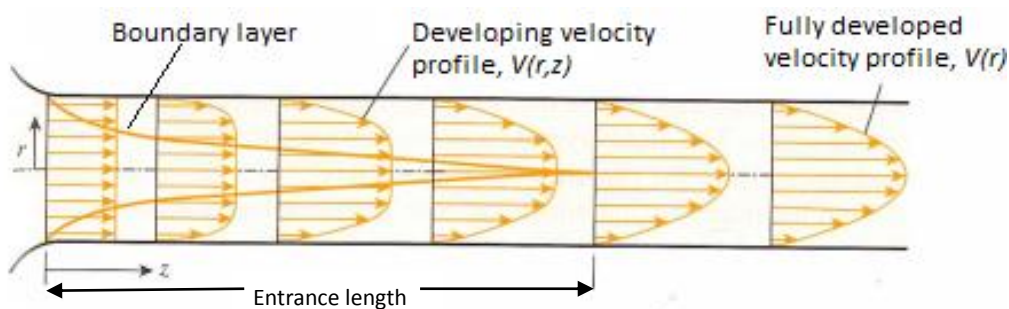


Figure 6: The development of the velocity profile in a circular pipe.  $V = V(r,z)$  and thus the flow is two-dimensional downstream when the velocity profile fully develops and remains unchanged in the flow direction (Çengel et al., 2011).

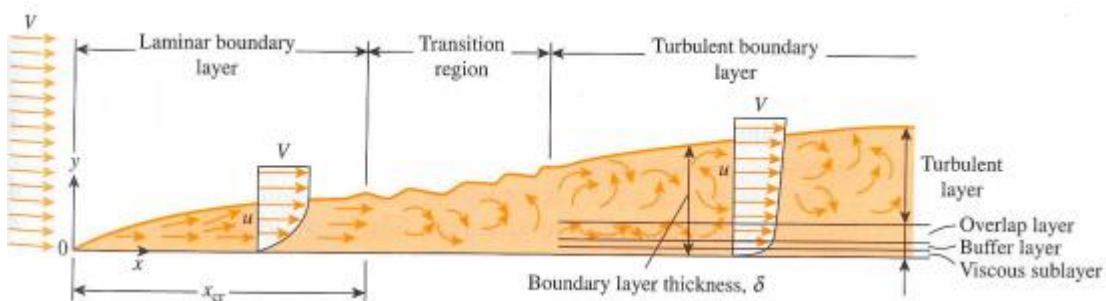


Figure 7: The development of the boundary layer for flow over a flat plate, and the different flow regimes (Çengel et al., 2011).

<sup>3</sup> A moving fluid in contact with a solid body will not have any velocity relative to the body at the contact surface (Prabhakara & Deshpande 2004).

### 2.1.2.3 Laminar and Turbulent Flow in Pipes

“At low velocities fluids tend to flow without lateral mixing, and adjacent layers slide past one another as playing cards do” (McCabe et al. 2005). In this case, there are neither crosscurrents nor eddies<sup>4</sup> and this regime is called laminar flow. When the velocity increases, turbulence appear, eddies form, which leads to lateral mixing (Figure 8) (McCabe et al. 2005). What is actually happening is that at low flow velocities, the pressure drop in the fluid increases directly with the fluid velocity (laminar flow), whereas at high velocities the pressure drop increases more rapidly (turbulent flow) (McCabe et al. 2005).

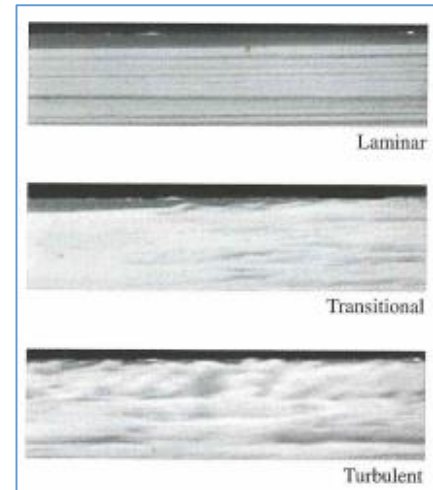


Figure 8: Right: Laminar, transitional and turbulent flows (Çengel et al., 2011).

### 2.1.2.4 Shear Stress vs. Shear Rate

The relationship between shear stress and shear rate in a real fluid is explained previous in this chapter, as it is the foundation of the science of rheology. However, in this thesis the shear stress at the artificial membrane wall is especially important, due to the mass transfer through the membrane in the small intestine device.

The shear stress and shear rate is, as presented in Figure 3, depended on the type of fluid. To explain how the shear stress and shear rate is connected to the velocity profiles, a shear diagram is useful. A shear diagram is a profile of the shear stress of a fluid flowing through a pipe with constant pressure. The shear stress develops due to friction between the fluid layers and the pipe wall. Figure 9 is a sketch of the velocity profile compared to its shear stress in a laminar flow. The shear stress is highest at the wall, and decreases towards the centre of the pipe. This can be calculated when knowing the pressure distribution in the pipe from the Equation 7.

Comparing Figure 9 and Figure 6, shows that the velocity gradient (shear rate) is smaller for turbulent flow, resulting in that the shear stress at the wall is larger for turbulent flow than laminar flow.

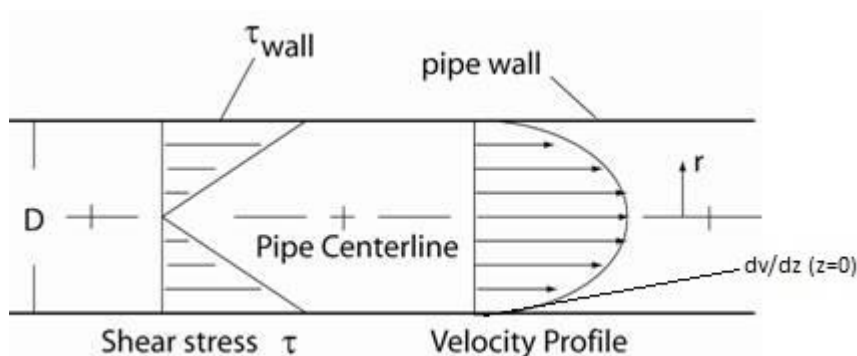


Figure 9: Shear diagram vs. velocity profile of a laminar flow where  $dv/dz$  present the velocity gradient, also known as the shear rate (Sleigh and Noakes, 2009).

<sup>4</sup> Eddy: a current at variance with the main current in a stream of liquid or gas, especially one having a rotary or whirling motion (Dictionary 2014).

Equation 7: Shear stress at the pipe wall (Salas-Bringas et al. 2009).

$$\tau_{wall} = \frac{((\Delta P_{Measured})r)}{(2L)}$$

Where  $\Delta P_{Measured}$  is the pressure drop between the points  $P_1$  and  $P_2$

$L$  is the length between [mm]

$r$  is the pipe radius [mm] (Figure 9)

This equation only applies to laminar and steady flow, where the fluid is incompressible, the temperature is constant and there is no slip at the pipe wall. The properties should also be time and pressure independent and the pressure drop should be linear (Salas-Bringas et al. 2009).

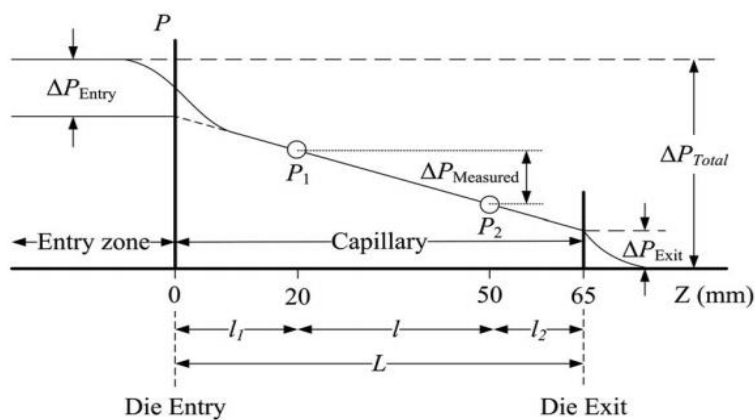


Figure 10: Diagram of the pressure distribution in a pipe, where the pressure drop is linear (Salas-Bringas et al. 2009).

#### 2.1.2.4.1 Shear Rate of Power Law Fluids

Once  $n$  is estimated, the shear rate ( $\gamma$ ) in a power law fluid can be calculated (Equation 8).

Equation 8: The shear rate of a power fluid, relevant in laminar flow (Smith 2011).

$$\gamma = \left( \frac{3n + 1}{4n} \right) \left( \frac{8u}{D} \right)$$

Where  $D$  is the pipe's diameter

In the case of fluid flow through the artificial membrane at a velocity of  $1.66 \cdot 10^{-4}$  m/s, the shear rate against an increasing value of  $n$  is plotted in Figure 11.

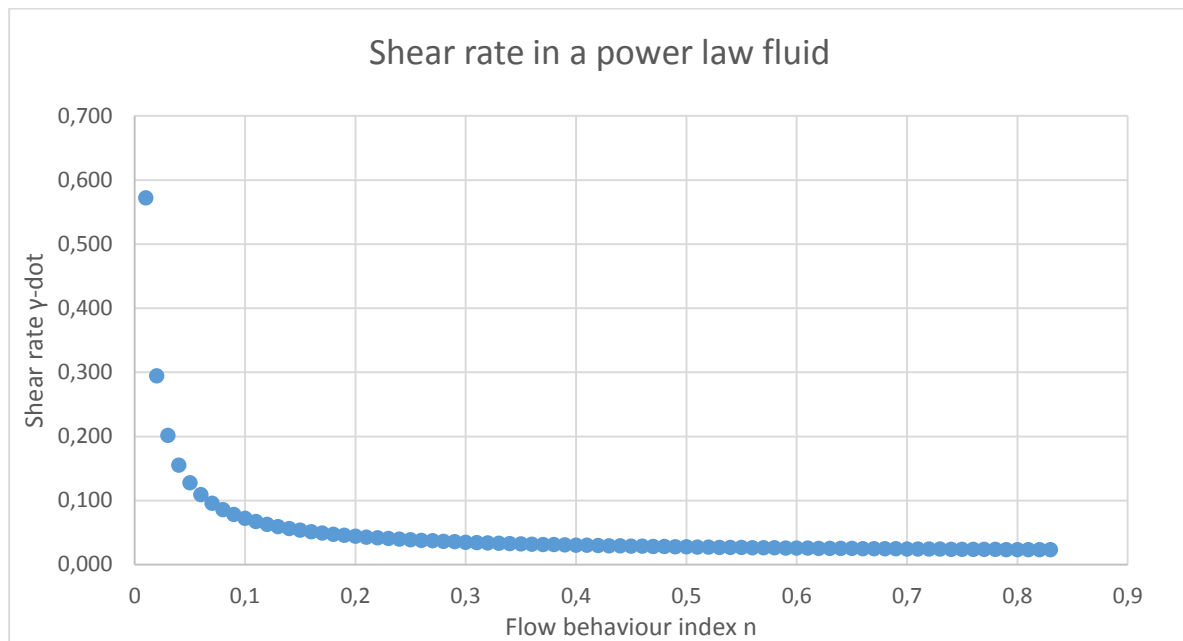


Figure 11: The shear rate in a power law fluid, where the flow is laminar, at different values of  $n$  (Schüller 2014). The fluid is flowing in a pipe with an inner diameter of 0.03 m and a mean velocity at 0.00016667 m/s. As the  $n$ -value increases toward 1 (Newtonian fluid), the shear rate becomes linear. See chapter 0 for calculations of the velocity and diameter.

The significance of this  $n$ 'th power can also be demonstrated in velocity profiles, see Figure 5.

### 2.1.2.5 Reynolds Number

Reynolds number ( $Re$ ) is a dimensionless group of variables describing the ratio of inertial forces to viscous forces, which gives a prediction of similar flow behaviour in different fluid flow scenarios.

Equation 9: Reynolds number for a Newtonian fluid.

$$Re = \frac{D\bar{V}\rho}{\mu} = \frac{D\bar{V}}{\nu}$$

Where:  $D$  is the inner diameter of the tube [m]

$\bar{V}$  is the liquid's average velocity [m/s]

$\rho$  is the liquid's density [kg/m<sup>3</sup>]

$\nu$  is the liquid's kinematic viscosity [m<sup>2</sup>/s]

Observations have shown that the transition from laminar to turbulent flow occurs over a wide range of Reynolds numbers ( $Re$ ), depended on the circumstances. Relevant for this thesis, is the issue of flow through a pipe. Reynolds numbers below 2100 (the fluids critical Reynolds number) is always laminar in the case of Newtonian fluids. However when eliminating effects like disturbance at the entrance of the pipe and the pipe wall's roughness; also Reynolds number well above 2100 indicates laminar flow. In normal circumstances, Reynolds number over 4000 is turbulent, and the area between is a transition phase (Figure 8).

In the case of non-Newtonian power law-fluids, the equation above is no longer useful. A new power law-equation (Equation 10) is a wide used definition, however it is somewhat arbitrary (McCabe et al. 2005).

Equation 10: The Reynolds number for a non-Newtonian liquid.

$$Re = 2^{3-n} \left( \frac{n}{3n+1} \right)^n \frac{D^n \rho \bar{V}^{2-n}}{K}$$

The fluids critical Reynolds number (the fluid is laminar below this number) is also different when the fluid is a non-Newtonian power law-fluid, see Equation 11.

Equation 11: The Reynolds critical number, which under indicates laminar flow.

$$Re < \frac{6464n(2+n)^{(2+n)/(1+n)}}{(1+3n)^2} = Re_{critical}$$

#### 2.1.2.5.1 Reynolds Stress

As mentioned previous, shear stress at the pipe wall is much larger with turbulent flow than with laminar flow. These turbulent shear stresses are called Reynolds stresses, and are directly related to the varying shear rate. When eddies occur in the flow, as it do in turbulent flow, the shear rate (velocity gradient) varies between having a positive or a negative value (see Figure 12). All in all this requires an equation for turbulent stress (Equation 12).

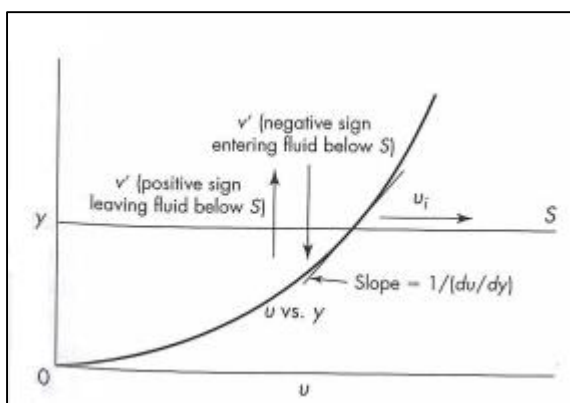


Figure 12: Reynolds stress. A fluid in turbulent flow is moving in the positive  $x$  direction, and surface  $S$  is parallel to the flow (McCabe et al., 2005). The mean velocity of the flow is  $u$ . When an eddy moves towards the wall, its flow rate  $v'$  has a negative value, and away from the wall, its flow rate is positive.

Equation 12: Turbulent viscosity, called the Reynolds stress (McCabe et al. 2005).

$$\tau_t = \overline{\rho u'v'} = E_v \left( \frac{du}{dy} \right)$$

Where  $u'$  is the mean velocity

$v'$  is the flow rate

$\rho$  is the density

$\tau_t$  is the Reynolds stress (turbulent stress)

$E_v$  is the eddy viscosity

x

The eddy viscosity is analogous to the absolute viscosity  $\mu$ , and is presented as the equation below.

Equation 13: The eddy viscosity (McCabe et al. 2005).

$$E_v = \frac{\mu}{\rho}$$

The total shear stress of a liquid in turbulent flow is then the turbulence stress added to the original equation for viscous stress.

Equation 14: The total shear stress in a turbulent fluid is the sum of the viscous stress and the turbulent stress (McCabe et al. 2005).

$$\tau = (\mu + E_v) \frac{du}{dy}$$

### 2.1.2.6 Entry Length

The entrance length in a pipe is the length from the inlet to the point where the flow is fully developed (Figure 6). Poole and Ridley (Poole & Ridley 2007) developed a model which calculates the entry length for non-Newtonian (power-law) fluids where  $n$  is between 0.4 and 1.5. The model is presented in Equation 13 and plotted in Figure 13 (Salas-Bringas et al. 2009).

Equation 15: The entry length ( $L_e$ ) of a non-Newtonian in-elastic power fluid.

$$\frac{L_e}{D} = [(0.246n^2 - 0.675n + 1.03)^{1.6} + (0.0567Re)^{1.6}]^{1/1.6}$$



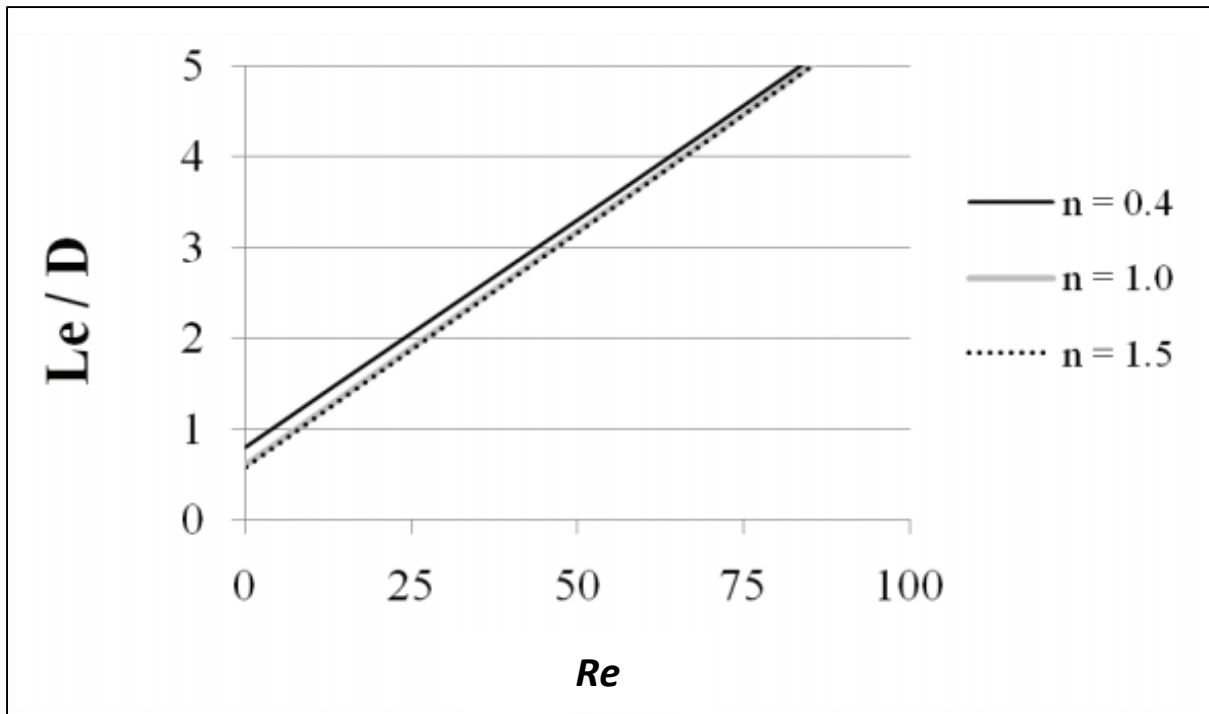


Figure 13: Entry length for different diameters,  $n$  values and Reynolds numbers for inelastic power law fluids (Salas-Bringas et al. 2009).

Where  $L_e$  is the entry length [mm]

$Re$  is the Reynolds number

## 2.2 Diffusion of Soluble Products through a Membrane

Diffusion is the movement of an individual component through a mixture. This movement is under the influence of a physical stimulus, which can be a concentration-, an activity-, a pressure- or a temperature gradient. The most common is with a concentration gradient, which is also the case in this thesis. A diffusion can be either at a steady state where the gradient is maintained by constantly supplying the diffusing component, or it can be un-steady where the gradient and fluxes decrease with time as equilibrium is approached (McCabe et al. 2005).

In membrane separations, diffusion occurs in the two fluids on either side of the membrane and in the membrane itself (McCabe et al. 2005).

Five diffusion quantities are used in diffusion theory (McCabe et al. 2005);

- ❖ Velocity  $u$  [length/time]
- ❖ Flux across a plane  $N$  [mol/area-time]
- ❖ Flux relative to a plane of zero velocity  $J$  [mol/area-time]
- ❖ Concentration  $c$  and molar density  $\rho_M$  [mol/volume]
- ❖ Concentration gradient  $dc/db$ ,  $b$  is the length in direction of diffusion [m]

Using Fick's first law of diffusion (Equation 16), one can calculate the molar flux  $J$  of a mass component  $A$  through a liquid. The law states that the mass transport occurs due to a mass concentration gradient (McCabe et al. 2005).

Equation 16: Fick's first law of diffusion (McCabe et al. 2005).

$$J_A = -D_v \frac{dc_A}{db}$$

Where  $D_v$  is the volumetric diffusivity [area/time]

### 2.2.1 Diffusion in Liquids

The diffusivity  $D_v$ , for large spherical molecules (MW > 400) in a dilute solution, can be estimated from Equation 17 below. This equation considers the drag on a sphere moving in a continuous fluid (McCabe et al. 2005).

Equation 17: Stokes-Einsteins equation (McCabe et al. 2005).

$$D_v = \frac{7.32 \times 10^{-16} T}{r_0 \mu}$$

Where  $T$  is the absolute temperature [K]

$r_0$  is the molecular radius [cm]

$\mu$  is the viscosity [cP]

#### 2.2.1.1 Passive Diffusion of Peptides Across a Immobilized Artificial Membrane

A group of scientist evaluated the effect of size and charge on the permeation characteristics of peptides across the intestinal mucosa in 1997 (Pauletti et al. 1997). In this research, they found the diffusivity flux of a negatively charged amino-acid (molecular weight 616 g/mol) through an artificial membrane to be 10.04 cm/s. Knowing this flux, they could calculate the amino acids molecular radius to be  $3.3 \cdot 10^{-8}$  cm. Using this as an example of diffusion of milk components through the artificial membrane in this project, one can calculate the dimensionless numbers  $Sc$ ,  $Sh$  and  $Gz'$ .

### 2.2.2 Dimensionless Numbers $Sc$ and $Sh$ and $Gz'$

Schmidt, Sherwood and Graetz number are all dimensionless groups of mass transfer.

#### 2.2.2.1 Schmidt Number

Schmidt number is the ratio of the kinematic viscosity to the molecular diffusivity and is given by Equation 18.

Equation 18: Schmidt number (McCabe et al. 2005).

$$Sc = \frac{v}{D_v} = \frac{\mu}{\rho D_v}$$

For typical mixtures, the Sc number range from about  $10^2$  to  $10^5$ , and it decreases with increasing temperature due to the effect on the viscosity and the diffusivity.

### 2.2.2.2 Sherwood Number and Graetz Number

Sherwood number relates the mass flux to the concentration difference and the mass diffusivity coefficient (McCabe et al. 2005).

Equation 19: Sherwood number relevant for fluid flow over a flat plate (McCabe et al. 2005)

$$Sh = \frac{k_c D}{D_v}$$

Where  $k_c$  is the mass transfer coefficient

However, when regarding a flow inside a pipe, the  $Sh$  number is adjusted. An example, relevant for this thesis, is when the wall concentration is a function of axial position, as in a counter flow membrane separator. The  $Sh$  number, in a laminar flow, is therefore given in Equation 20.

Equation 20: Sherwood number relevant for laminar fluid flow inside a pipe (McCabe et al. 2005).

$$Sh = 1.76Gz'^{1/3}$$

Where  $Gz$  is the Graetz number for mass transfer:

Equation 21: Graetz number (McCabe et al. 2005).

$$\frac{\dot{m}}{\rho D_v L} = Gz' = \left(\frac{\pi}{4}\right) Re Sc \left(\frac{D}{L}\right)$$

Where  $\dot{m}$  is the mass flow rate.

For turbulent flows, with high Schmidt number (typical for mixtures), the  $Sh$  number is:

Equation 22: Sherwood number relevant for a turbulent fluid flow (McCabe et al. 2005).

$$Sh = 0.0096Re^{0.913}Sc^{0.346}$$

### 2.2.3 Types of Membranes in the Relevant Size Region

Depending on the size of the solute, different types of filtration is used. The purpose of the artificial small intestine is to filtrate out smaller molecules (<3.5 kDa). Due to this fact, only the relevant filtration methods are mentioned here.

#### 2.2.3.1 Ultra- and Microfiltration

Micro- and ultrafiltration are pressure driven processes. Solutes with low MW and water passes through the filter, and solutes with high MW are retained. A concentration gradient (Figure 14) is built up on the inside of the membrane wall, which results in a gel formation at the wall. When the rate of transfer of solute toward the membrane is equal to the diffusion rate of solute away from the membrane, due to this gel formation, the system is at steady state (Shuler & Kargi 1992).

The volumetric filtration flux  $J_v$  through a membrane with gel formation is given by:

*Equation 23: The volumetric filtration flux through a membrane with gel formation (Shuler & Kargi 1992).*

$$J_v = k \times \ln \frac{C_w}{C_B}$$

Where  $J_v$  is the volumetric filtration flux [ $\text{m}^3/\text{m}^2\cdot\text{s}$ ]

$C_B$  is the concentration at the boundary ( $X=0$ )

$C_w$  is the concentration where the layer starts ( $X=\delta$ )

$k$  is the mass transfer coefficient, given by Equation 24.

*Equation 24: The mass transfer coefficient (Shuler & Kargi 1992).*

$$k = \frac{D_v}{\delta}$$

Where  $\delta$  is the gel layers thickness [m].

As mentioned in the previous chapters, the mass transfer coefficient is a function of fluid and solute properties, and is directly related with the  $Re$ ,  $Sh$  and  $Sc$  number (Shuler & Kargi 1992).

The size of the solute separates micro- from ultrafiltration. Where microfiltration is usually used to separate species like bacteria and yeast, which has the size  $0.1 \cdot 10^{-6}\text{m}$  to  $10 \cdot 10^{-6}\text{m}$ , ultrafiltration is used when the size of the solute has a MW above 5-500kDa. With even smaller molecules, dialysis is used instead.

#### 2.2.3.2 Dialysis

Dialysis is a membrane separation used for the removal of solutes with low MW (< 500) from a solution. A known example is the use of artificial kidneys (dialysis membranes) to filtrate out urine (Shuler & Kargi 1992). Due to the size of the components in milk, which are intended to be pass though the membrane, it is assumed that ultrafiltration, dialysis, or a combination of the two will be used.

The dialysis membrane is selective, which separates a solution in two phases, where one contains low MW and one contains high. The MW cut-off (often given in the size Da) is low in dialysis membranes, which makes the low MW molecules, move from a high to a low concentrated area, until it reaches its equilibrium (Shuler & Kargi 1992).

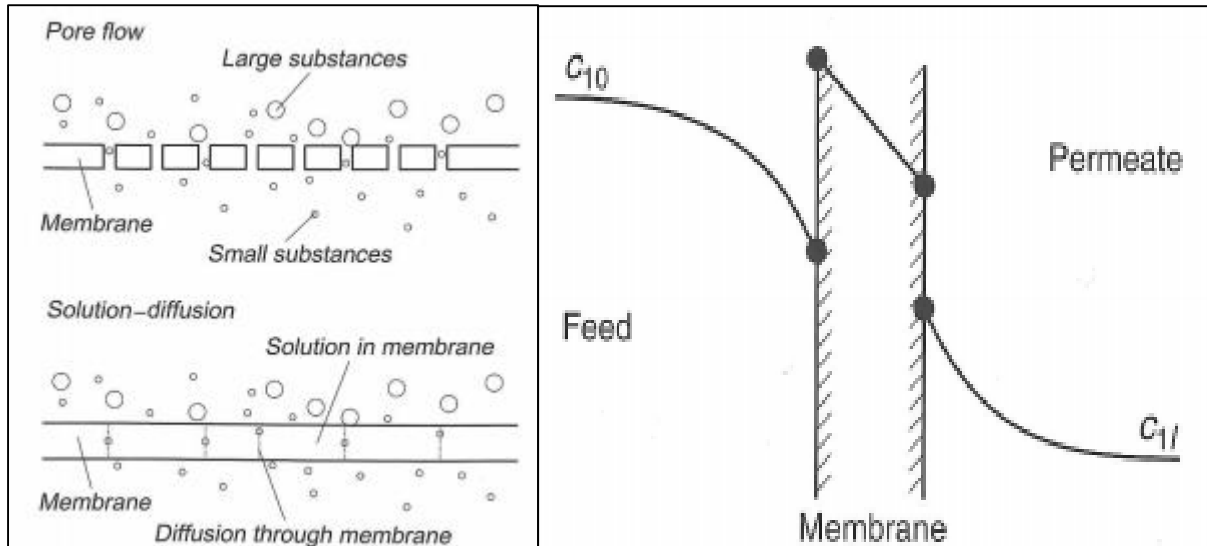


Figure 14: Left: Sketch of the principle of dialysis (diffusion) vs. ultrafiltration (Lekang 2013). Right: The concentration gradient across a membrane, from left to right (Cussler 2009).

The transport mechanism in these types of membranes (often dense or compact regarding dialysis), is diffusion or solubility of the membrane material. It is therefore important that the membrane is adapted to the permeate, to have transport across it. In diffusion through dense materials, the pressure on the inside of the membrane is an important factor to push through the permeate. This depends on the membrane's thickness. However, regarding the membrane types that will be used in this apparatus, the membranes are relatively thin, which lowers the importance of this factor (Lekang 2013).

### 2.2.3.3 Cross Flow

A method of partial elimination of the gel formation is to have the fluid flows (inside and outside the membrane) counter current. The method is called tangential flow filtration, causing a decrease in the pressure directly at the membrane (Shuler & Kargi 1992). For laminar flow, the pressure drop through the pipe can be found through the Hagen-Poiseuille equation.

Equation 25: The Hagen-Poiseuille equation for pressure drop in cross-flow filtration (Shuler & Kargi 1992).

$$P_{inlet} - P_{outlet} = \Delta P = \frac{C\mu LQ}{D}$$

Another version of the same equation gives the permeate flux (Equation 26). The membrane's permeability depends on if it is dense (typical dialysis) or porous (typical micro- or ultrafiltration), and its structure (Lekang 2013).

Equation 26: Hagen-Poiseuille equation, which fits when the model is a cylindrical pore micro- or ultrafiltration (Lekang 2013).

$$J_v = \frac{\varepsilon r_p^2}{8\tau_{tor}} \times \frac{\Delta P_m}{L_m \mu}$$

Where  $J_v$  is the permeate flux [L/m<sup>2</sup>·h]

$\Delta P_m$  is the pressure drop across the membrane

$\tau_{tor}$  is the tortuosity (path length in relation to pore diameter)

$r_p$  is the pore's radius

$L_m$  is the length across the membrane

$\varepsilon$  is the surface porosity, which is found by Equation 27

Equation 27: The membrane's porosity (Lekang 2013).

$$\varepsilon = \frac{n_p \pi r_p^2}{A_m}$$

Where  $n_p$  is the numbers of pores in the membrane area  $A_m$

In general, ultrafiltration membranes usually have a porosity of 0.1-1%, while microfiltration membranes have a porosity of 5-70%.

## 2.3 The Dynamics and Biomechanics of the Digestive System

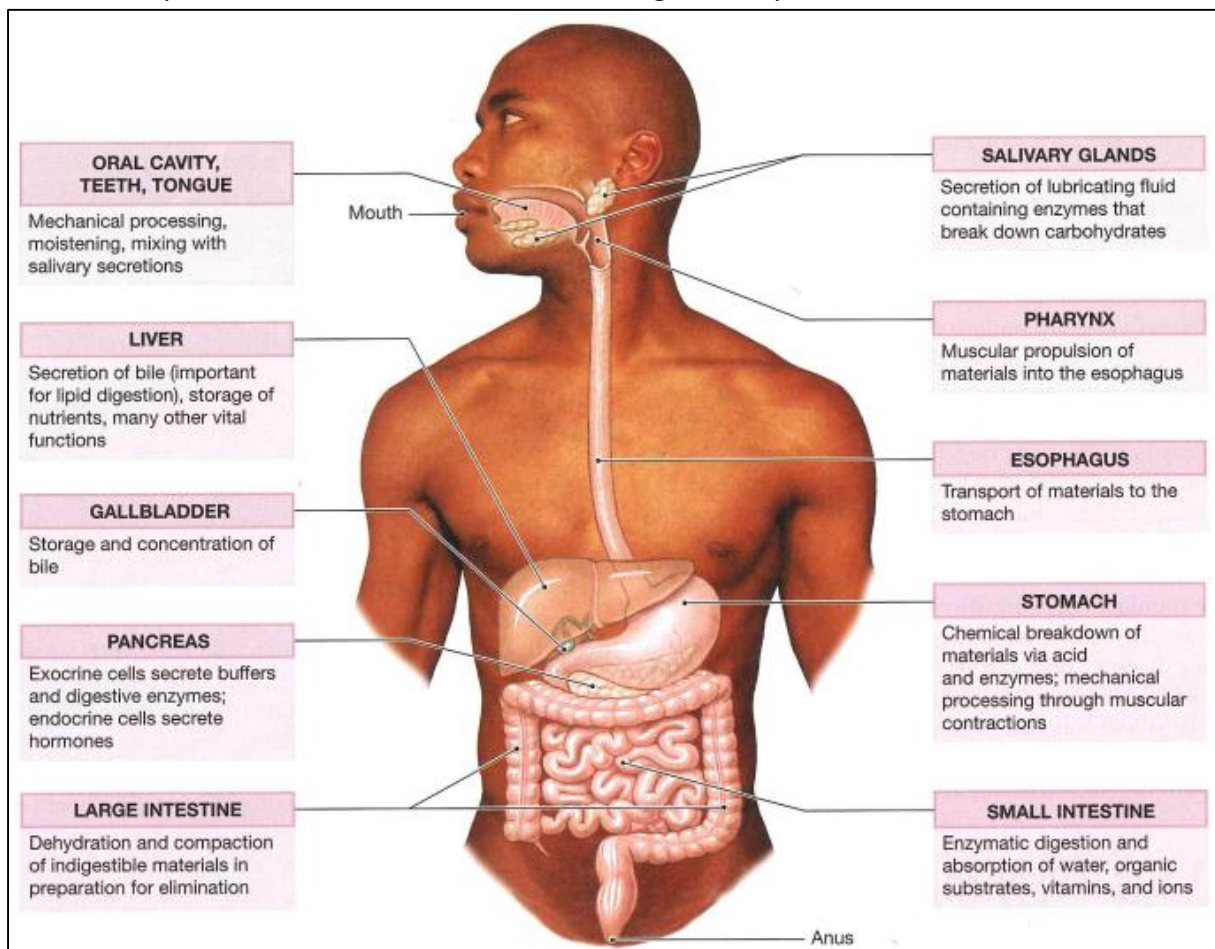


Figure 15: The components of the human digestive system (Martini & Nath 2009).

In the human body, the digestion of food starts in the mouth where it is chewed and moistened by the saliva amylase. This turns the solid food to a food bolus, whereas liquids are directly swallowed. It then moves down the esophagus by peristaltic movements, and into the stomach. Peristalsis is a wave of contraction of the wall, forcing the content forward, like a peristaltic pump (Tharakan 2008).

The stomach functions as a storage, mixer and emptier. Gastric juices, along with the peristaltic movements from the stomach wall, helps to mix and homogenize the food, and turn it into a multiphase slurry called chyme. Gastric juices are secreted from the glands lining the stomach and contain gastric acid, bile salts, and digestive enzymes, which lowers the level of pH to below 2. The more intensive peristaltic movements then push the content into the duodenum, now as a substance called chyme (Kong & Singh 2008). Studies have indicated that duodenal receptors mediate with a negative feedback mechanism, making sure that a limited amount of energy (8.4 to 16.8 kJ/min) is delivered to the duodenum from the stomach (Faas et al. 2002). The particle size of the content entering the duodenum is less than 1 to 2 mm during fed state (Thomas 2006).

The duodenum is the first of three parts of the small intestine. In the duodenum, duodenal juices from the pancreas, liver and intestine dissolves the food, making it ready for absorption. Most of the nutrient absorption occurs through the small intestinal walls, including the absorption of water. After passing through the small intestine, the food moves to the large intestine (colon). The remaining water in the, by then indigestible food, is absorbed through the walls of the large intestine. The waste products moves through and out of the large intestine for excretion (Kong & Singh 2008).

The fluid flow velocity through the small intestine is varying, and it depends on the digestive content. However, Guyton has given a flow velocity of  $1.667 \cdot 10^{-4}$  m/s (Guyton & Hall 2006) through a small intestine with a diameter of 0.03 m (Ganong & Barrett 2005). The Reynolds for the fluid in the small intestine is within a range between the orders  $10^{-3}$  and 10, which indicates laminar flow and not a good mixing of the content. However, the movements in the intestinal walls generates the mixing needed.

### 2.3.1 Movements of the Intestinal Walls

The movements of the intestinal wall causes the food content to mix with the enzymes. These movements are also responsible of moving the nutrients close to the absorptive epithelium in the intestinal membrane (Macagno & Christensen 1980).

There are two different movements/contractions in the gastro intestinal tract, peristalsis and segmentation.

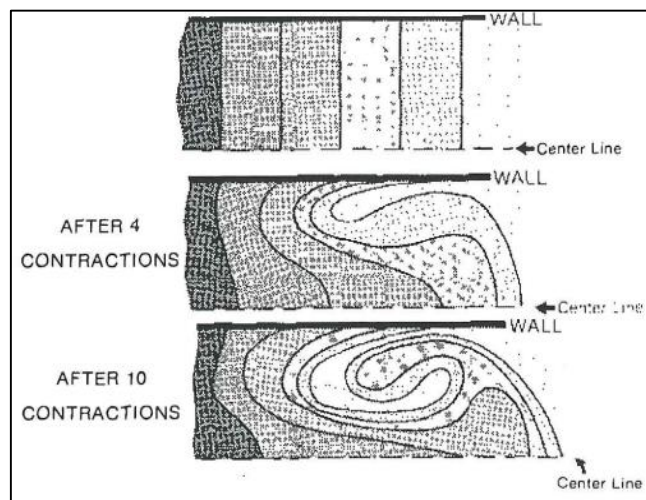


Figure 16: Lagrangian description of flow induced by longitudinal contractions (Macagno & Christensen, 1980).

Figure 16 presents a model describing the flow induced by peristaltic contractions, visualizing the turbulence created in the small intestine.

#### 2.3.1.1 Peristalsis

Peristalsis is a reflex response that consists of waves of the muscular (both longitudinal and circular) contractions that moves small oval mass of digestive content, along the length of the digestive tract (Martini & Nath 2009). Squeezing toothpaste out of a tube is a similar movement, and a mechanical peristaltic pump uses the same principle (Figure 17).

#### 2.3.1.2 Segmentation

Segmentation is a movement the intestinal walls use to mix the intestinal content. This provides time for digestion and absorption, and is most frequent in the small intestine (Ganong & Barrett 2005). This contraction does not follow a set of patterns, nor does it push the content in any direction (Martini & Nath 2009).



Macagno and Christensen recorded the time between any two successive segmental contractions in a human duodenum, after a subject had ingested a glass of skimmed milk. The result is shown in Figure 17, where the most frequent contractions is 5-6 seconds apart.

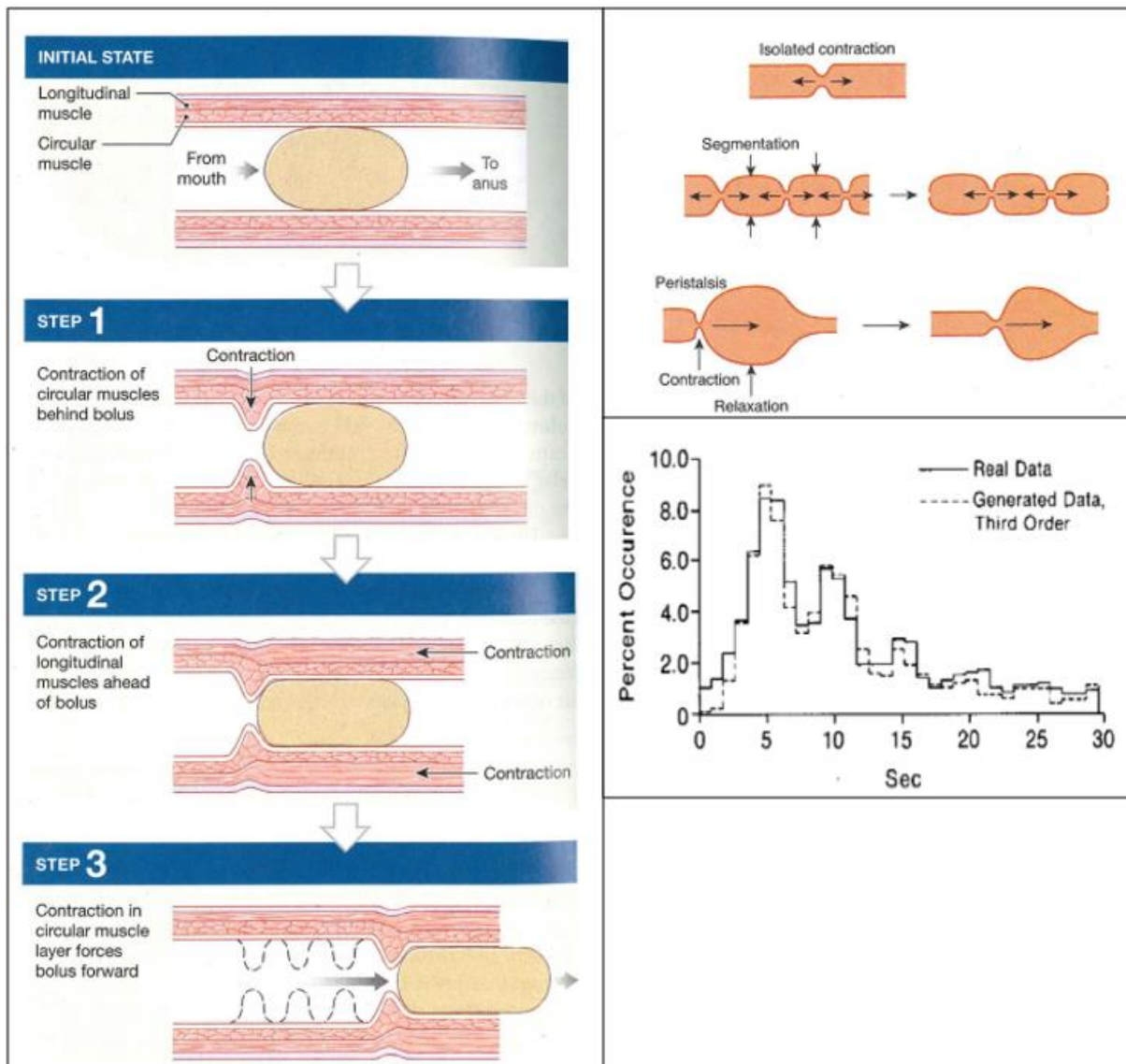


Figure 17: Left: Peristalsis movements. Right on top: Segmentation movements in contrast to the related peristalsis movements (Ganong & Barrett, 2005). Right on bottom: Frequency distribution of intercontractile times in the human duodenum (Macagno & Christensen, 1980).

### 2.3.2 The Small Intestine

Responsible for most of the nutrient absorption, the small intestine is the part of the digestive system that is the focused area on building a dynamic in-vitro model. The small intestinal membrane is also the most critical and difficult part to simulate. Figure 18 gives a solid description of the different aspects of the complicated intestinal wall.

The small intestine is divided into three part; first one short duodenum, then two longer sections jejunum and ileum. The duodenum is approximately 25 cm, and the total length of the jejunum and the ileum combined is approximately 260 cm (Ganong & Barrett 2005). Every section has its own functions.

The duodenum's prime function is to receive chyme from the stomach and neutralize its acid levels before they can damage the absorption surfaces of the intestinal walls. As the first section of the small intestine, the duodenum have few *plicae circulares* (see Figure 18(a)), and small villi. The next section is the jejunum, and it is here that most of the absorption occurs. The occurrence of *plicae circulares* and size of villi in this section of the intestine, is much more prominent than earlier. In the last section of the ileum, these structures are almost non-existing. The ileum is the last section the digested content passes before entering the large intestine (colon). The prime function of the ileum is therefore to protect the small intestine from bacteria that are normal inhabitants of the colon (Anatomy 2014).

The absorption of chemicals and nutrients is minimal in the duodenum, increases in the jejunum, and is non-existing in the ileum.

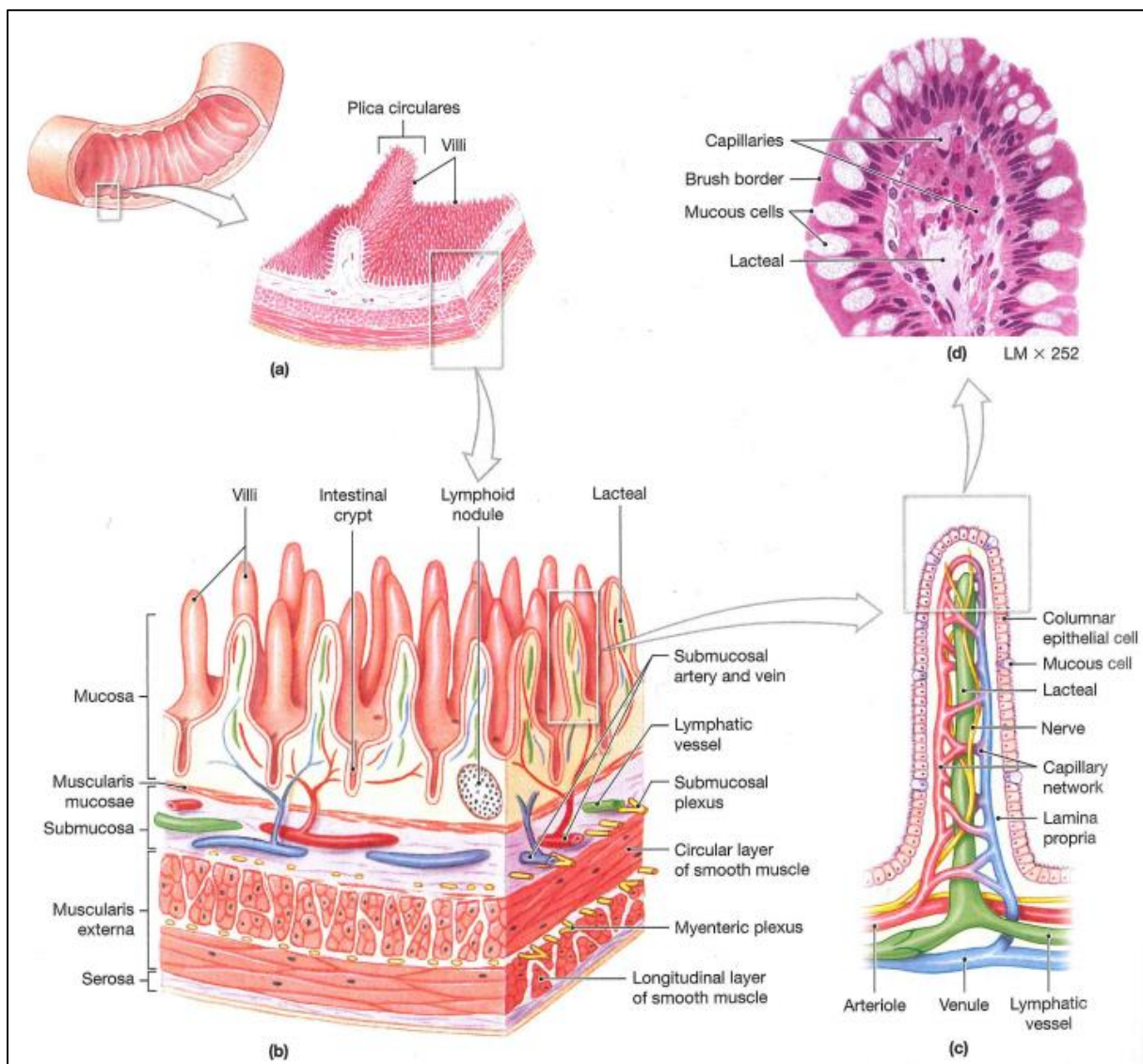


Figure 18: **The intestinal wall.** (a) A single *plicae circulares* and multiple villi. (b) The organization of the intestinal wall. (c) Internal structure in a single villus, showing the capillary and lymphatic supplies. (d) A villus in sectional view. (Martini & Nath 2009).

### 2.3.2.1 Size of Villi

The absorption efficiency of the different sections in the small intestine is directly related to the occurrence and size of plicae circulares, villi (see chapter above) and microvilli (Figure 20). Note that the plicae circulares occurs in only some mammals (humans) and not in mammals often used for research (rats) (Mayhew 1984), and is therefore not considered as a factor contributing to the roughness of the intestinal wall. Knowing the structure of the intestinal villi and microvilli, one can estimate this roughness.

#### 2.3.2.1.1 Roughness

The flow through the human small intestine is as previous mentioned, assumed to be turbulent due to the movements in the intestinal walls. In turbulent flow, a rough pipe (which the structure of the villi can be described as), leads to a larger friction factor for a given Reynolds number. Different types of roughness are presented in Figure 19.

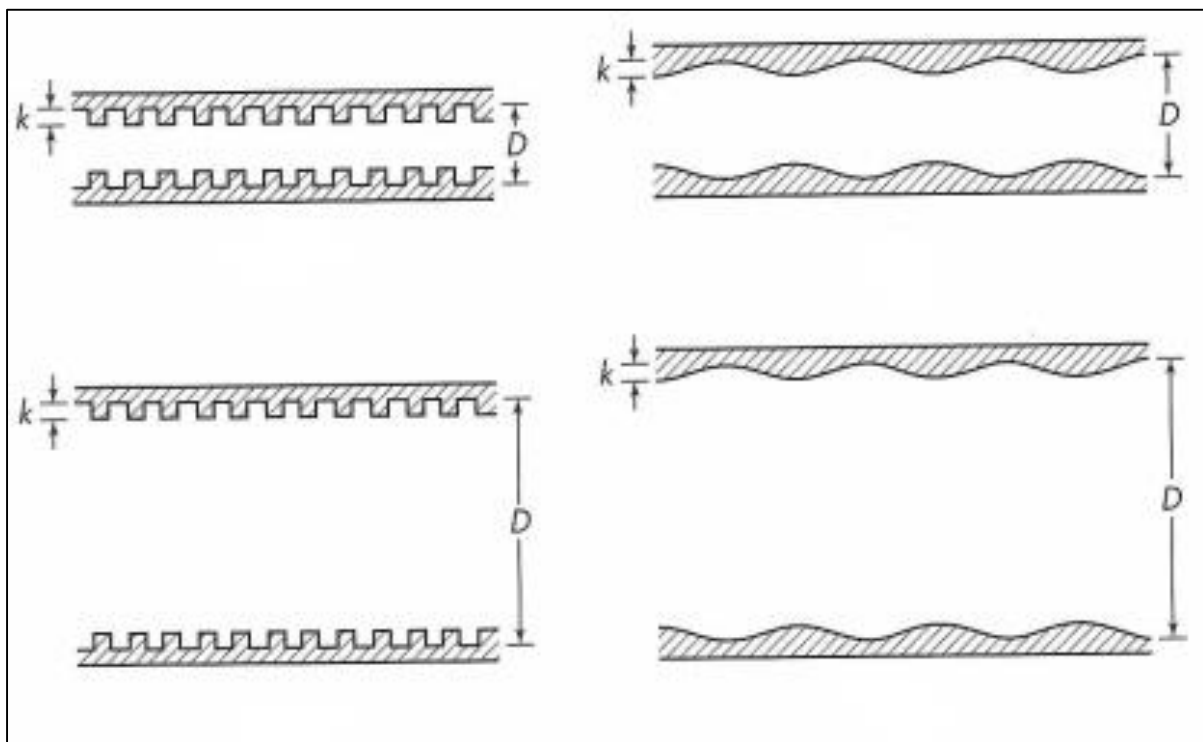


Figure 19: Types of roughness, with different diameters and roughness parameters.  $k/D$  is the relative roughness (McCabe et al. 2005).

Knowing the Reynolds number, the internal diameter of the pipe, it is possible to find the friction factor  $f$ , through the roughness parameter  $k$  and a friction factor plot (see Appendix K). The roughness parameter  $k$  is simply the height of each unit of roughness, which in this case is the height of the villi.

### 2.3.2.1.2 Microvilli

The dimensions of villi and microvilli (see Figure 20) vary from animal to animal. However, when measured, the height of the microvilli is usually close to  $1 \cdot 10^{-6} \text{m}$  with a width at  $7 \cdot 10^{-8} \text{m}$  in rats. Their distribution is arranged in a closed hexagon (see Figure 20). When counting the microvilli in a sample area, the population is found to cover approximately 60% of the surface area of a villi, and it increases the free surface by a factor of 24 (Palay & Karlin 1959). The gap between the microvilli is assumed to be approximately  $5 \cdot 10^{-8} \text{m}$ .

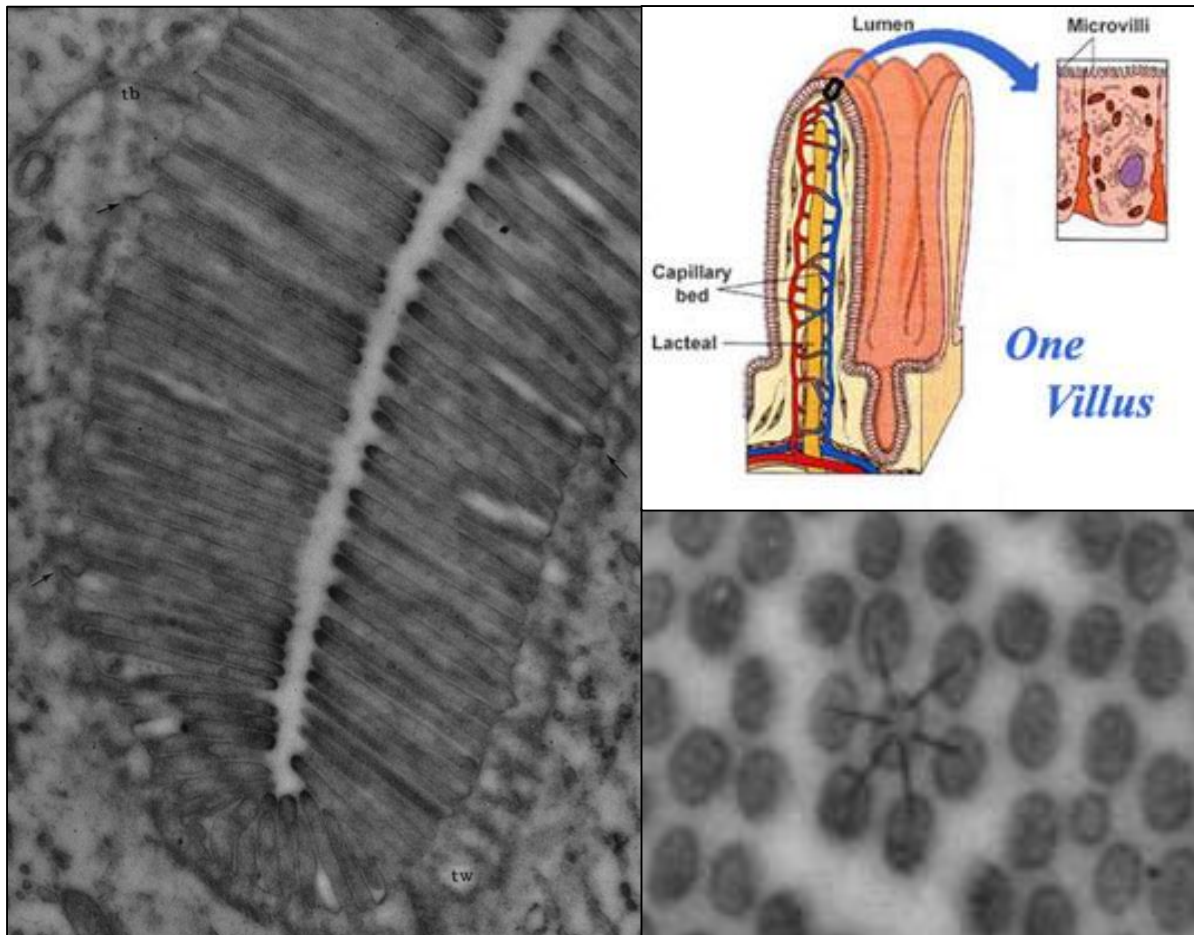


Figure 20. Left: The striated border of two neighboring epithelial cells in the depths of a fold in the surface of a villus, picture taken through an electron microscopy (Palay & Karlin 1959). Bottom right: Distribution of microvilli on the villus surface in the intestinal wall (Palay & Karlin 1959). Top right: A sketch demonstrating microvilli vs. villi (Nutter's Exus)..

### 2.3.2.1.3 Villi

The dimensions of villi is calculated from the table in Appendix N, giving approximately 30 villi in an area of  $1 \cdot 10^{-6} \text{m}^2$ , with an average height at  $3 \cdot 10^{-4} \text{m}$ . With a cross sectional area of  $2 \cdot 10^{-8} \text{m}^2$ , the villi covers about 60% of the surface area of the intestinal walls. This means that 40% of the area is gaps, which divided in between the 30 villi gives a gap of  $1.38 \cdot 10^{-8} \text{m}^2$  between each.

### 2.3.3 Transport Across the Intestinal Wall

The transport of nutrients and chemicals across the small intestinal wall occurs in three different ways or in a combination of two or three of them, depending on what is transported. The transport options are simple diffusion, facilitated diffusion, cotransport or a combination.

- ❖ Diffusion
  - A molecule crosses the membrane through the lipid portion of the membrane (lipids-soluble molecules), or through a membrane channel.
- ❖ Cotransport
  - Two substrates at a time, crosses the membrane with one carrier protein, following a concentration gradient for at least one of the substrates.
- ❖ Facilitated diffusion
  - A carrier protein transport a molecule across the plasma membrane without using energy, following a concentration gradient (*Anatomy 2014*).

Table 2: The major substrate groups in milk, and their transport across the intestinal mucosa (*Martini & Nath 2009*).

❖ Substrate group	Transport method
Carbohydrate	Facilitated diffusion and cotransport
Lipids	Diffusion
Proteins	Facilitated diffusion and cotransport

### 3 Components of the System

#### 3.1 The Apparatus and overall Design Requirements

##### 3.1.1 Designs from Previous Work

The research group responsible for this project had drawn some process diagrams examples as ideas to how the dynamic *in-vitro*<sup>5</sup> model could be built. Their final result is presented in Figure 21 and was used as base for this thesis.

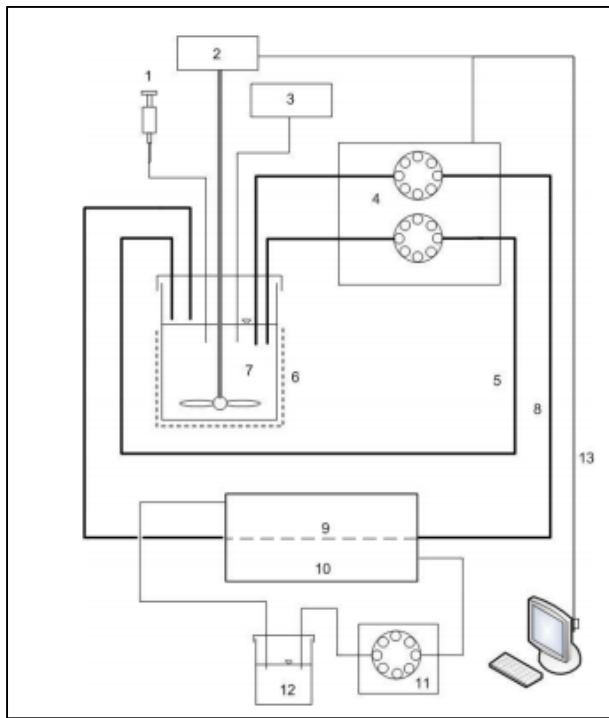


Figure 21: A process diagram of the full configuration of the dynamic *in-vitro* model that was the base for this project (Salas-Bringas et al. 2014).

Figure 21 is a process diagram of the basis for this project, used actively in the designing and building process of the apparatus. On the diagram, item 1 to 7 is representing the stomach and 8 to 12 is representing the small intestine. The syringe (item 1) is doing the mechanism of adding the gastric fluid to the stomach. The viscometer (item 2) mixes the digestive (item 7), at the same time as it measures the viscosity of the gastric fluids and the shear rate in the fluid during the digestion process. The titrator (item 3) adds different amounts of HCl depending on the buffering capacity of the food. The peristaltic pumps (item 4 and 11) replicates the peristaltic movements in the stomach and the small intestine. The pumps are connected to acid resistant hoses, and can pump continuously the gastric fluids (through item 5), the duodenal fluids (through item 8) and the buffer fluid (item 12). Item 6 is a jacket heater, which provides heat to the fluid of a stabile temperature of 37°C. The small intestine is represented by the porous media (item 9), immersed in the buffer volume inside a larger container (item 10). A computer is connected through item 13 to measure and control the viscometer and the peristaltic pumps (Salas-Bringas et al. 2014).

<sup>5</sup> *In-vitro* modelling is where the study of a biological phenomenon is done outside their normal biological context, in contrast to *in-vivo* studies which is done within its biological context (e.g. inside a human body).

### 3.1.2 Function

The main function of the apparatus is that it should simulate the digestive processes in the stomach and the small intestine, as a dynamic model.

Different factors needed to be considered when choosing the components that together would function as the digestive system. These factors are listed in Table 3.

Table 3: A summary of factors considered when choosing the components of the system and their significance.

Factors	Not significant	Significant	Crucial
User friendly		x	
Economy			x
Functionality			X
Appearance	x		
Cleanliness		x	
Delivery time			x
Volume limitations <sup>6</sup>			x

### 3.1.3 Design Requirements

The apparatus have several requirements to make the process through it, as similar to the real human digestive process as possible.

- ❖ Temperature
  - The temperature in the human gastrointestinal tract remains constant at 37°C (+/- 1°C). Since the behaviour of fluids is temperature-dependent, the apparatus has to be designed so that the temperature in the digestive content remains stable at 37°C (+/- 1°C).
- ❖ Viscosity
  - The system is required to continuously measure and report the viscosity of the digestive content.
- ❖ Volume
  - The total volume circulating in the apparatus cannot be more than 29 ml, which is the volume there is room for in the rheometer cup when all the tubes and the probe propeller is connected. This requirement directly affect the tube lengths and sizes, making the desired size of the whole apparatus, as small as possible.
- ❖ Fluid flow
  - The flow in the small intestine is turbulent despite the small velocity downstream. This is due to the peristalsis and segmentation movements of the wall. The turbulence contributes to the increased shear stress at the membrane wall and the membrane fluidity (Haidekker et al. 2000). However, in the artificial membrane where there is no contractions, the fluid velocity would have to be quite larger than in the real intestine to get a turbulent flow. The

<sup>6</sup> Volume limitations is due to the limited gastric and duodenal juice available, in addition to the limited room in the rheometer cup.

system is therefore required to be capable of controlling the fluid velocity, so that one can produce both turbulent and laminar flow.

- The volume requirement that result in the size limitation of the apparatus sets a new requirement regarding the fluid flow. The system is required to have a device that not only controls the fluid velocity, but also is capable of controlling three different fluid circuits.
- ❖ Transport of molecules
  - The system is required to provide the user an opportunity to withdraw samples from the small intestine device to measure the transport of molecules over the artificial membrane.

### 3.2 The Artificial Model of the Human Digestive System

Some parts of the human digestive system are not considered due to its complexity. The functions regarding the stomach and the small intestine that are not modelled in this thesis, as well as those that are modelled, are listed in Table 4.

Table 4: Functions of the human stomach and small intestine that are modelled and not modelled in the apparatus.

Function not modelled	Comments
Segmental contractions	Future possibility using some clamping device
Membrane wall with villus.	Future possibility using animal small intestine
The three parts of the small intestine and their separate functions	Future possibility
Function modelled	Device to simulate
Peristaltic movements	Peristaltic pump
Diffusion through membrane	Artificial membrane
Environment	Titration controlling the pH and heating container controlling the temperature

#### 3.2.1 The Peristaltic Pump

##### 3.2.1.1 Function

The peristaltic pump function as the systems circulation device. A peristaltic pump, as opposed to other types of pumps, is capable of mimicking the peristalsis movements of the stomach and the small intestine on some level.

##### 3.2.1.2 Requirements

Some of the requirements of the peristaltic pump are already discussed in the previous chapter. A summary of all the requirements considered choosing a pump, is listed in Table 5.

Table 5: Requirement considered choosing a pump for this project.

Requirement	Effect
Three channels	Economical- and space-efficient
Control channels separately	Flexible and reliable
Tube size compatible	Volume efficient
Adjustable flow rate	Flexible
Price	Within budget



## 3.2.1.3 Options

Table 6: Specifications for option 1.

Option 1	
Name	Reclo ICC
Supplier	VWR
Number channels	2-4
Separately channel control	Yes
Tube size i.d. range [mm]	0.13-3.17
Flow rate range [ml/min]	0.0002-35
Price	28 780 NOK



Figure 22: Reclo ICC.

Table 7: Specifications for option 3.

Option 2	
Name	MCP Standard (easy load)
Supplier	VWR
Number channels	1
Separately channel control	Not included
Tube size i.d. range [mm]	0.8-8.0
Flow rate range [ml/min]	0.066-1100
Price	32 875 NOK



Figure 23: MCP Standard pump with an easy-load pump-head.

Table 8: Specifications for option 4. \*The information is not available.

Option 3	
Name	LP-BT100-2J
Supplier	Houm
Number channels	1
Separately channel control	Not included
Tube size i.d. range [mm]	N/A*
Flow rate range [ml/min]	0.0002-380
Price	11 500 NOK



Figure 24: The LP-BT100-2J, a classical peristaltic pump.

Table 9: Specifications for option 5. \*The information is not available.

Option 4	
Name	LP-BT100-IL
Supplier	Houm
Number channels	Multiple
Separately channel control	No
Tube size i.d. range [mm]	N/A*
Flow rate range [ml/min]	0.0002-500
Price	N/A



Figure 25: The LP-BT100-IL.

### 3.2.1.4 Final Solution

Option 1 (Table 6) was the only option that met all the requirements and was therefore bought for this project. See Appendix A.

## 3.2.2 The Tubes

### 3.2.2.1 Function

The tubes function as the circulating device connected to the peristaltic pump.

### 3.2.2.2 Requirements

Table 10: Requirement of the tubes.

Requirement	Effect
Size 2-4 mm i.d.	Volume efficient
Autoclave-able	Easy to clean
Acid resistant material	Resistant to low pH in stomach fluid
Transparent material	Visual control

### 3.2.2.3 Options

One option was considered after choosing the peristaltic pump, from the same supplier as the pump. The Tygon 3350 tubes, with clamps, is compatible with the Reclo ICC pump. The material is platinum tempered silicon, with a smooth surface. It is highly elastic, biocompatible (compatible with food articles). It is resistant against ozone and UV, in addition to being autoclave-able.

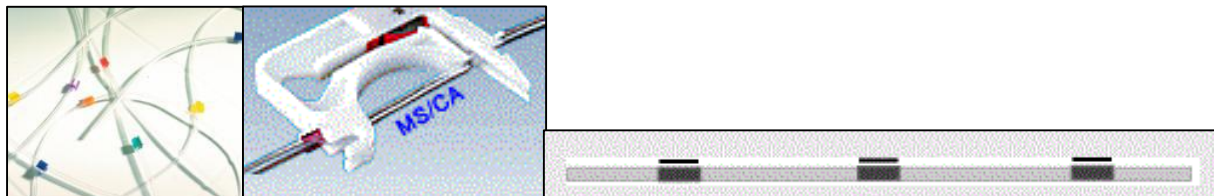


Figure 26: Example of tubes in different sizes in the same series (VWR 2014). They all have three stoppers (right picture) so that they fit in the cassette (middle picture).

### 3.2.2.4 Final Solution

Only one option was considered. Regarding the different tube sizes, final sizes were chosen after doing the preliminary test, presented in chapter 4.1.1. The VWR catalogue number for the tube size 2.54 mm i.d., is 224-2522<sup>7</sup>. The catalogue number for the 3.17 mm i.d. tubes is not available, since this ordering was done through a contact at VWR (see chapter 3.3.2).

Using these tubes, presents a new challenge regarding the lumps in the coagulated milk circulating in the stomach circuit. Since the tubes are only 400 mm long each, they are extended by extending plugs. These plugs have a narrower diameter than the tubes, increasing the possibility of the lumps to get stuck.

<sup>7</sup> 2.54mm i.d. was the tube-size that was ordered. However, the wrong tubes were sent (size 2.72 mm i.d.) Due to the similarity between the, the apparatus functioned with the wrong size, and the mistake was not noticed before the thesis was finished. New tubes were ordered at the end of the thesis-period.

### 3.2.3 The Small Intestine

#### 3.2.3.1 Function

The small intestine device (also referred to as the duodenum device) primary function is to simulate the upper part of the small intestine. A membrane is to be placed inside the device, where desired lipids/peptides etc. can diffuse from the digestive fluid to the buffer fluid.

Even though it is in the jejunum-part of the small intestine where most of the absorption of nutrients occurs, the duodenum is where the digestive enzymes is secreted and mixed with the chyme. Due to this, the NMBU-group in charge of this project decided to name this device for the duodenum. However, throughout this thesis, it is often referred to as the small intestine device, to avoid the confusion of its purpose.

#### 3.2.3.2 Requirements

Table 11: Requirements for the small intestine device.

Requirement	Effect
Max. 20 ml volume in membrane part	Volume efficient
Autoclave-able	Easy to clean
Removable membrane part	Flexible
Transparent material	Visual control

#### 3.2.3.3 Options

Table 12: Specifications for option 1.

Option 1	
Name	Tube-A-Lyzer
Supplier	Spectrum Labs
Available membrane sizes [kDa]	0.1-0.5, 3.5-5, 8-10, 20, 50, 100
Sample chamber volume [ml]	8-10 or 25-30
Removable membrane	No
Transparent material	Yes
Number of chambers	1 or 2
Price	1 058 NOK or 1 297 NOK



Figure 27: Tube-A-Lyzer with one chamber.

Table 13: Specifications for option 2.

Option 2	
Name	Hollow Fiber Dialysis Modules
Supplier	Spectrum Labs
Available membrane sizes [kDa]	10
Sample chamber volume [ml]	100-10 000+
Removable membrane	No
Transparent material	Yes
Number of chambers	3
Price	1 985 NOK

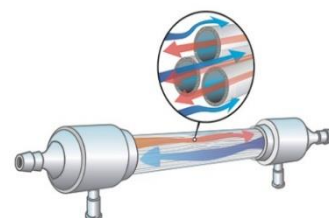


Figure 28: Hollow Fiber Dialysis Module.

Table 14: Specifications for option 3.

Option 3	
Name	American manufactured glassware
Supplier	Adams & Chittenden Scientific Glass
Available membrane sizes [kDa]	Flexible
Sample chamber volume [ml]	Flexible
Removable membrane	Yes
Transparent material	Yes
Number of chambers	Flexible
Price	1 024 NOK + shipping from USA

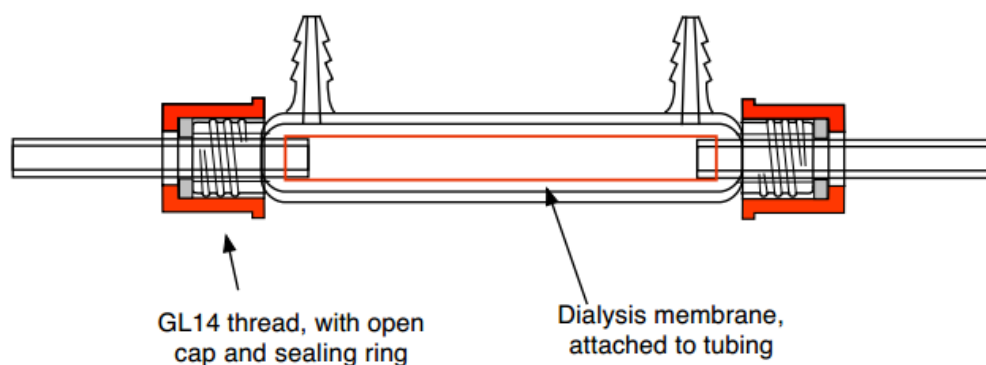


Figure 29: A simple sketch done by Adams &amp; Chittenden Scientific Glass, in the price-inquiry process.

Table 15: Specifications for option 4.

Option 4	
Name	Norwegian manufactured glassware
Supplier	Adams & Chittenden Scientific Glass
Available membrane sizes [kDa]	Flexible
Sample chamber volume [ml]	Flexible
Removable membrane	Yes
Transparent material	Yes
Number of chambers	Flexible
Price	610 NOK

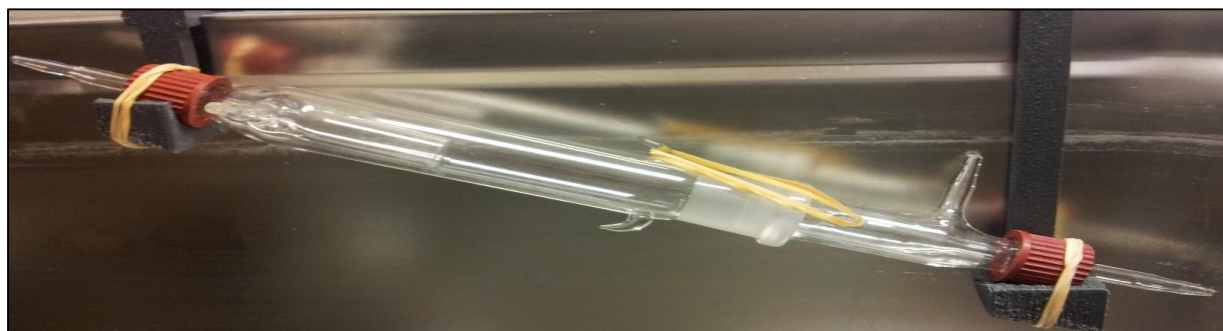


Figure 30: Manufactured glassware made of Stein Høydaahl at UiO, from the designs from this thesis.

### 3.2.3.4 Final Solution

Option 3 and 4 was both accepted solutions, due to their flexibility. However, option 4 was chosen due to the supplier's location. If anything breaks, it is easier replaced, than if the part needs to be shipped from another country.

The small intestine device is divided in four separate pieces, six counting the red lids at the ends (Figure 31). There is two outer ends (named buffer-tube) and two inner ends (named membrane-tube). The inner ends are identical. A simple guide of how to put the parts together with the membrane and the pump is presented in Appendix J.



Figure 31: Left: Short outer buffer tube with inserted inner membrane-tube. Middle: Long outer buffer tube. Right: Inner membrane tube, there is two identical in the system.

## 3.2.4 The Artificial Membrane

### 3.2.4.1 Function

The membrane is functioning as a porous wall where compositions like proteins and peptides diffuse from the digestive fluid to the buffer volume.

### 3.2.4.2 Requirements

Table 16: Requirements of the membrane. \*Internal diameter.

Requirement	Effect
The same i.d.* mm size is represented in several porosity sizes.	The small intestine device can be designed to one membrane size, and still give the possibility of different porosity sizes.
Transparent material	Visualization

### 3.2.4.3 Options and Final Solution

Due to the requirements, and the group's previous experience with products from spectrum labs, the standard RC (Regenerated Cellulose) membrane was chosen for the project. This is a ready-to-use membrane, equilibrated in water and packaged wet in 0.05% sodium azide solution<sup>8</sup>. See Appendix B for product specifications.

<sup>8</sup> The product should be stored cold in the refrigerator.

### 3.2.5 The Rheometer

#### 3.2.5.1 Function

The rheometer continuously measured the viscosity of the digestive composition. In addition to this prime function, the container (the rheometer cup) functions as the stomach compartment.

#### 3.2.5.2 Requirements

Table 17: Requirements for the rheometer.

Requirement	Effect
Interchangeable probe	Flexible
Able to measure low viscosity at different shear rate, like milk.	Flexible
Temperature control	Stable

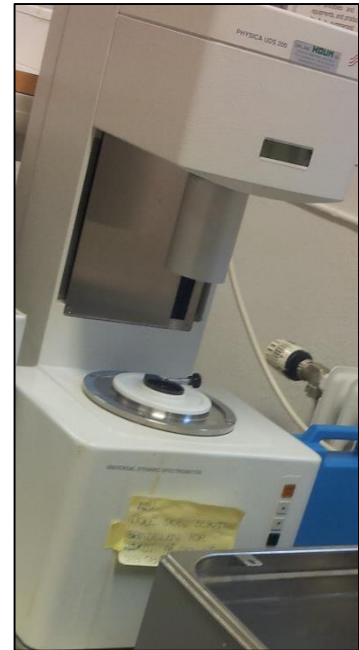


Figure 32: Anton Paar Physica UDS 200, the rheometer of choice.

#### 3.2.5.3 Options and Final Solution

There was only one option in this case. This was the Anton Paar Physica UDS 200 (Figure 32), which was already in IKBM's possession. The dimensions are presented in Appendix H.

##### 3.2.5.3.1 The Probe Propeller

The probe propeller is connected to the rheometer, producing a shear rate in the digestive liquid, which produces a shear stress in the rheometer cup. The model usually used in this particularly rheometer, is the EMKA600 probe, shown in Figure 33. However, for the case of this study, this probe is not suitable. The probe should be made in titanium, to resist the acidification from the digestive fluid with low pH. Due to the length of the titrator sensor, the probe should be much longer (dimensions are presented in Appendix C). The size of the propeller blades, and their design, also needs to be modified to match the limited room in the rheometer cup. None of these modifications are prioritized in this thesis, but they are important for future work.



Figure 33: Left: The probe sketched in SW (scanned in a 3D-scanner). Right: The EMKA600 model in its container.

### 3.2.5.3.2 The Rheometer Cup

There was two available models of the cup fitted to the rheometer; one was made in titanium and one in stainless steel. Due to the same reason as with the probe, the titanium cup were best suitable. The dimensions are presented in Appendix D.



Figure 34: The rheometer cup used in this apparatus.

### 3.2.6 The Heating Container

#### 3.2.6.1 Function

The heating container works like an incubator, keeping the temperature of the circuits steady at 37°C (+/- 1°C).

#### 3.2.6.2 Requirements

Table 18: Requirements for the heating container.

Requirement	Effect
Temperature control	Steady temperature
Enough volume to keep the small intestine immersed	Room for several components

#### 3.2.6.3 Options and Final Solution

IKBM was already in possession of a heating container (Figure 35), which met the requirements. The model is from Grant UK.



Figure 35: The heating container from Grant UK, used in this project. The peristaltic pump is placed beside the heating controller, saving room and volume of the entire apparatus.

### 3.2.7 The Titrator

#### 3.2.7.1 Function

The titrator, combined with a titration sensor, controls and regulates the pH level in the digestive fluid to the level corresponding to the system (stomach – low pH, intestine – neutral pH).

#### 3.2.7.2 Options and Final Solution

Prior to this thesis, the research group had already chosen the Compact Titrator G20 (Figure 36) with the DGi102-Mini titration sensor. The technical specifications are presented in Appendix G.



Figure 36: The Compact Titrator G20 on the left, with the titration sensor DGi102-Mini, used in this apparatus.



### 3.3 Building the Apparatus

#### 3.3.1 Step-by-Step Digestive Fluids

The mechanical steps of the dynamic simulation are described in chapter 2.3. The digestive composition starts as milk, and after several steps it ends up as a digested fluid nothing like the starting point. The steps are presented in Table 19.

Table 19: The composition of the digestive fluid in the apparatus, divided in four steps. \*Acid or base needed to calibrate the pH level to  $pH < 2$  is included in this volume.

Step	Added component	Volume [ml]	New total volume [ml]	pH	Time approximately before next step [min]	Comment
1	Milk	3.625	3.625	6-7	0	Mixed and pH measured outside the apparatus.
2	Saliva	3.625	7.250	6-7	0	
3	HGJ	7.250*	14.500	>2	30	All three components are mixed in the cup.
4	HDJ	14.500*	29.000	6-7	60	Added to the mix in the cup.

Figure 37 shows the steps as they fill up the rheometer cup. The different tubes and the titrator sensor are presented in the figure to give a perspective on the volume limitations in the cup.

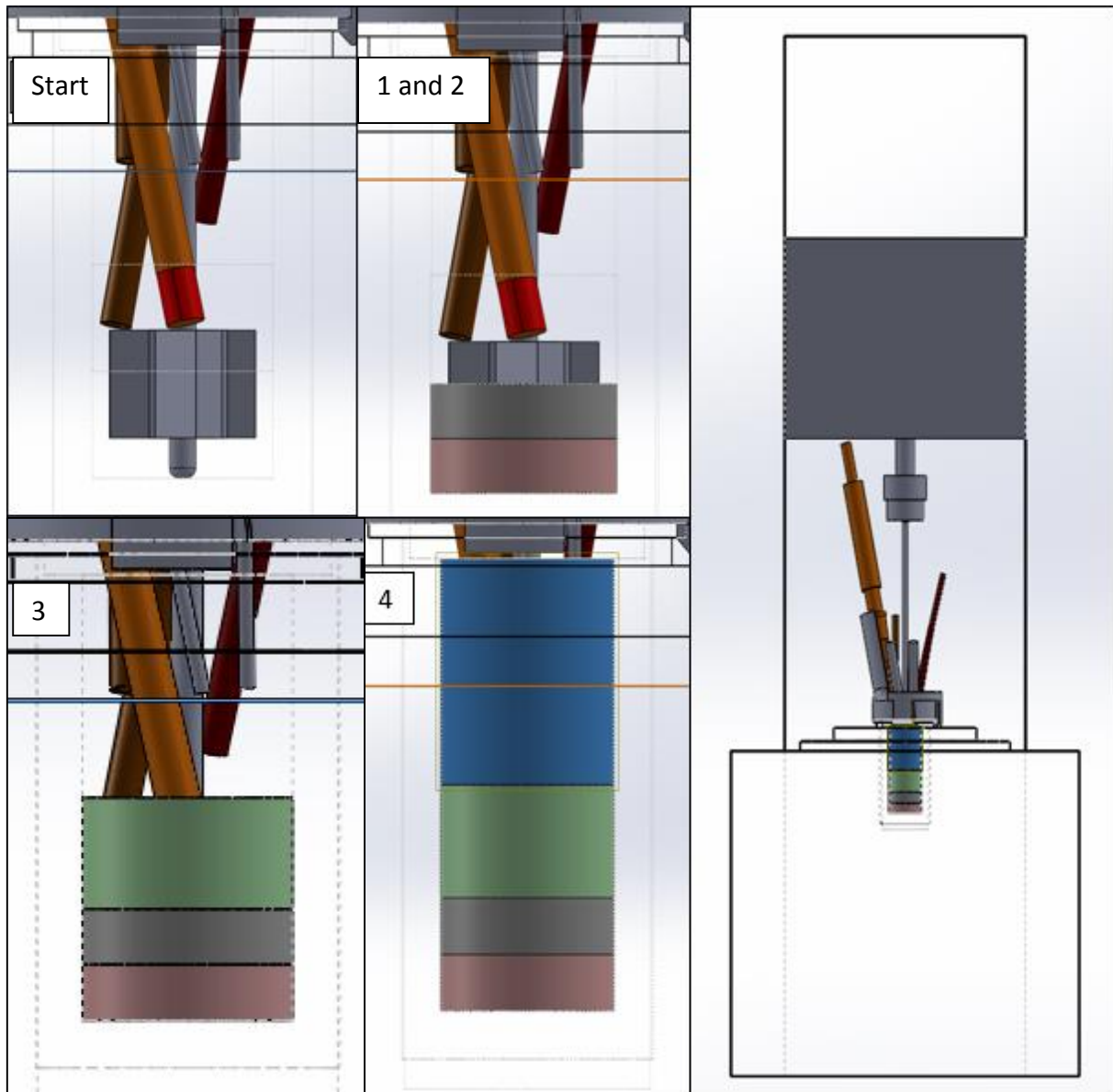


Figure 37: The steps through the simulated digestive process. After step 3, the fluid starts to circulate in the stomach circuit, emptying a part of the cup. After step 4 the fluid starts to circulate the small intestine circuit, emptying a part of the cup again. The orange cylinder with the red tip represents the titrator sensor, where the red tip has to be immersed in the fluid to be able to measure the pH value. This is the reason that step 1 and 2 is mixed and measured first outside the cup. The last picture on the right is the rheometer with the cup full.

## 3.3.2 The Total Apparatus

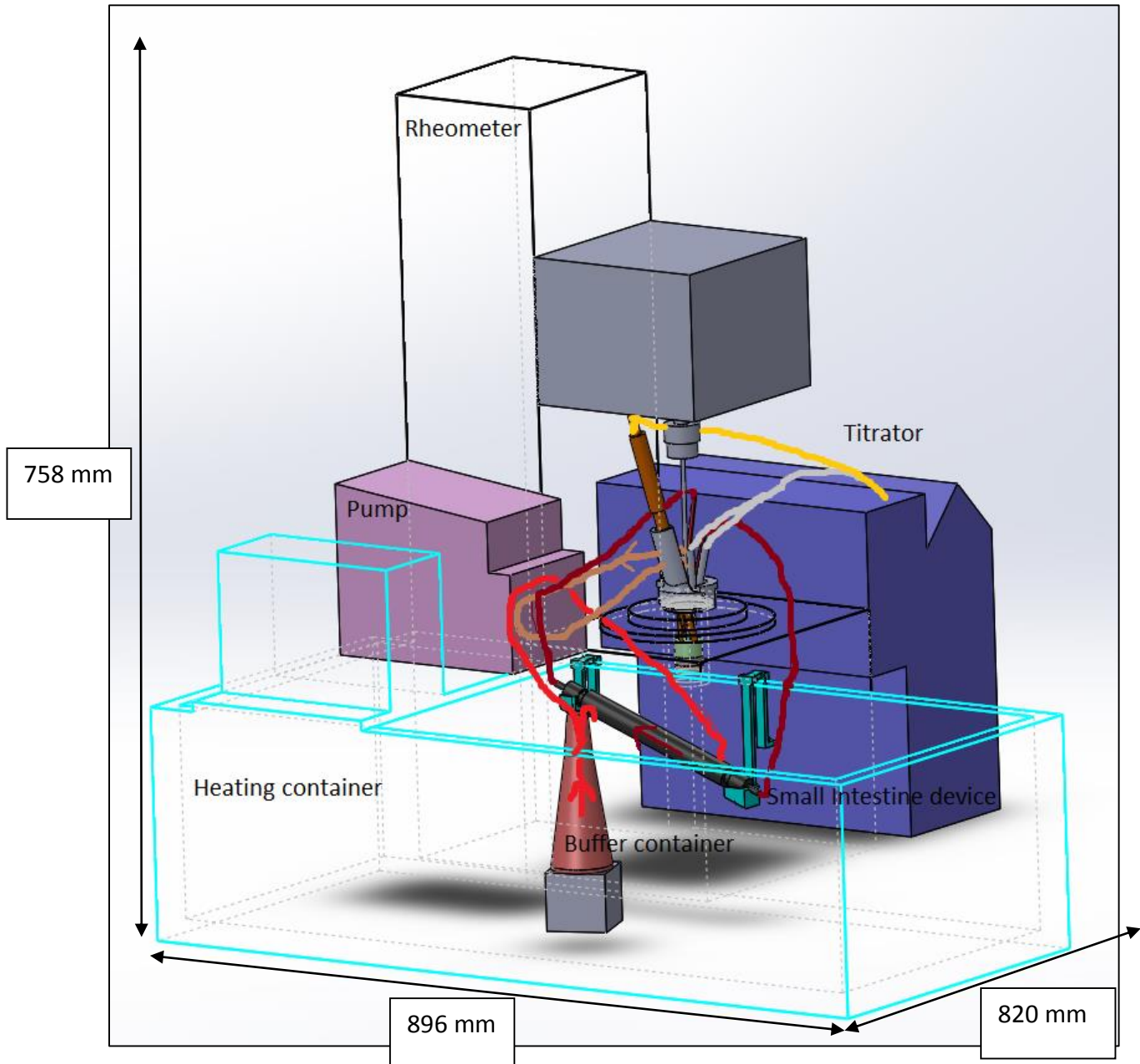


Figure 38: A sketch done in SW of the whole apparatus, with all the components described in chapter 1. Light brown circuit represents the stomach circuit. Dark red represents the small intestine circuit, with the light red as the buffer circuit.

Information about the suppliers and their contacts, for new components bought for this project, is listed in Table 20.

Table 20: Suppliers list.

Component	Supplier	Contact	Email	Mobile
Reclo ICC with tubes	VWR	Helle Juul Garder	<a href="mailto:helle.garder@no.vwr.com">helle.garder@no.vwr.com</a>	+47 47 35 14 43
The small intestine device	UiO	Stein Høydahl/ Terje	<a href="mailto:stein.hoydahl@uio.no">stein.hoydahl@uio.no</a>	+47 41 17 27 94/ +47 22 85 56 23

## 4 Experimental Work

### 4.1 Testing of Equipment

#### 4.1.1 Selection of Tubing Sizes

To select the tube sizes for the stomach-part of the apparatus, a simple experiment was done.

##### 4.1.1.1 Purpose

The purpose of this test was to see how the coagulated milk (milk with lowered pH), would behave in different tube sizes. A relative small tube size was preferable due to the volume limitations of the total system. However, when coagulated milk is circulating, one obstacle is that the lumps will get stuck and not pass through the tube. This was the main concern when choosing the tube sizes that would later be ordered from the supplier.

##### 4.1.1.2 Method

Three silicon tubes were tested, each with different tube size (i.d. 1.6, 3.2 and 8.0 mm). By using the peristaltic pump that was available (323U, Watson Marlow), borrowed from a lab at IKBM, coagulated milk was pumped through each tube. Notes were made on the tubes capability of keeping a continuous flow (no lumps blocking the passage), and capability of emptying itself (no lumps left stuck at the walls). The latter can occur if the tube size is too big compared to the small volume flow passing through, not causing enough force to push the lumps through the tube.



Figure 39: The method used for the selection of tubing size.

#### 4.1.1.3 Result

The results from this test is presented in Table 21. These notes were evaluated together with the concern of the volume limitations, and made the foundation for picking the tube size i.d. 3.17 mm for the “Stomach-circuit”.

In the small intestine-part of the apparatus, the issue of coagulated milk was almost non-existing, due to the pH increase in the fluid at that point. The only concern in this part was the strict volume limitations. Due to this, the smallest tube size available, and compatible with the peristaltic pump used in the apparatus, was chosen.

*Table 21: Results of the test with the coagulated milk pumped through the different tubes. The pump used for this test was a one-channel peristaltic pump, burrowed at IKBM.*

Tube size i.d. [mm]	Flow through	Lumps stuck	Concerns
1.6	No	Yes	No flow through, lumps stuck in the opening.
3.2	Yes	Minimal	Although most of the lumps got through, some stayed stuck to the tube wall, when trying to empty the tube.
8.0	Yes	No	Lumps stays stuck to the wall, the wetted perimeter was too small.

## 4.2 The Stomach

As mentioned previous in chapter 3, the cup in the rheometer is functioning as the stomach. The peristaltic pump will circulate the fluid through a tube, and the probe propeller from the rheometer will contribute to mix the content.

### 4.2.1 The Lid

From the cup (stomach and then the small intestine) to the peristaltic pump, a number of tubes are connected. Four different tubes are going inside the cup, in addition to the tubes injecting acid and base from the titrator and the titrator sensor. This sums up to no less than seven different items placed inside the cup. To keep everything in their strategic place, in addition to keeping room for the propeller, a lid for the cup was made.

#### 4.2.1.1 Purpose

The purpose of making the lid for the rheometer-cup was to make sure that all of the items, which were connected to the cup, were positioned where they could do their job without interfering with another item’s function.

#### 4.2.1.2 Prototyping and Final Design

Before the final product was finished, this process went through a number of prototypes. Designing the whole system in SW made it possible to continuously change details of the lid as more information and experience with the apparatus was learned. No less than 10 different examples were sketched. Figure 40 presents three of the best prototypes of the lid.

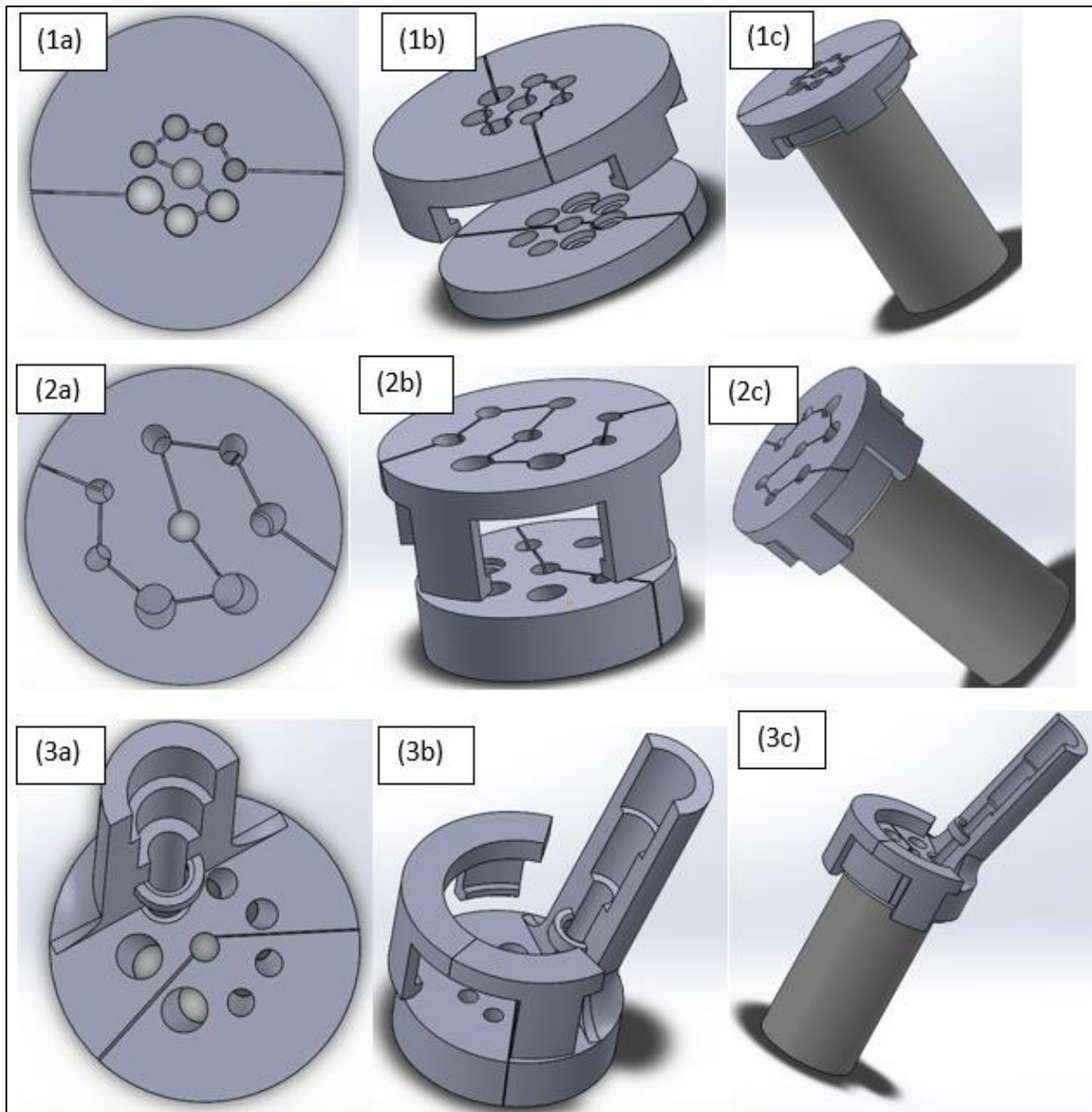


Figure 40: Development of the lids in the prototyping process. 1-3 presents the three of the best prototypes. Every example consists of four parts: two upper and two bottom lids. 1c, 2c and 3c presents the lids combined with the rheometer cup.

#### ❖ Prototype 1

- This prototype has rings carved out, 1.44 mm (90% of 1.6 mm) deep, around the holes for the silicon tubes. In the carvings, there is room for O-rings (thickness 1.6 mm diameter) that will tighten around the tubes, keeping them in place. Prototype nr 1 was printed, but after experiencing that the silicon tubes had no use for the O-Rings to be kept in place, the idea was dismissed.

#### ❖ Prototype 2

- In the second prototype presented here, one can still see a carving around one of the holes. The idea of O-rings was here considered to keep the titrator sensor in place. This prototype was not printed. The holes in this prototype is angled.

❖ Prototype 3

- Due to the weight of the titrator sensor support-fundament replaced the function of the O-ring, shown in 3a-c (Figure 40). This was the final prototype, and is not yet printed. The dimensions are given in Appendix E.
- The model is similar to prototype nr 9 which was printed (Figure 42), the only difference is adjusted dimensions for the titrator support.



Figure 42: The titrator sensor placed in one of the parts of prototype 9 of the lid. Prototype 9 is similar to prototype 10, which is presented in Figure 40.



Figure 41: The hose clamp around the first printed prototype. A screwdriver with a flat head is used to tighten the hose clamp.

A hose clamp (Figure 41) is used to tighten the lid around the cup in all the prototypes. An idea of using small screws to do the same was considered. However; considering the fact that this would produce smaller parts, making it more difficult to handle, the idea of screws was quickly rejected. The simplest solution is often the most user-friendly.

### 4.3 The Small Intestine

#### 4.3.1 Preliminary Studies – Flow Simulations

##### 4.3.1.1 Purpose

The part of the digestive system focused on in this thesis, is the small intestine and the device that will function as it. In the beginning of the process, the group<sup>1</sup> decided that a device functioning as a dialysis tube would be the best solution. The main challenge to consider while designing the device was that the flow would go from the narrow tube (i.d. 2,54 mm) into the wider membrane (i.d. 12,65 mm). This would cause some turbulence flow into the membrane (Figure 43), and the main considerations in the design was to limit this turbulence as much as possible, and still consider the volume limitations. To get a better characterization of the flow inside the membrane, laminar flow is preferable. This is despite the fact that turbulent flow will increase the shear stress at the membrane wall, which will increase the fluidity of particles through it. Different solutions were considered, however a simple cone-design was chosen (Figure 44).

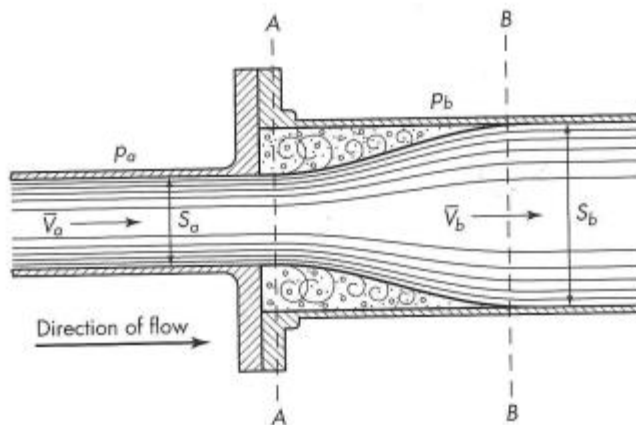


Figure 43: Simple sketch of eddies that should be avoided in the active membrane part of the small intestine device (McCabe et al. 2005).



Figure 44: Simple sketches of two different solutions to overcome the turbulence. The sketch to the left is a cone-solution, chosen for this thesis. The sketch in the middle and the right demonstrates the flow separated by pipes to minimize the turbulence.



#### 4.3.1.2 Flow Simulations

Flow simulations in SW (simulations of flowing water in the membrane tube) were done at different angles (Figure 46) and with different flow velocities. Table 22 presents the general settings and initial conditions for the flow simulation.

Table 22: General settings and initial conditions set in SW for the flow simulation with inlet volumetric flow 0.2 ml/s. Every setting is set at default.

General settings	
Analysis type	Internal
Heat conduction in solids	No
Radiation	No
Time-dependent	No
Gravity	No
Rotation	No
Fluids	
Fluids	Water (Liquids)
Wall conditions	
Wall thermal condition	Wall temperature
Roughness	0 $\mu\text{m}$
Initial conditions	
Parameter Definition	User Defined
Thermodynamic pressure	101325 Pa
Temperature	293.2 K
Velocity parameters	0 m/s
Turbulence length	0.0001365 m
Turbulence intensity	2 %

Table 23 presents every scenario tested and its results. Figure 45 shows distance between drawn lines in the wider cylinder, which gave a XY-plot of the results after the simulations were finished running.

Figure 47 presents an example of this XY-plot. When using these plots, it was possible to evaluate the fluids entry length in the membrane. This could also be calculated, using Equation 15.

The scenario that resulted in the shortest entry length, gave the dimensions for the tube connecting the hose and membrane, to prevent turbulent flow through the membrane part. Figure 48 presents an example of a cut-plot done of the flow trajectories in one of the simulations.

Table 23: Results from the flow simulations. Highlighted in yellow is the solution with the best result. \*See Figure 46. \*\*Represents the entry length.

Inlet velocity [ml/s]	Angle [degrees]*	Laminar flow at distance [mm]**
5	25	>80
5	35	>80
5	45	70
2	25	80
2	35	70
2	45	55
2	55	50
2	65	50
2	75	40
2	85	50
0,35	45	40
0,2	15	30
0,2	25	35
0,2	35	40
0,2	45	43

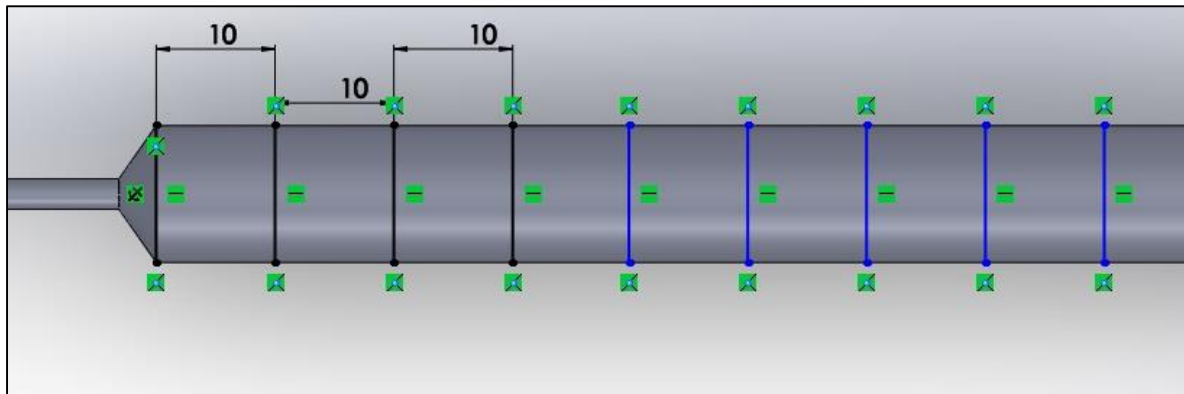


Figure 45: Lines used for plotting the result from the flow simulations in XY-plots, and the gap between them.

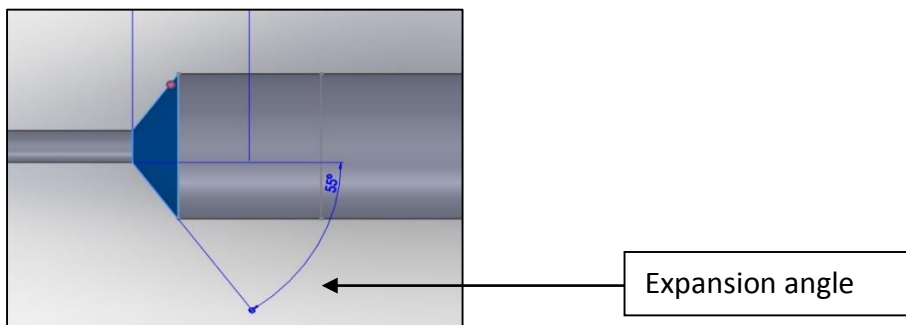


Figure 46: Sketch done in SW of the inner small intestine part used for flow simulations. Flow simulations were done at different angles (Table 23).

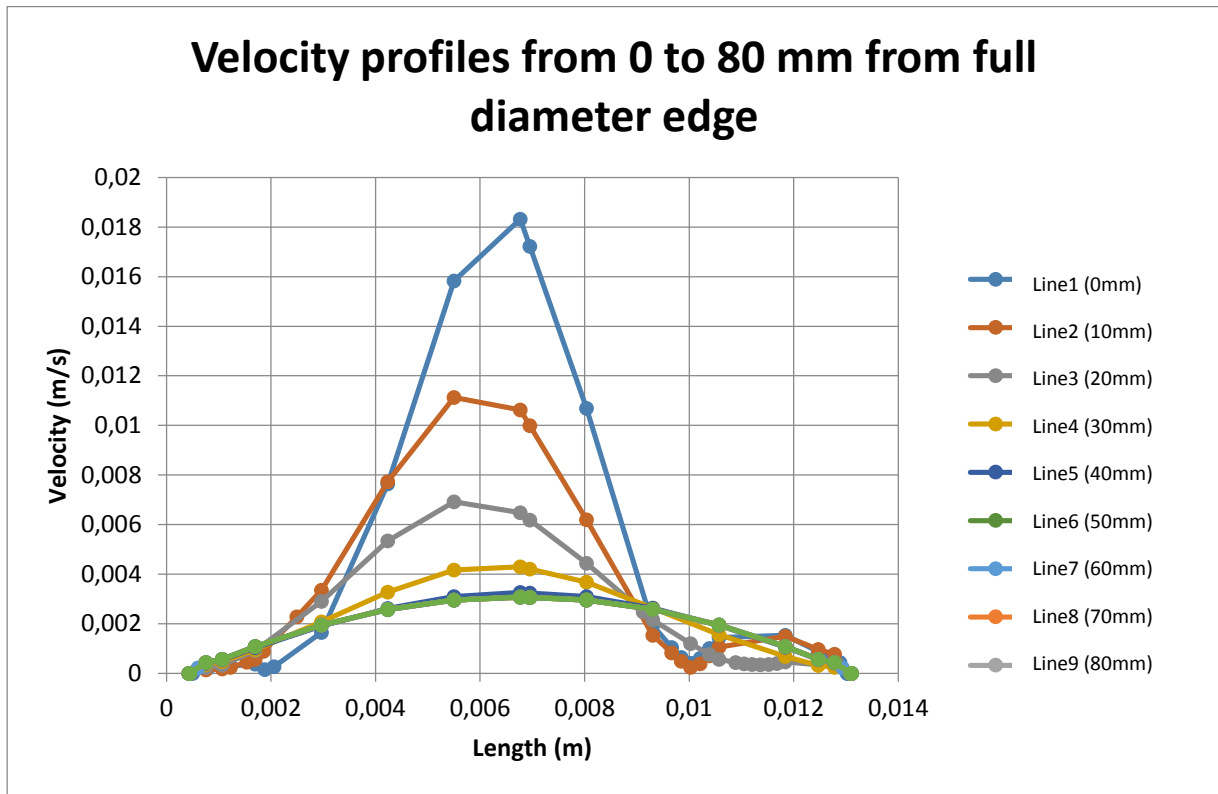


Figure 47: XY-Plot of the best solution found with the simulations, where the expansion angle is  $15^\circ$  and the inlet volume flow is 0.2 ml/s. The liquid was water in the simulations, which is Newtonian. The lines from the top to bottom goes from 0 mm and to 80 mm distance from the inlet of the wider cylinder. Line4 (30 mm distance) marks where the flow becomes laminar (the entry length). These dimensions resulted in the shortest entry length among the scenarios in this particular test. The unsymmetrical curved lines (0-20 mm lines) is due to the turbulent flow.

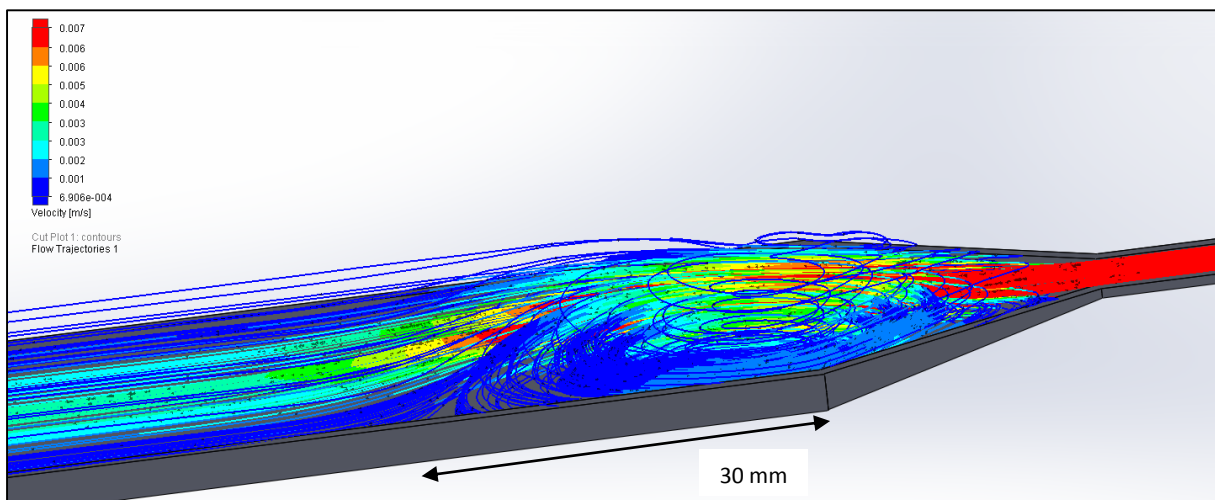


Figure 48: A flow trajectories plot of the simulation giving the best conditions for laminar flow in the membrane region (Table 23). The flow through the tube has an inlet velocity of 0.2 ml/s and an expansion angle of 15 degrees. This plot demonstrates the cross between turbulent and laminar flow in the tube. The flow projectors are 250 lines with arrows, and the sketch is of the inner small intestine tube.

#### 4.3.1.2.1 Calculation of the Theoretical Entry Length

The theoretical entry length is calculated, using the equation from chapter 2.1.2.6. It is assumed that the flow behaviour index is  $n = 0.4$  and the Reynolds number is  $Re < 53.2$  (Salas-Bringas et al. 2009).

$$L_e = \left[ \left[ (0.246n^2 - 0.675n + 1.03)^{1.6} + (0.0567Re)^{1.6} \right]^{1/1.6} \right] D$$

$$L_e = \left[ \left[ (0.246(0.4)^2 - 0.675(0.4) + 1.03)^{1.6} + (0.0567(53.2))^{1.6} \right]^{1/1.6} \right] 12.65 \text{ mm}$$

$$= \left[ \left[ 0.69886 + 5.85048 \right]^{1/1.6} \right] 12.65 \text{ mm} = 40.95 \text{ mm}$$

The theoretical entry length is calculated to be 40.95 mm for a power law fluid. This is almost 11 mm longer than the results from the flow simulations suggested. However, in the flow simulations, the fluid was water, which as a Newtonian fluid ( $n = 1$ ) have a different behaviour than a power law fluid ( $n < 1$ ). One should also consider the difference in the pressure distribution in the pipe, due to the angled elevation of the small intestine device. With all this considered, an entry length of 30 mm is a qualified estimate.

#### 4.3.1.3 Final Design

Based on the results from the flow simulations and ideas from dialysis tubes on the marked, the designing part could start. A simple sketch (Figure 49) with the wanted dimensions for the small intestine device was made for Stein Høydahl at UiO. He used this sketch to make the tubing in glass and the finished product is shown in Figure 30.

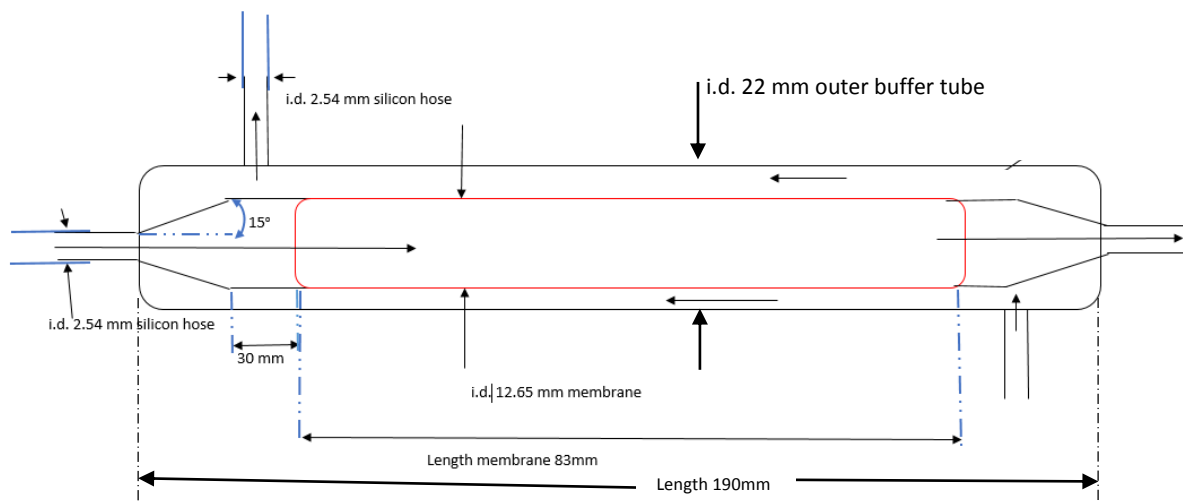


Figure 49: Sketch of the wanted dimensions for the small intestine tube, sent to Høydahl at UiO.

## 4.3.2 Functionality Test of the Small Intestine Device

### 4.3.2.1 Purpose

With the membrane and the small intestine-parts all put together, a test with water flowing through was done. The purpose of this test was to check for leakages, and determine the best solution to hold the membrane stuck to the tube. The membrane became slippery when it was immersed in liquid, and had a tendency of slipping off the glass tube.

### 4.3.2.2 Method

The small intestine system was fully connected to the peristaltic pump, with water flowing in both the circuits (small intestine- and buffer-circuit).

As mentioned previous in chapter 1, the flow velocity in a human small intestine with a 0.03 m diameter, is approximately  $1.667 \cdot 10^{-4} \text{m/s}$ . However, due to the complexity of the intestinal wall movements and structure of villi, the real flow is not possible to simulate in the apparatus as it is.

The flow rate in both the circuits (co-current) is therefore set to 0.2 ml/s, which corresponds to the flow rate from the flow simulations in SW.

### 4.3.2.3 Result

#### 4.3.2.3.1 Calculations of the Flow through the Artificial Membrane

Using the equation of continuity (Equation 2), the flow velocity of water through the artificial membrane was calculated. The volumetric flow rate in the tube connected to the peristaltic pump and the inner membrane-end, is the same as the flow rate in the expanded artificial membrane.

$$V_2 = \frac{A_1 u_1}{A_2} = \frac{(5.07 \times 10^{-6} \text{m}^2)(0.03947 \text{m/s})}{1.26 \times 10^{-4} \text{m}^2} = 0.00159 \text{m/s}$$

Table 24: The flow velocity ( $u_2$ ) in the artificial membrane is calculated to be 0.00159 m/s, in an ideal pipe flow. The flow velocity at the inlet is the same as in the previous flow simulations (0.2 ml/s).

	Parameter	Value	Unit
Inner membrane end cross sectional area	$A_1$	$5.07 \cdot 10^{-6}$	$\text{m}^2$
Membrane cross sectional area	$A_2$	$1.26 \cdot 10^{-4}$	$\text{m}^2$
Tube flow velocity	$u_1$	0.03947	m/s
Membrane flow velocity	$u_2$	0.00159	m/s
Volumetric flow rate	Q	0.2	ml/s

#### 4.3.2.3.2 Membrane vs. Slippery Glassware

When immersed in liquid, the membrane expands with 10%, in addition to getting very slippery. The glass material also gets very slippery when immersed in liquid. Some simple tests were done to see what might be the best solution to hold the membrane in place and prevent leakages.

##### 4.3.2.3.2.1 Without any Bands to hold the Membrane

The pros of this solution is simple that it is more efficient to not include any more parts. In the beginning of the test, there was no leakages. However, when the peristaltic pump empties the membrane, with the force this creates, it pulls the membrane of the glass.

##### 4.3.2.3.2.2 O-Rings (i.d. 11.5 mm)

The O-rings are made of a strong material (nitrile) that will not break, nor will it expand. However, the thickness (1.6 mm) of this O-ring will interfere with the flow of the buffer liquid due to a narrow outer end-tube (Figure 50). It also slipped of the membrane in this test, which makes it unsuitable for as a solution.

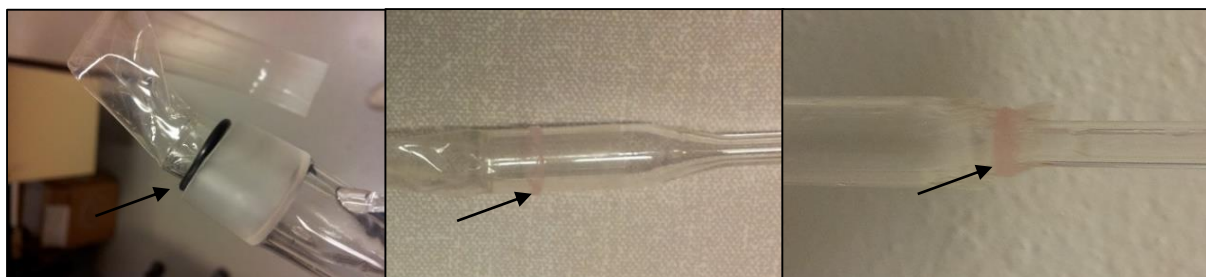


Figure 50: Left: Due to the thickness of the O-ring, it will cut of the buffer liquids flow outside the membrane. Middle: small rubber bands on the wide tip. Right: Small rubber bands on the narrow tip.

##### 4.3.2.3.2.3 Small Rubber Bands (i.d. 13 mm) at the Wider Tip

These rubber bands are elastic enough to go around the wider end of the tube, and still be thin enough for no interference with the buffer liquids flow. However, the band is not strong enough to keep the membrane from slipping of the tube, nor is its elasticity as long lasting as the O-rings.

##### 4.3.2.3.2.4 Small Rubber Bands (i.d. 13 mm) at the Narrow Tip

The same rubber bands described in chapter 4.3.2.3.2.3. Their function to keep the membrane from slipping of the glass is better using this method. However, the membrane-folds this method creates within the band, makes the contact between the membrane and the glass not complete. A consequence of this is that leakages occurred, after the membrane had been immersed in fluid for 30 minutes.

## 4.3.2.3.2.5 Summary of Membrane vs. Slippery Glassware

No accepted solution was found to this problem during this thesis. One possible solution is to change the design of the small intestine device to a solution where the roughness of the white part of the outer buffer-ends (Figure 51) is utilized. This material can be added to the wall on the part of the inner membrane-ends that are in contact with the membrane, making it less slippery.

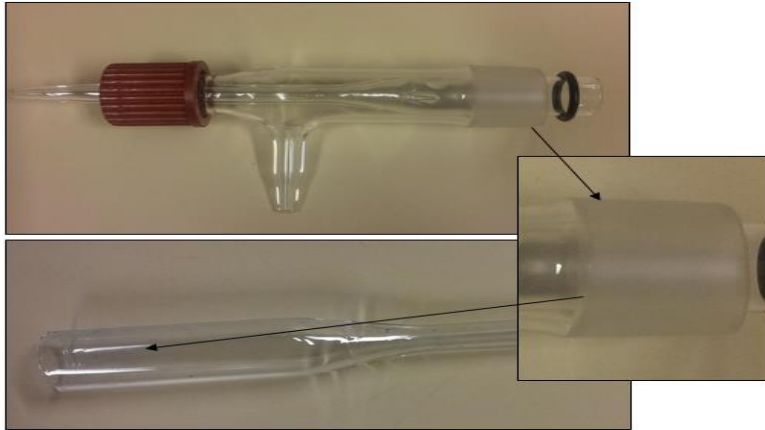


Figure 51: Idea for solution of the problem with the slippery membrane.

## 4.3.3 Optimization

The first thing noticed in the test was that due to the low velocity in the wider membrane part, an air bobble appeared at the roof of the membrane, covering the entire length. This air bobble stayed in the membrane as long as the device was vertically balanced (Figure 52).

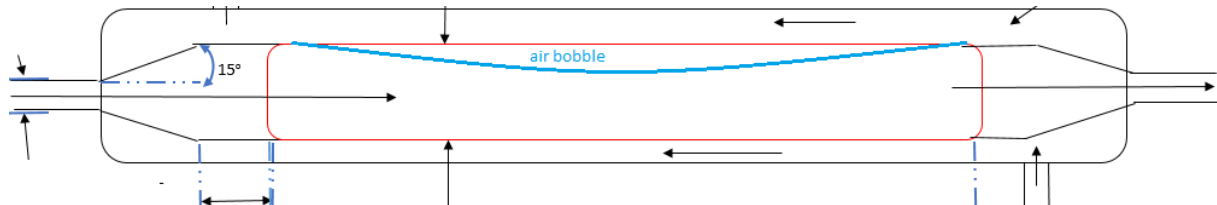


Figure 52: Simple sketch showing the air bobble in the membrane.

By elevating the outlet end, by at least 10 degrees, the air bobble went out the tube due to gravity (air has a smaller density than water, and most other liquids). The new solution is shown in Figure 53 where two new devices (dimensions presented in Appendix F) was designed in SW and 3D-printed to help hold the small intestine device in place.

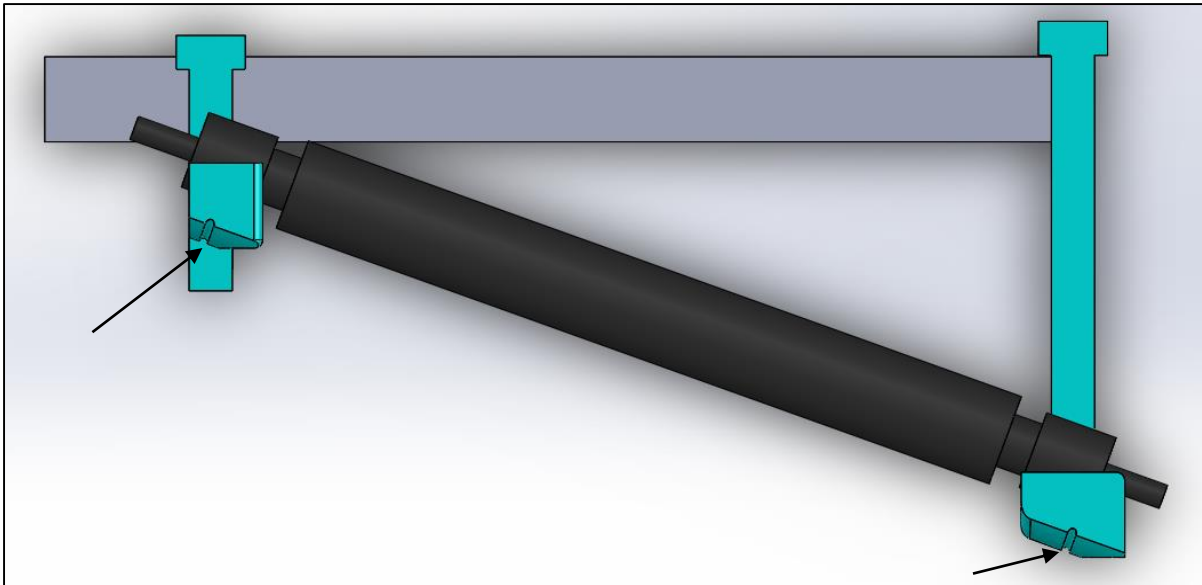
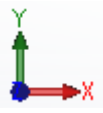


Figure 53: The new devices printed are painted in turquoise, with a simple sketch of the small intestine device in black. The outlet end is elevated with 15 degrees, avoiding the air bobble developing. The narrow gap (see where the arrows are pointing) is added to the design for the use of a rubber band to keep the devices attached to each other.

#### 4.3.3.1 Simulations Considering Gravity

Table 25: General settings and initial conditions set in SW for the flow simulation with inlet volumetric flow 0.2 ml/s. Every setting, except the gravity, is the default setting. The gravity setting is set so the elevation is in a 15° angle as in the apparatus.

General settings		
Analysis type		Internal
Heat conduction in solids		No
Radiation		No
Time-dependent		No
Gravity 	X component	$2.53901583 \text{ m/s}^2 \left( \sin 15 \times 9.81 \frac{\text{m}}{\text{s}^2} \right)$
	Y component	$-9.47573236 \text{ m/s}^2 \left( \cos 15 \times \left( -9.81 \frac{\text{m}}{\text{s}^2} \right) \right)$
	Z component	$0 \text{ m/s}^2$
Rotation		No
Fluids		
Fluids		Water (Liquids)
Wall conditions		
Wall thermal condition		Wall temperature
Roughness		0 $\mu\text{m}$
Initial conditions		
Parameter Definition		User Defined
Thermodynamic pressure		101325 Pa
Temperature		293.2 K
Velocity parameters		0 m/s
Turbulence length		0.0001365 m
Turbulence intensity		2 %



#### 4.3.3.1.1 Pressure Cut-plot

After adjusting the angle of the small intestine device, with the new holders, a new flow simulation was done, which is used as a starting point for future improvements of the design. In the new flow simulation, gravity was considered due to the angled elevation (Figure 54).

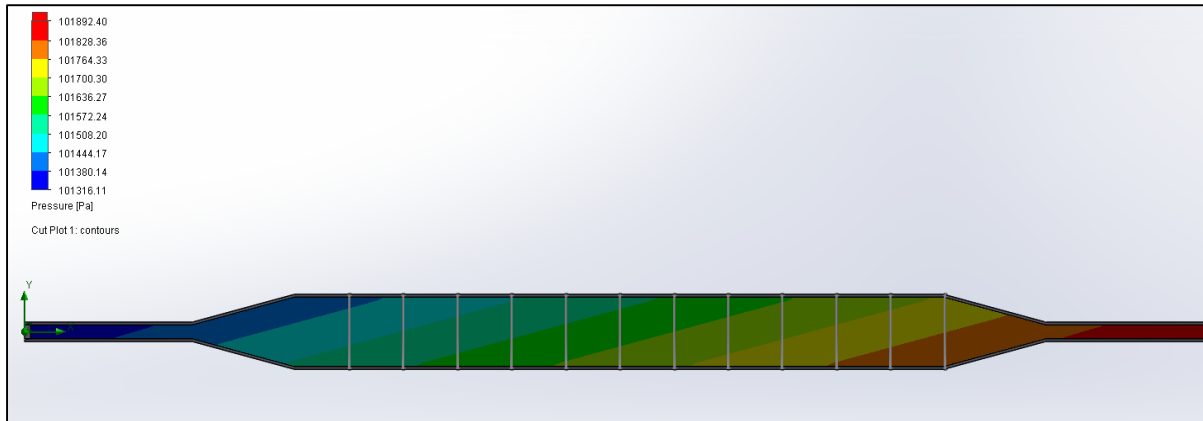


Figure 54: A static pressure cut plot of flow simulation where the inlet volume flow (right inlet) was 0.2ml/s. The pressure scale starts at blue (low) and continues to red (high). The plot shows that the pressure is highest at the bottom, and angled related to the angle (15°) the inner small intestine device is elevated.

##### 4.3.3.1.1.1 Shear Stress at the Membrane Wall

$$\tau_{wall} = \frac{((\Delta P_{Measured})R)}{(2l)}$$

$$\tau_{wall} = \frac{((126.1 Pa) \times 0.01265m)}{(2 \times 0.050m)} = 15.95 Pa$$

The shear stress at the artificial membrane wall is calculated to be 15.95 Pa. This is when the fluid is water which, as mentioned earlier, has very different flow behaviour than milk (or digestive fluids in general). One can assume that shear stress at the wall will be higher when the fluids is non-Newtonian ( $n \neq 1$ ).

#### 4.3.3.2 Particle Study

Based on the results from the first flow simulations, a particle study was done with water particles in water. With a particle study, one can easier see the distribution of the fluid in the tube. The result is presented in Figure 55, and it presents a new possibility for a better design of the small intestine device. A new and improved design is presented in Appendix I.

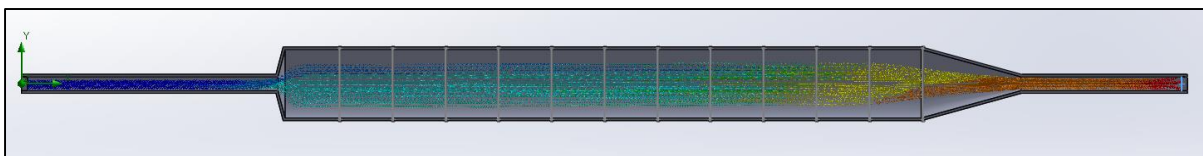


Figure 55: Particle study shows the distribution when 250 water-particles is flowing from the inlet (right end). The dimensions of the small intestine is in this picture adjusted, to fit the distribution better. This is a proposal for future improvements to the design; the sketch is presented in Appendix I.

#### 4.3.3.3 Flow Simulations with Updated Information

A second round of flow simulations were done to simulate the effect of lowering the velocity below the values tested in chapter 4.3.1.

##### 4.3.3.3.1 Calculations to Connect the Velocity in the Human Intestine to the Artificial Membrane

The continuity equation (Equation 1) is used to find a new inlet velocity ( $u_3$ ) that is more realistic than the one used in the previous velocities. The calculations are based on the information regarding fluid characteristics of the human small intestine, mentioned previous in chapter 2.3. Table 26 presents the result.

Table 26: The parameters used to calculate the new inlet velocity ( $u_3$ ) in the narrow tube (right end in Figure 34), for a more realistic flow velocity through the membrane. The volumetric flow rate is based on information given in chapter 2.3.

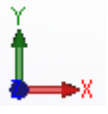
	Parameter	Value	Unit
Human small intestine cross section area	$A_1$	$7.069 \cdot 10^{-4}$	$m^2$
Human small intestine flow velocity	$u_1$	$1.667 \cdot 10^{-4}$	m/s
Artificial membrane cross sectional area	$A_2$	$1.257 \cdot 10^{-4}$	$m^2$
Artificial membrane flow velocity	$u_2$	$9.374 \cdot 10^{-4}$	m/s
Tube inlet cross sectional area	$A_3$	$5.067 \cdot 10^{-6}$	$m^2$
<i>Tube inlet flow velocity</i>	$u_3$	$2.325 \cdot 10^{-2}$	m/s
Volumetric flow rate	Q	0.1178	ml/s

##### 4.3.3.3.2 Flow Simulation Giving a Shorter Entry Length

Based on the calculations in the previous chapter, a new flow simulation was done, similar to the ones done in chapter 4.3.1. The only difference was lowering the inlet volumetric flow rate from 0.2 ml/s to 0.1178 ml/s. The new result is shown in Figure 57 as a XY-plot demonstrating the new entry length, and in a flow trajectories plot (Figure 56) demonstrating the cross between turbulent and laminar flow.

Table 27 presents the general settings and initial condition for this simulation.

Table 27: General settings and initial conditions set in SW for the flow simulation with inlet volumetric flow 0.1178 ml/s. Every setting, except the gravity, is the default setting. The gravity setting is set so the elevation is in a 15° angle as in the apparatus.

General settings		
Analysis type		Internal
Heat conduction in solids		No
Radiation		No
Time-dependent		No
Gravity 	X component	$2.53901583 \text{ m/s}^2 \left( \sin 15 \times 9.81 \frac{\text{m}}{\text{s}^2} \right)$
	Y component	$-9.47573236 \text{ m/s}^2 \left( \cos 15 \times \left( -9.81 \frac{\text{m}}{\text{s}^2} \right) \right)$
	Z component	0 m/s <sup>2</sup>
Rotation		No
Fluids		
Fluids		Water (Liquids)
Wall conditions		
Wall thermal condition		Wall temperature
Roughness		0 μm
Initial conditions		
Parameter Definition		User Defined
Thermodynamic pressure		101325 Pa
Temperature		293.2 K
Velocity parameters		0 m/s
Turbulence length		0.0001365 m
Turbulence intensity		2 %

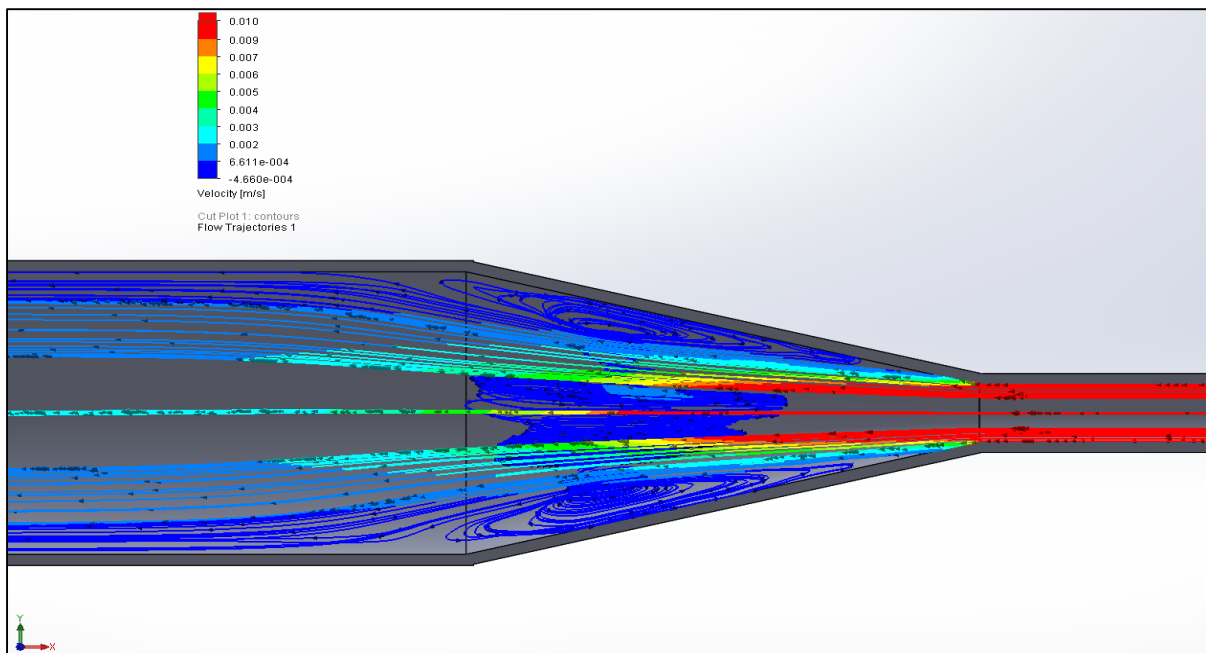


Figure 56: A flow trajectories plot of the simulation done in SW with an inlet volumetric flow at 0.1178 ml/s, and an expansion at 15°. The plot demonstrates the transition between turbulent and laminar flow, showing less turbulence than the previous simulation (Figure 48). The flow projectors are 250 lines with arrows.

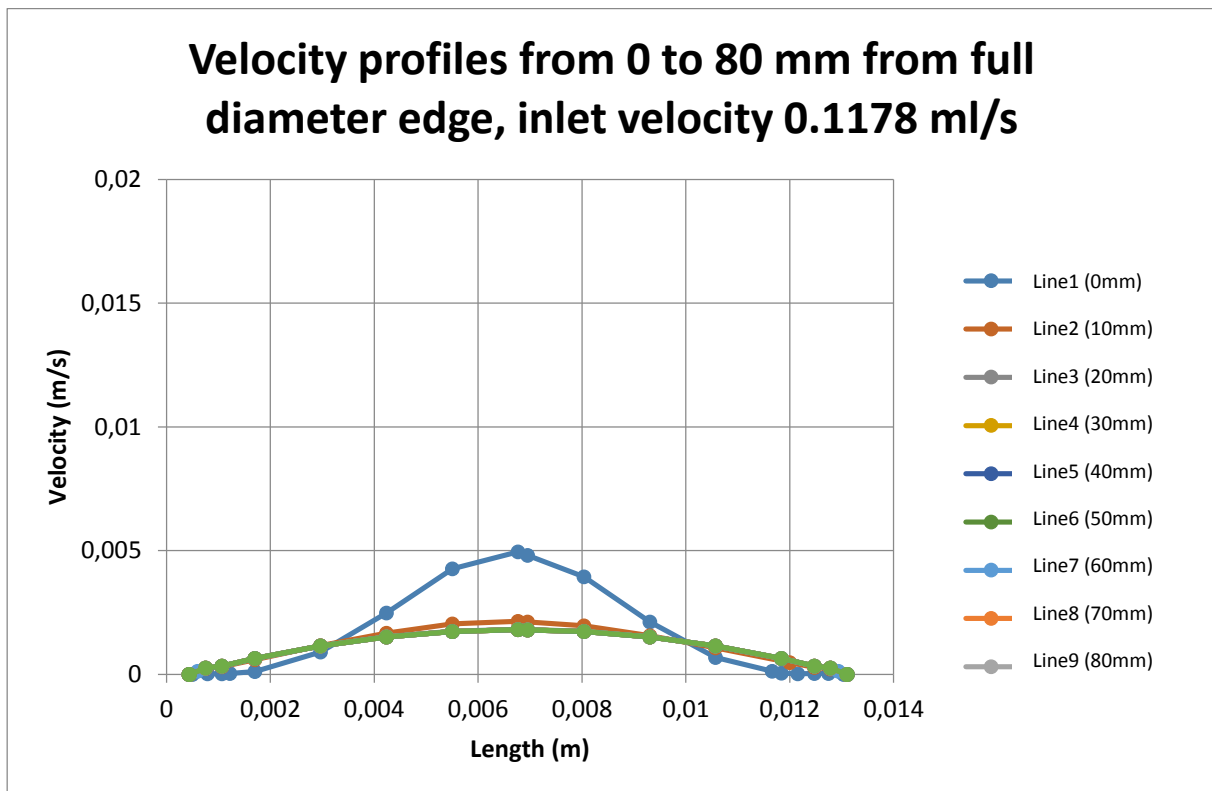


Figure 57: XY-Plot of second simulation, where the expansion angle is  $15^\circ$  and the inlet volume flow is 0.1178 ml/s. The liquid was water in the simulations, which is Newtonian. The lines from the top to bottom goes from 0 mm and to 80 mm distance from the inlet of the wider cylinder. Line2 (10 mm distance) marks where the flow becomes laminar (the entry length). The unsymmetrical curved lines (0mm line – line1) is due to the turbulent flow.

The simulations (Figure 56 and Figure 57), resulted in a shorter entry length than in the first simulations (chapter 4.3.1). A new sketch with new dimensions for the small intestine part was done, based on this result combined with the results from the particle study. The new dimensions decreases the volume, which is a positive effect on the initial volume limitation. The sketch is presented in Appendix I.

#### 4.3.4 Permeability Test

##### 4.3.4.1 Purpose

The purpose of these laboratory tests, was to measure and visualize the permeability of the membranes.

##### 4.3.4.2 Method

The membrane available for test had a cut-off size of 3.5 kDa. Table 28 gives the molecular sizes of the two colorants used. With the knowledge, these assumptions were made; Evan's Blue would diffuse through the membrane and Myoglobin would not. Both dynamic and static flow was tested. Samples was taken from the buffer fluid and sent to IKBM for a full spectrum spectroscopy analysis, to check if there was any diffusion.

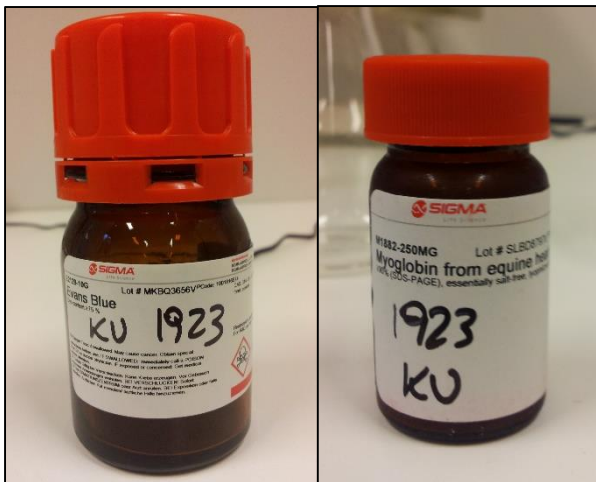


Figure 58: Left: Evan's Blue colorant. Right: Myoglobin colorant.

Table 28: Sizes of the two colorants used in this test. The membrane cut-off size was 3.5 kDa.

Colorant	kDa
Evans Blue	0.96081
Myoglobin from equine heart	16.95149 (Zaia et al. 1992)

##### 4.3.4.2.1 Dynamic

The dialysis flow rate was 0.2 ml/s due to the flow simulations in SW from the preliminary studies of the small intestine, where the optimal flow was 0.2 ml/s.

The dynamic test was divided in three parts, every part with its own assumption.

Table 29: Purposes of the different tests was to measure and visualize there three different events, based on these assumptions.

Test	What	Assumption
1	Myoglobin	No diffusion
2	Evan's Blue	Diffusion
3	Mixed	Diffusion of blue

Photos (Figure 56) and samples for spectroscopy documented every test. The samples from a buffer volume of 150 mL water continuously circulating, was taken with a time interval to see the development (Table 30).

Table 30: The time interval between every sample sent for spectroscopy.

Product	Sample ID	Time interval [min]
Myoglobin	1	5
Myoglobin	2	10
Myoglobin	3	15
Myoglobin	4	25
Sample from Myoglobin liquid	5	-
Evan's Blue	6	5
Evan's Blue	7	10
Evan's Blue	8	15
Evan's Blue	9	25
Sample from Evans Blue liquid	10	-
Mixed	11	5
Mixed	12	10
Mixed	13	15
Mixed	14	25
Sample from mixed liquid	15	-

#### 4.3.4.2.2 Static

In this test, the conditions were static. Only solution of Evan's Blue was sent through the inner circuit. The time interval between the samples are presented in Table 31.

Table 31: The time interval between the samples in the static permeability test.

Sample ID	Time Interval [min]
1	0
2	5
3	10
4	15
5	20
6	25
7	30

#### 4.3.4.3 Result

Neither the dynamic nor the static test showed any diffusion.



Figure 59: Above: The dynamic permeability test through the membrane where the colorant Evan's Blue was used. Bottom left: The static permeability test with Evan's Blue. Bottom right: Leakage after two hours of dynamic flow.

## 4.4 Fluid Calculations

### 4.4.1 Reynolds Number

In order to use Equation 9 to calculate the Reynolds number of the fluid, some conditions and fluid properties (Appendix L) are collected. The conditions and properties that are relevant for this system are listed in Table 32.

Table 32: Parameters used to calculate the Reynolds number (Fellows 2009)

Fluid	D [m]	v [m/s]	$\rho$ [kg/m <sup>3</sup> ]	$\mu$ [N·s/m <sup>2</sup> ] <sup>9</sup>
Water	0.01265	0.0395 <sup>10</sup>	1000	1.79·10 <sup>-3</sup>
Whole milk	0.01265	0.2325	1030	2.12·10 <sup>-3</sup>

#### 4.4.1.1 Water

In both the flow simulations and the permeability tests, the fluid flowing through the membrane was water. The water's Reynolds number during these tests is calculated below.

$$Re = \frac{D\bar{V}\rho}{\mu} = \frac{0.01265m \times 0.0395m/s \times 1000kg/m^3}{0.00179Ns/m^2} = 279.15$$

The Reynolds number estimates that the flow inside the artificial membrane is in the laminar region, which is the same results as the flow simulation showed.

#### 4.4.1.2 Milk

No experiments with flow of milk (or coagulated milk) through the membrane have been done in this thesis. However, a rough estimate of the Reynolds number is possible to calculate.

As mentioned in chapter 2.1.2.5, a new equation is used to calculate the Reynolds number of non-Newtonian power law-fluids.

$$Re_x = 2^{3-n} \left( \frac{n}{3n+1} \right)^n \frac{D^n \rho \bar{V}^{2-n}}{K}$$

$$Re_x = 2^{3-0.55} \left( \frac{0.55}{3(0.55)+1} \right)^{0.55} \frac{0.01265^{0.55}m \times 1030kg/m^3 \times 0.2325^{2-0.55}m/s}{0.85}$$

$$= 2^{2.45} (0.421128)(11.227945) = 25.84$$

<sup>9</sup> At 20°C for the milk and 0°C for the water.

<sup>10</sup> 12 ml/min equals to 0.0395 m/s in the artificial membrane.



Where the consistency coefficient  $K$  is estimated to be 0.85, a mean value of the  $K$  values for yoghurt. The flow behaviour index is estimated to be 0.55 (Appendix M). It is assumed that the milk will have a consistency more similar to yoghurt than the original milk, when entering the small intestine. This is a rough estimate; however, it is clear that the Reynolds number indicates a laminar flow, due to that it is below the critical Reynold number (calculated below).

$$Re_{critical} = \frac{6464n(2+n)^{(2+n)/(1+n)}}{(1+3n)^2} = 2364.55$$

#### 4.4.2 Schmidt, Sherwood and Graetz Number in the Digestive Composition

To calculate the dimensionless numbers  $Sc$ ,  $Sh$  and  $Gz'$ , some assumptions are needed to be made.

First, the example from chapter 2.2.1.1 is used to assume a diffusivity of an amino acid in milk, even though peptides would be more relevant for this thesis due to its smaller molecular weight. However, in order to use the *Stokes-Einstein* equation without having to consider the association parameter for the solvent ( $\psi_B$ ), the molecular weight has to be above 400, which is the case of the amino acid.

Second, the viscosity is assumed to be the same as the measured viscosity after added HDJ in Devle's research (Figure 4) (Devle et al. 2012). The temperature is assumed to be the same as in the apparatus. Therefore, the diffusivity  $D_v$  is calculated below, from Equation 17.

$$D_v = \frac{7.32 \times 10^{-16}(310K)}{(3.3 \times 10^{-8}cm)7cP} = 9.8234 \times 10^{-7}cm^2/s$$

##### 4.4.2.1 Schmidt Number

From this result, the Schmidt number is calculated:

$$Sc = \frac{\mu}{\rho D_v} = \frac{7cP}{1.03g/cm^3 \times 9.8234 \times 10^{-7}cm^2/s} = 6918310$$

This is a number within the region  $10^5$  which is typical for mixtures (McCabe et al. 2005).

##### 4.4.2.2 Graetz Number

Knowing the  $Sc$  and  $Re$  number, the  $Gz'$  number is calculated:

$$Gz' = \left(\frac{\pi}{4}\right) ReSc \left(\frac{D}{L}\right) = \left(\frac{\pi}{4}\right) (25.84)(6918310) \left(\frac{0.01265m}{0.06m}\right) = 29602043$$

Where  $L$  is the length of the tube, here assumed to be the same length as the active membrane part in the apparatus, and  $D$  as the membranes diameter. A Graetz number over 1000 indicates a fully developed velocity profile (McCabe et al. 2005).

#### 4.4.2.3 Sherwood Number

Knowing the  $Gz'$  number, the  $Sh$  number is calculated:

$$Sh = 1.76Gz'^{1/3} = 1.76(29602043)^{1/3} = 544.44$$

### 4.4.3 Volume Calculations

#### 4.4.3.1 Purpose and Method

Due to the critical volume limitations in the rheometer cup, it was essential to know the exact volume of the fluids circulating in the apparatus. One at a time, the fluids in the circuits was weight on a scale, to calculate the volume from the density of water.

Volumes of all the items relevant for this test, were collected from SW prior to the volume calculations. These volumes are shown in Table 33.

Table 33: Volumes collected from drawing in SW.

Item	Volume [mm3] SW	Volume [m3] SW	Volume [ml] SW
Only propeller	1101,42	1,10142E-06	1,10142
Probe in the cup	1620,09	1,62009E-06	1,62009
Inside cup total	36833,79	3,68338E-05	36,83379
Inside cup - probe total	35213,7	3,52137E-05	35,2137
Bottom volume	12719,17	1,27192E-05	12,71917
Bottom volume - propeller	11617,75	1,16178E-05	11,61775
Titration sensor	475,57	4,7557E-07	0,47557
Tube 1 2,54	849,24	8,4924E-07	0,84924
Tube 2 2,54	849,24	8,4924E-07	0,84924
Tube 1 3,17	1322,76	1,32276E-06	1,32276
Tube 2 3,17	1322,77	1,32277E-06	1,32277
Acid tube	131,95	1,3195E-07	0,13195
Base tube	131,95	1,3195E-07	0,13195
<i>Total tubes and pH</i>			5,08348
Total volume inside cup - all tubes, pH, probe			
<b>29,68643</b>			

#### 4.4.3.2 Results

##### 4.4.3.2.1 The Stomach Circuit

Table 34: Volume of the fluid circulating in the stomach circuit. \*This is after subtracting the volume left in the cup in-between the blades of the propeller that is not possible for the peristaltic pump so suck out. The volume available for circulation is less than the volume that is needed to circulate.

Stomach circuit	Value
Total volume in the system [ml]	14.84
Volume in the cup for fluid [ml]	14.84
Total volume available for circulation [ml]	3,34*
Total volume in the tubes circulating [ml]	5.48 <sup>11</sup>
Numbers of tubes connected (length 400 mm each)	2
Tube i.d. [mm]	3.17

The total volume in the stomach circuit should at one point of the process fit in the cup, in addition to the HDJ and all the tubes with the propeller.

##### 4.4.3.2.2 The Small Intestine Circuit

Table 35: Volume of the fluid circulating in the small intestine circuit.

Small intestine circuit	Value
Total volume in the system [ml]	29.68
Volume in the cup for fluid [ml]	29.68
Total volume available for circulation [ml]	18,18*
Total volume in the tubes circulating [ml]	18.63
Numbers of tubes connected (length 400 mm each)	3
Tube i.d. [mm]	2.72 <sup>12</sup>

In both the stomach and the small intestine circuits, the available volume for circulation is less than what is actually circulating in the tubes. Due to the probe propeller, some fluid at the bottom will not be sucked out of the cup. Designing a new propeller will compensate for this and a simple sketch of a new design is presented in Appendix P.

#### 4.4.4 Roughness Calculations

Knowing the height of a villi in the small intestine in a rat (chapter 2.3.2.1), and the intestine's diameter, one can estimate relative roughness at the intestinal wall. The diameter of a rat's small intestine is assumed to be  $1 \cdot 10^{-2}$  m.

The relative roughness is in this case, calculated to be:

$$\frac{k}{D} = \frac{0.0003m}{0.01m} = 0.03$$

<sup>11</sup> Measured on a scale in grams - and converted to ml.

<sup>12</sup> After the thesis was finished, it was noticed that the tube size was not what was ordered. The tube size in the small intestine circuit is supposed to be 2.54 mm i.d.

Combining the relative roughness with the Reynolds number of the fluid, one can find the friction factor from Appendix O. Note that roughness has no effect on the friction factor in laminar flow, unless  $k$  is over a value which makes the diameter uncertain (McCabe et al. 2005). Note that the relative roughness calculation is based on the assumption that the length between each villi is equal to its width. This is not accurate, as the villi covers 60% of the intestinal surfaces. It is however, an acceptable estimate.

#### 4.5 Equations Used to Describe the Possible Flow Conditions in the System

Table 36: Mathematical models: Equations, which is possible to use, using data obtained from the system, to describe flow conditions both in the rheometer cup and in the artificial membrane. Regarding other equations described in this thesis not mentioned here, the current system does not provide enough information to use.

Name	Equation	Parameter	X = Obtained from apparatus C = Fluids coefficient	Description of which flow condition
Shear stress in a power fluid	$\tau_v = K(\gamma)^n$	$\gamma$	X	The shear stress in the fluid in the rheometer cup at the given shear rate from the rheometer.
		$K$	C	
		$n$	C	
Shear rate in a power fluid	$\gamma = \left(\frac{3n+1}{4n}\right)\left(\frac{8u}{D}\right)$	$n$	C	The shear rate inside the artificial membrane.
		$D$	X	
		$u$	X	
Re-number in a non-Newtonian fluid	$Re = 2^{3-n} \left(\frac{n}{3n+1}\right)^n \frac{D^n \rho \bar{V}^{2-n}}{K}$	$n$	C	The Re-number inside the artificial membrane, describing if the flow is laminar or turbulent.
		$K$	C	
		$D$	X	
		$\bar{V}$	X	
		$\rho$	C	
Stokes-Einstein's equation	$D_v = \frac{7.32 \times 10^{-16} T}{r_0 \mu}$	$T$	X	The diffusivity for large molecules through the fluid.
		$r_0$	C	
		$\mu$	X	
Schmidt number	$Sc = \frac{\mu}{\rho D_v}$	$\mu$	X	Describes the relationship between the fluids viscosity vs molecular diffusivity.
		$\rho$	C	
		$D_v$	X	
Sherwood number	$Sh = 1.76 Gz'^{1/3}$	$Gz'$	X	Describes the mass flux through the laminar liquid inside the artificial membrane.
Graetz number	$Gz' = \left(\frac{\pi}{4}\right) Re Sc \left(\frac{D}{L}\right)$	$\frac{D}{L}$	X	Mass transfer through the artificial membrane.
		$Sc$	X	
		$Re$	X	

## 5 Discussion and Conclusion

### 5.1 Functionality of the Apparatus and its Limitations

#### 5.1.1 Results from Experimental Work

##### 5.1.1.1 Tubing Sizes

After an evaluation of the results from the preliminary test where the fluid flow of coagulated milk was tested through different tube sizes, acceptable tube sizes was chosen for both the stomach and the small intestine circuit. The primary challenge of the coagulated milk was, as described in chapter 4.1, the lumps blocking the passage. However, the tubes in the requested size that was delivered with the pump was only 400 mm long (chapter 0), which needed to be extended. This were done connecting two tubes together with extending plugs. This introduced the same challenge again, as the diameter inside the extending plugs is narrower than the tube itself. This has not been tested with coagulated milk, but it is assumed to be a problem.

A possible solution for this problem could be to get a longer tube with the size 3.17 mm from another supplier, and glue on some stoppers so that the tube will be compatible with the peristaltic pump.

##### 5.1.1.2 Stomach

###### 5.1.1.2.1 Volume Limitations

The limited volume available of the fluid (chapter 1.2.3), has been a concern which is considered throughout the designing process. The volume flowing through the different circuits, as well as the volume inside the rheometer cup, was therefore measured either physical (by a weight scale) or through simulated sketches in SW (chapter 4.4.3). As mentioned in chapter 4.4.3.2.2, the available volume for circulation in both the stomach and the small intestine circuits, is less than what needs to be circulating the tubes (with the current tubes sizes). Due to the probe propeller, some fluid at the bottom will not be sucked out of the cup, causing an ineffective circulation of the fluid. Increasing the available fluid to circulate, by decreasing the size of the probe propeller, is a possible solution for this challenge (chapter 5.2.1.2).

###### 5.1.1.2.2 Lid – Limited Visualization

The lid was designed to keep all the different devices (tubes, titrator sensor and probe propeller) in a strategic position in the rheometer cup. Using SW, several computational designs was done to find the best solution (chapter 4.2.1). It was also possible to visualize the organization of the different devices within the cup, using SW. Through several prototypes, one final design was made. This considered the problem with volume limitations inside the cup, as well as the organization of the different devices above the lid in consideration of the pump, the titrator and the rheometer.

The final design of the lid does not eliminate the challenge regarding the volume limitations. Due to all the devices taking up room inside the rheometer cup, there is limited room for the digestive composition fluid (Figure 37). Considering the first stages of the digestive composition, the gastric fluids will cause the milk to coagulate. It is assumable that these created lumps in the fluid, will be stuck between the tubes, probe propeller and the titrator sensor inside the cup. This will limit the circulation of the digestive fluid in the stomach circuit. The lack of visualization inside the cup when the system is running makes this a problem that can possibly stop the entire system due to blockages.

A possible solution to this problem is discussed in chapter 5.2.1.3.

#### 5.1.1.3 The Small Intestine Device

The small intestine device was designed considering the larger size of the artificial membrane that was going to be used, compared to the narrower silicon tube in where the digestive composition was going to circulate. This expansion was expected to cause the development of a turbulent flow in the wider membrane (Figure 43). Considering this issue, combined with the fact that laminar flow gives a better characterization of the fluid behaviour, flow simulations in SW were done to simulate how long the entry length (Equation 15) in the membrane was expected to be.

The flow simulations in SW (chapter 4.3.1) were an acceptable tool to use, to get a visualization of the expected fluids behaviour through the membrane. The design of the small intestine device, based on these simulations, made a good first prototype.

##### 5.1.1.3.1 Challenges with Computational Simulations

Computational simulations will never be as accurate as the model in reality. The model used in SW did for example not consider the material of the membrane, which made a significant difference in the real dynamic model. Nor did it consider the fluids characteristics (milk), as the fluid in the simulations was water, which is a Newtonian fluid.

Through the experimental tests (chapter 1), several new challenges appeared to the design, which had not been considered earlier.

One of the first challenges was the air bubble that appeared within the membrane (chapter 4.3.3). A simple angled elevation eliminated this problem. A second challenge that appeared was the membrane's material, which got very slippery against the smooth glass material of the inner small intestine ends, when immersed in fluid. Tests were done (chapter 4.3.2.3.2) to find a good solution to keep the membrane in place. However, no acceptable solution was found.

##### 5.1.1.4 Permeability Tests

The permeability tests (chapter 4.3.4), both the dynamic and the static, resulted in no diffusion of the colorant *Evan's Blue* through the artificial membrane. Prior to the test, it was assumed that there would be some diffusion through the membrane, due to the much smaller MW of *Evan's Blue* (Table 28) than the membrane's cut-off size (3.5 kDa). This was however not the case, and the reasons for this could be several. One possibility for this failed diffusion stands out, namely the pressure difference across the membrane was not favourable for diffusion.

#### 5.1.1.4.1 Pressure difference across membranes

As mentioned in chapter 2.2.3, the concentration gradient across the membrane is a common transport inducer. However, this is not the only element that is important in the diffusion process. The pressure difference between the two sides of the membrane, needs to be high enough to push the permeate through. This is especially a significant factor in materials where the cut-off is as small as it is in the case of this system (Table 28).

In the first test, the system was kept flowing, with the same volumetric flow on the inside of the membrane (small intestine circuit) as the outside (buffer circuit). In the second test, the system was kept static, thus no volumetric flow on either of the sides. This produced no real pressure difference to push the permeate through the membrane, and is assumed to be one of the major reasons there was no diffusion in the test.

#### 5.1.1.4.2 Laminar vs. Turbulent Flow

As mentioned in chapter 2.1.2.4, turbulent flow increases the shear stress at the membrane wall, compared to laminar fluid flow. This increase the diffusion rate through a membrane in turbulent fluid conditions. However, in this system, the fluid flow inside the artificial membrane kept laminar. The decrease of shear stress, which this laminar condition vs. turbulent condition causes, can possibly be a factor contributing to no diffusion in the permeability tests.

#### 5.1.1.5 A Mathematical Model

Listed in Table 36, is the equations in which data obtained from the apparatus, can be applied to model the fluid's behaviour through the system. Several equations is applicable, though there are still some limitations to the characterization of the system.

##### 5.1.1.5.1 The Mathematical Model's Limitations

###### 5.1.1.5.1.1 Power law model's significance on the fluids behaviour

The power law model appears in almost every equation modelling the fluid behaviour through this apparatus. When the shear rate and the viscosity are known, which is measured by the rheometer (UDS200, Germany), the power model can use the parameters  $n$  and  $K$  to characterize the fluids behaviour (Equation 6). The fluid behaviour index  $n$  and the consistency coefficient  $K$  depends on the characteristic of the fluid, which means that to get a realistic description of the fluids flow behaviour through the entire system, these parameters needs to be known. As the dynamic model is at this point, there is no description of these parameters as the fluid content changes throughout the system.

###### 5.1.1.5.1.2 The limited description of the membranes permeability

The model for the membranes permeability (Equation 26) is not listed in Table 36 due to the one missing parameter; the membranes porosity. This information about the membrane used in this apparatus, is not available.

This equation modelling the membranes permeability would however be a significant contribution to the characterization of the fluid flow through the system.

## 5.2 Ideas for Further Optimization

### 5.2.1 Ideas for New Optimized Designs

#### 5.2.1.1 *The small intestine device*

Due to the experience with the fluid flow through the small intestine device, combined with the knowledge from the flow simulations, an evaluation of the size of device was done. Every result from relevant tests done through this thesis, indicates that the device should be shorter. The new design is presented in Appendix I.

Regarding the slippery membrane-issue discussed earlier, one idea of a stands out. This is presented earlier in the thesis, in Figure 51.

#### 5.2.1.2 *Probe propeller*

As discussed previous, the volume limitations in the rheometer cup presents a problem of the lumps in the fluid getting stuck between all the devices. An idea of a solution to these is shorter blades at the bottom, combined with a second set of narrower blades placed further up on the probe. A simple sketch of this idea is presented in Appendix P

#### 5.2.1.3 *Rheometer cup*

A second tool that can help with the volume limitation issue is visualization. Making the rheometer cup in a transparent material, which in addition handle the low pH, combined with placing the cup above the “seat” of the rheometer, can make this part of the system visual.

### 5.2.2 Permeability test

To improve the chance of successful diffusion in a future permeability test, one should try keeping the internal flow rate (the small intestine circuit) dynamic, while the outer flow rate (buffer circuit) is kept static. It is assumed that this can contribute to the pressure difference across the membrane, increasing the permeate’s diffusivity through the membrane.

### 5.2.3 Factors of the human digestive system which can, with some modifications, be simulated

As mentioned several times earlier, turbulent flow increases the diffusion rate through a membrane, compared to laminar flow. In the human small intestine, the movements in the intestinal walls, creates this turbulent flow, despite the low Reynolds number of the fluid (chapter 2.3).

In this apparatus, the peristaltic pump simulates some peristaltic contractions. This however, does not effect the fluid conditions in the artificial membrane, due to the distance between the small intestine device and the pump. Segmental contractions are not simulated at all in the system.

An idea for future development of these movements, which will increase the fluid turbulent flow through the membrane at low velocities, is creating some kind of a clamping device around the membrane. These clamps will contract with a frequency similar to the frequency presented in Table 17. Tharakan (Tharakan 2008), used this method in his system with success.



## 6 Conclusion

The apparatus, with its many challenges, is an acceptable first prototype of an *in-vitro* dynamic model of the stomach and the small intestine for milk products. Either the challenges and limitations met during the experimental work have been improved, or ideas for further optimization has been presented.

Preliminary tests of the built system indicating the parameters, which describe the physical and chemical environment in the apparatus, have either had a successfully result, or values have been obtained from other research relevant for this objective.

The description of several equations, which can be used to characterize the fluid's behaviour through the system, is presented in the thesis. This includes information of other parameters that would be significant contributors to this model.

### 6.1 Further Work

For further optimization of the dynamic model, the new ideas for the designs that are discussed in chapter 5.2.1, should be evaluated and possibly implicated in the apparatus.

There are still several functions in the human digestive that are not considered in this thesis to be a part of the apparatus, which can be considered. These include dividing the small intestine device into a duodenum-device, a jejunum-device and an ileum-device, to achieve a more realistic simulation of the digestion through the small intestine. It also includes a further development and optimization of the diffusion through the artificial membrane, as well as a further development of the mathematical model represented in chapter 4.5.

Other further development of the system is discussed in chapter 5.2.3.

## 7 References

- Anatomy of the small intestine.* (2014). Available at: <http://pixgood.com/intestines-anatomy.html> (accessed: 13.11.2014).
- Çengel, Y. A., Ghajar, A. J. & Kanoğlu, M. (2011). *Heat and mass transfer: fundamentals and applications*. Singapore: McGraw-Hill. XXI, 902 s. : ill. pp.
- Cussler, E. L. (2009). *Diffusion: mass transfer in fluid systems*: Cambridge university press.
- Damodaran, S., Parkin, K. & Fennema, O. R. (2008). *Fennema's food chemistry*. Boca Raton: Taylor & Francis. 1144 s. : ill. pp.
- de Kruif, C. G. (1997). Skim Milk Acidification. *Journal of Colloid and Interface Science*, 185 (1): 19-25.
- Devle, H., Naess-Andresen, C. F., Rukke, E.-O., Vegarud, G. E., Ekeberg, D. & Schuller, R. B. (2012). Rheological characterization of milk during digestion with human gastric and duodenal enzymes. *Annual Transactions of the Nordic Rheology Society*, 20.
- Diamond, J. M., Karasov, W. H., Cary, C., Enders, D. & Yung, R. (1984). Effect of dietary carbohydrate on monosaccharide uptake by mouse small intestine in vitro. *The Journal of physiology*, 349 (1): 419-440.
- Dictionary.com.* (2014). Available at: <http://dictionary.reference.com/browse/eddies> (accessed: 23.11.2014).
- Faas, H., Steingoetter, A., Feinle, C., Rades, T., Lengsfeld, H., Boesiger, P., Fried, M. & Schwizer, W. (2002). Effects of meal consistency and ingested fluid volume on the intragastric distribution of a drug model in humans—a magnetic resonance imaging study. *Alimentary pharmacology & therapeutics*, 16 (2): 217-224.
- Fellows, P. (2009). *Food processing technology: principles and practice*. Boca Raton, Fla.: CRC Press. 1 online resource (xv, 913 s.) : ill pp.
- Ganong, W. F. & Barrett, K. E. (2005). *Review of medical physiology*, vol. 22: McGraw-Hill Medical ^ eNew York New York.
- Guyton, A. C. & Hall, J. E. (2006). *Textbook of Medical Psysiology*. 11th ed. Philadelphia, USA: Elsevier Inc.
- Haidekker, M. A., L'Heureux, N. & Frangos, J. A. (2000). *Fluid shear stress increases membrane fluidity in endothelial cells: a study with DCVJ fluorescence*, vol. 278. H1401-H1406 pp.
- Kong, F. & Singh, R. (2008). Disintegration of solid foods in human stomach. *Journal of food science*, 73 (5): R67-R80.
- Lekang, O.-I. (2013). *Aquaculture engineering*: John Wiley & Sons.
- Lucey, J. A. (2002). Formation and Physical Properties of Milk Protein Gels. *Journal of Dairy Science*, 85 (2): 281-294.
- Macagno, E. O. & Christensen, J. (1980). Fluid mechanics of the duodenum. *Annual review of fluid mechanics*, 12: 139-158.
- Martini, F. H. & Nath, J. L. (2009). *Fundamentals of anatomy & physiology*. San Francisco: Pearson Benjamin Cummings. XXXIX, 1123 s. : ill. pp.
- Mayhew, T. (1984). Geometric model of the rat intestinal mucosa for stereological evaluation of villus amplification factors. *Journal of microscopy*, 135 (3): 337-346.
- McCabe, W. L., Harriott, P. & Smith, J. C. (2005). *Unit operations of chemical engineering*. 7th ed. Boston: McGraw-Hill. XXV, 1140 s. : ill. pp.
- Nutter's Exus - The celiac lifestyle against the grain.* Available at: <http://www.nutters.com/nexus/celiacpg3.html> (accessed: 08.12.2014).
- Palay, S. L. & Karlin, L. J. (1959). An electron microscopic study of the intestinal villus I. The fasting animal. *The Journal of biophysical and biochemical cytology*, 5 (3): 363-371.
- Pauletti, G., Okumu, F. & Borchardt, R. (1997). Effect of Size and Charge on the Passive Diffusion of Peptides Across Caco-2 Cell Monolayers via the Paracellular Pathway. *Pharmaceutical Research*, 14 (2): 164-168.
- Poole, R. J. & Ridley, B. S. (2007). Development-Length Requirements for Fully Developed Laminar Pipe Flow of Inelastic Non-Newtonian Liquids. *Journal of Fluids Engineering*, 129 (10): 1281-1287.

- Prabhakara, S. & Deshpande, M. (2004). The no-slip boundary condition in fluid mechanics. *Resonance*, 9 (5): 61-71.
- Rao, M. A. (2014). Flow and functional models for rheological properties of fluid foods. In *Rheology of Fluid, Semisolid, and Solid Foods*, pp. 27-61: Springer.
- Salas-Bringas, C., Lekang, O.-I., Rukke, E. O. & Schuller, R. B. (2009). Development of a New Capillary Rheometer that uses Direct Pressure Measurements in the Capillary. *Annual Transactions of the Nordic Rheology Society*, 17.
- Salas-Bringas, C., Rukke, E.-O., Devold, T., Vegarud, G., Naess-Andresen, C. F. & Schuller, R. B. (2014). Developing an In-Vitro Dynamic Model of the Stomach and Small Intestine for Milk Products with Rheological Monitoring. *Annual Transactions of the Nordic Rheology Society*, 22.
- Schüller, R. B. (2014). *Shear rate plot*.
- Shuler, M. L. & Kargi, F. (1992). *Bioprocess engineering: basic concepts*. Englewood Cliffs, N.J.: PTR Prentice Hall. XVI, 479 s. : ill. pp.
- Smith, P. G. (2011). *An Introduction to Food Process Engineering*: Springer.
- Steffe, J. F. (1996). *Rheological methods in food process engineering*: Freeman press.
- Tharakan, A. (2008). *Modelling of physical and chemical processes in the small intestine*: University of Birmingham, Department of Chemical Engineering. 285 pp.
- Thomas, A. (2006). Gut motility, sphincters and reflex control. *Anaesthesia & Intensive Care Medicine*, 7 (2): 57-58.
- VWR. (2014). *VWR store catalog*: VWR store catalog (accessed: 28.11.2014).
- Zaia, J., Annan, R. S. & Biemann, K. (1992). The correct molecular weight of myoglobin, a common calibrant for mass spectrometry. *Rapid Commun Mass Spectrom*, 6 (1): 32-6.

## Reglo ICC Independent Channel Control Peristaltic Pump

By providing individually addressable control of each fluidic channel, the new Ismatec® Reglo ICC eliminates the clutter of multiple pumps on the bench top as well as allowing you, the scientist, to solve your application complexity in a single pump. Long hailed in Europe as the gold standard of Swiss precision, Ismatec drives will now power four channels, each independently programmable from the pump or the computer.

### Volumetric Dispense

- ▶ Continuous pumping or precision dispensing
- ▶ Flexibility of bi-directional flow in each channel
- ▶ Easy-to-use tubing cassettes allow quick changeovers
- ▶ Independent channel calibration minimizes the tube to tube differences resulting in the best calibration accuracy possible in a multichannel peristaltic pump
- ▶ New easy-to-use USB interface makes connections quickly

### Technical Specifications

- ▶ Available with four channels, each with independent functionality
- ▶ Flow range per channel: 0.0002 to 35 mL/min
- ▶ PC control or keypad control



ISM4408

Pump Specifications	
Motor Type	Stepper Motor (1/channel)
Speed Range	0.1–100 RPM
Speed Setting	RPM (Resolution = 0.01 RPM)
Flow Rate Range	0.0002–35 mL/min/channel (tubing dependent)
Number of Channels	2–4
Number of Rollers	8 Ertalyte® rollers standard; 6 and 12-roller options also available
Cassettes	MS/CA Click'n'Go (POM-C; alternatives available)
Dimensions (HxWxD)	6.7" (170 mm) x 5" (125 mm) x 8.1" (205 mm)* (*-for 3-channel model)
Weight	6 lbs. (2.7 kg)
Power Consumption	30 W (Max) Main Voltage: 100–264 V AC / 50/60 Hz (Requires use of included power supply, cables)
Protection Rating	IP 30
Differential Pressure	1.0 bar / 14.5 psi (Max)

Flow Rate Range		
Tubing ID (mm)	Flow Rate (mL/min per channel)	
	0.1 RPM	100 RPM
	Minimum	Maximum
0.13	0.0002	0.11
0.25	0.0005	0.41
0.51	0.0017	1.7
0.76	0.0036	3.6
1.02	0.0063	6.3
1.22	0.0088	8.8
1.52	0.013	13
1.85	0.017	17
2.54	0.027	27
3.17	0.035	35

Available Tubing Sizes	
Inner Diameter Range	0.13–3.17 mm (tubing material dependent)
Wall Thickness	0.8 mm

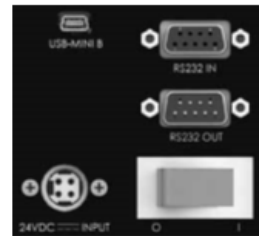
Please note: all tubing must have stoppers with correct spacing to be used with MS/CA cassettes

Environmental Conditions		
	Operational	Storage
Temperature Range	-5 °C to +40 °C (+41 °F to +104 °F)	-10 °C to +50 °C (+14 °F to +122 °F)
Relative Humidity	up to 80% (non-condensing)	up to 80% (non-condensing)

### Supported Communication Protocol

Each channel can be independently controlled via the front panel, USB interface, or RS-232 interface.

#### Rear Panel Connections:



RS-232 In (DB9-female)

RS-232 Out (DB9-male)

USB 2.0, Mini-B

### Operating Modes

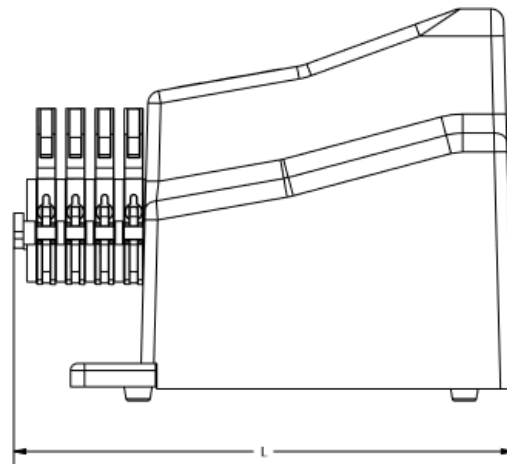
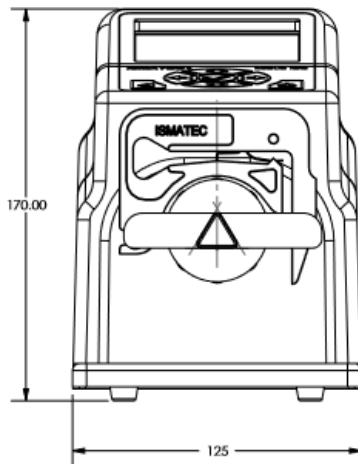
<b>Flow Rate</b>	Continuous operation at a set rate and direction
<b>Volume Over Time</b>	Dispensing a desired volume over a desired time
<b>Volume</b>	Dispensing a desired volume at a set flow rate
<b>Time Mode</b>	Dispensing for a set time duration with a set flow rate
<b>Volume With Pause</b>	Dispensing a set volume over multiple cycles with defined pause time in between
<b>Time With Pause</b>	Dispensing for a set time duration over multiple cycles with defined pause time in between
<b>Calibration</b>	Allows each channel to be calibrated for dispensed fluid volume accuracy

More complex routines are available through the use of the supplied software. Additionally, up to eight pumps can be connected to a computer at once, either by a USB hub or daisy chaining the RS-232 in/out connectors on the pump(s). (Note: For full functionality of each channel via RS-232 control, each pump must be directly connected to a serial interface such as Hypercom or PuTTY.) In the ICC daisy chain configuration, the pumps can either be controlled in legacy mode where all of the pump channels on an individual pump perform the same, or all of the individual channels are programmed with one channel command, similar to channels 2, and 3 (or 4).



**Dimensions**

- Overall Height:** 170 mm (~6.7")
- Overall Width:** 125 mm (~4.9")
- Overall Length:** 193 mm (~7.6")—2-channel  
205 mm (~8.1")—3-channel  
218 mm (~8.6")—4-channel



ismatec® is a registered trademark of IDEX Health & Science LLC  
 ©2013 IDEX Health & Science LLC  
 IDEX1767-PDV03.2013

www.idex-hs.com | North/South America +1 866 339 4653 | Europe +49 1801 808 800 | Asia +86 10 6566 9090



Eastern Plastics | ERC | Ismatec | Isolation Technologies | Rheodyne | Sapphire Engineering | Systec | Upchurch Scientific

## Appendix B

<b>Standard RC Membrane Spectra/Por® 7 Pre-treated Dialysis Tubing</b>				
MWCO	Flat Width (mm)	Diameter (mm)	Volume/Length (ml/cm)	Part No.
1 kD	18	11.5	1.1	<a href="#">132103</a>
	38	24	4.6	<a href="#">132104</a>
	45	29	6.4	<a href="#">132105</a>
2 kD	18	11.5	1.1	<a href="#">132107</a>
	38	24	4.6	<a href="#">132108</a>
	45	29	6.4	<a href="#">132109</a>
3.5 kD	18	11.5	1.1	<a href="#">132110</a>
	45	29	6.4	<a href="#">132111</a>
	54	34	9.3	<a href="#">132112</a>
8 kD	8	5.1	0.20	<a href="#">128356</a>
	12	7.5	0.45	<a href="#">132113</a>
	18	11.5	1.1	<a href="#">128358</a>
	24	15	1.8	<a href="#">132114</a>
	32	20.4	3.3	<a href="#">132115</a>
	40	25.5	5.1	<a href="#">132116</a>
	50	32	7.9	<a href="#">132131</a>
10 kD	8	5.1	0.20	<a href="#">128408</a>
	12	7.5	0.45	<a href="#">132117</a>
	18	11.5	1.1	<a href="#">128418</a>
	24	15	1.8	<a href="#">132118</a>
	32	20.4	3.3	<a href="#">132119</a>
	45	29	6.4	<a href="#">132120</a>
15 kD	8	5.1	0.20	<a href="#">128458</a>
	12	7.5	0.45	<a href="#">132121</a>
	18	11.5	1.1	<a href="#">128458</a>
	24	15	1.8	<a href="#">132122</a>
	32	20.4	3.3	<a href="#">132123</a>
	45	29	6.4	<a href="#">132124</a>
25 kD	8	5.1	0.20	<a href="#">128508</a>
	12	7.5	0.45	<a href="#">132125</a>
	18	11.5	1.1	<a href="#">128518</a>
	24	15	1.8	<a href="#">128524</a>
	28	18	2.5	<a href="#">132126</a>
	34	22	3.7	<a href="#">132127</a>
50 kD	12	7.5	0.45	<a href="#">132128</a>
	28	18	2.5	<a href="#">132129</a>
	34	22	3.7	<a href="#">132130</a>
Price:				\$266

Appendix C

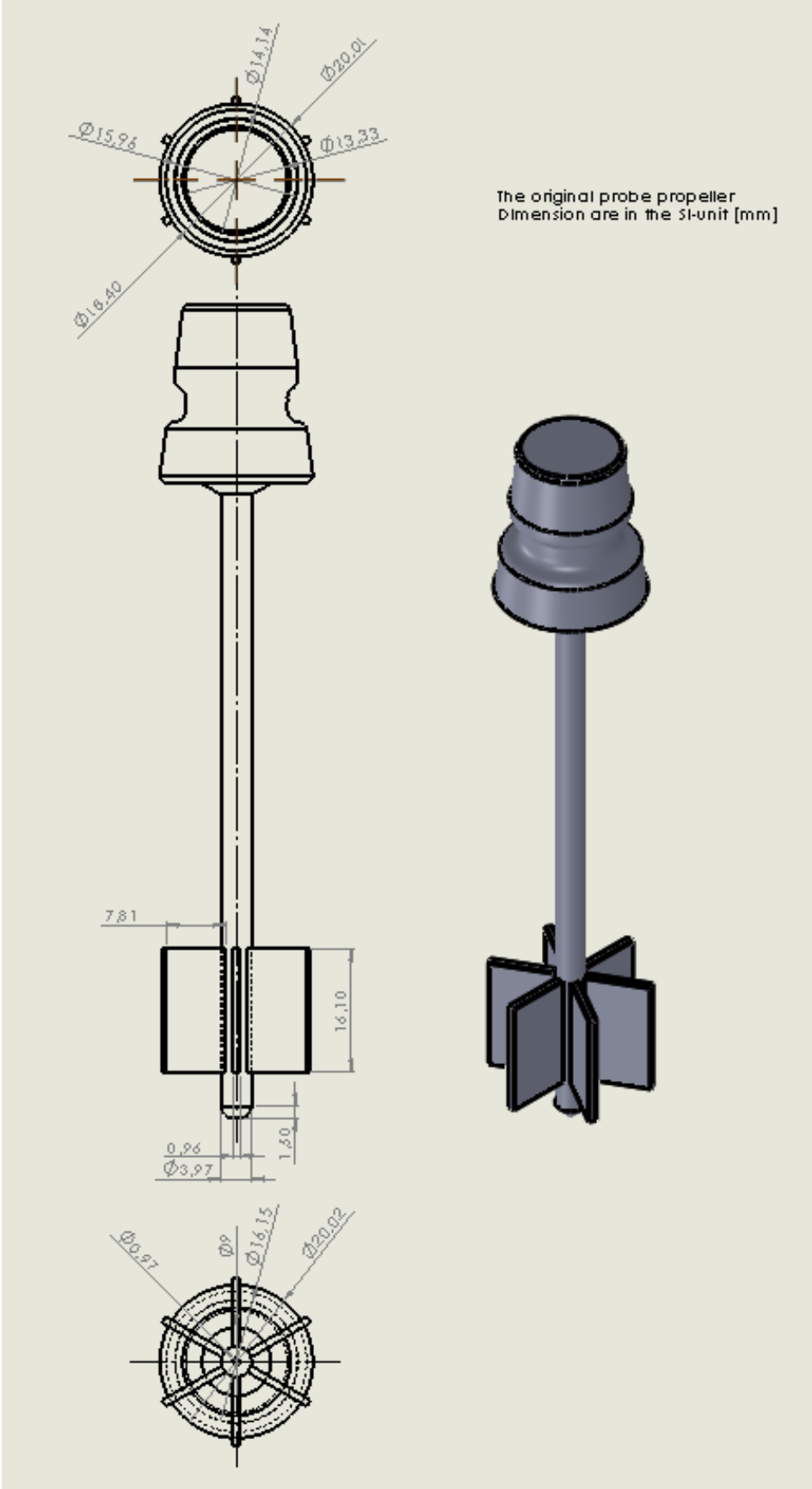


Figure 60: Dimensions [mm] probe propeller.



# Appendix D

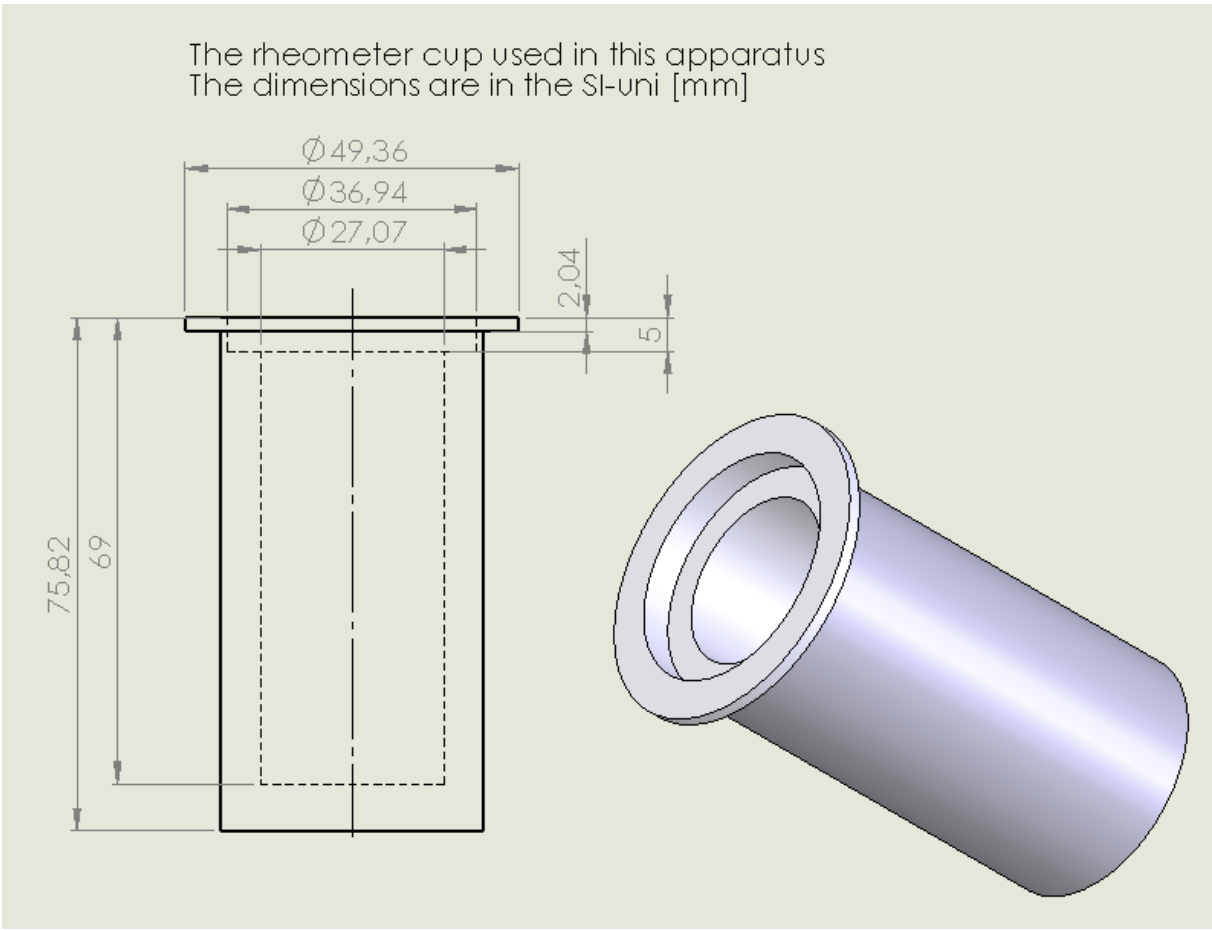


Figure 61: Dimensions [mm] rheometer cup.

Appendix E

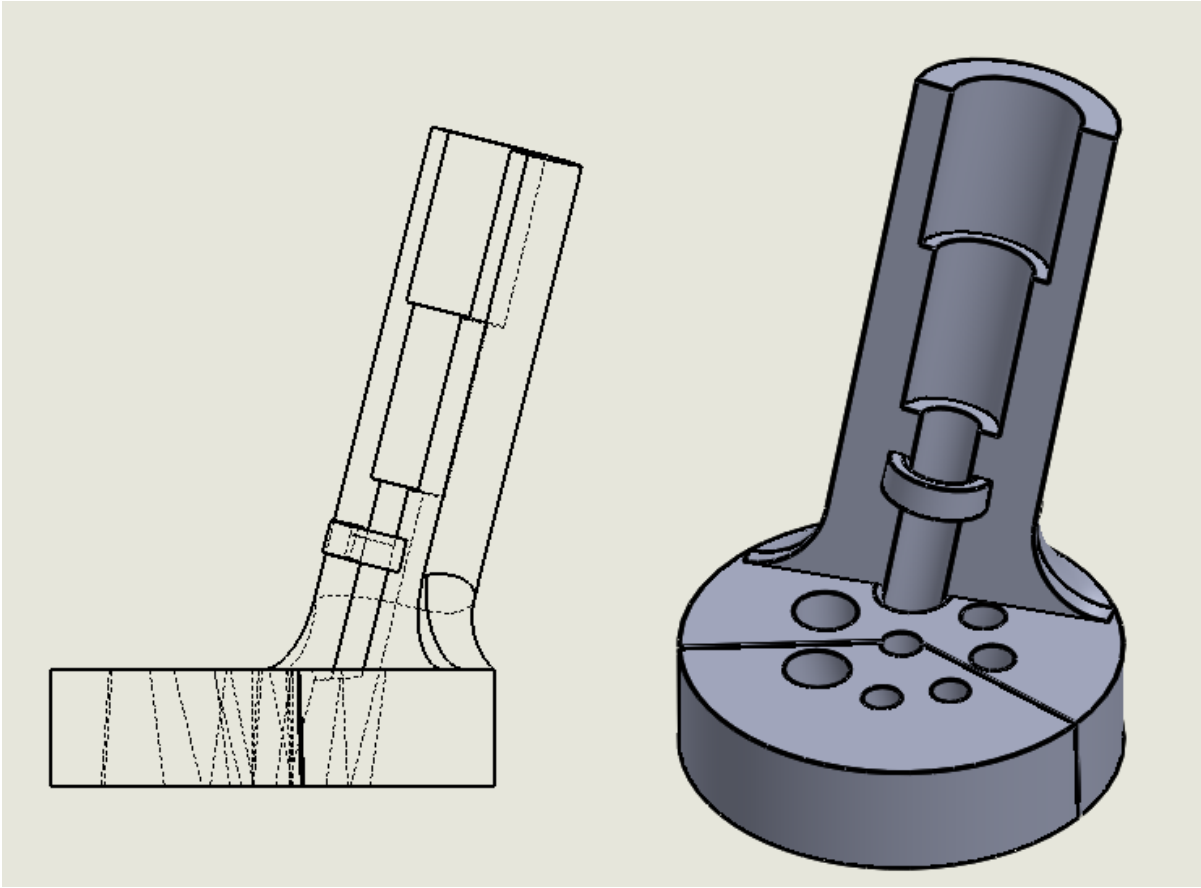


Figure 62: Dimensions [mm] lid, prototype nr 10.

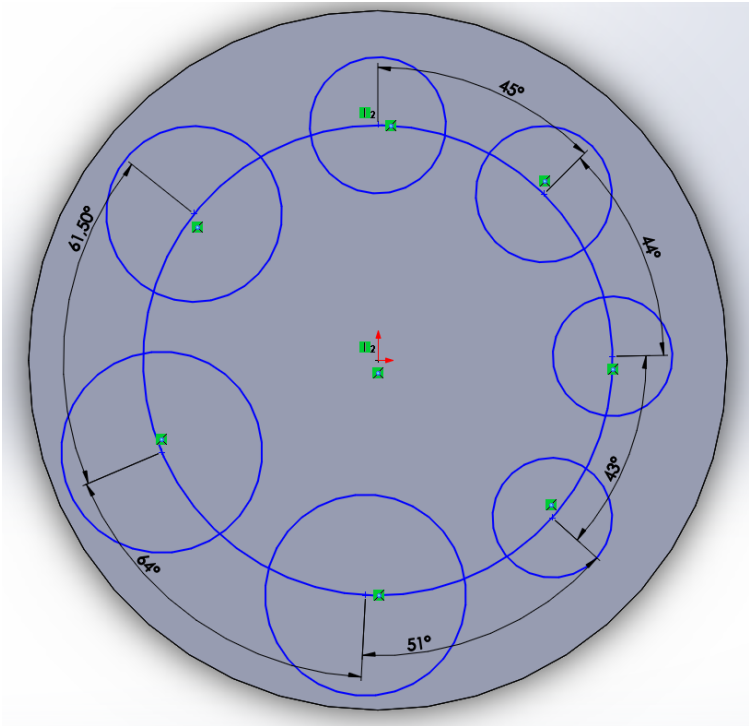


Figure 63: Placement of the holes in the lid.

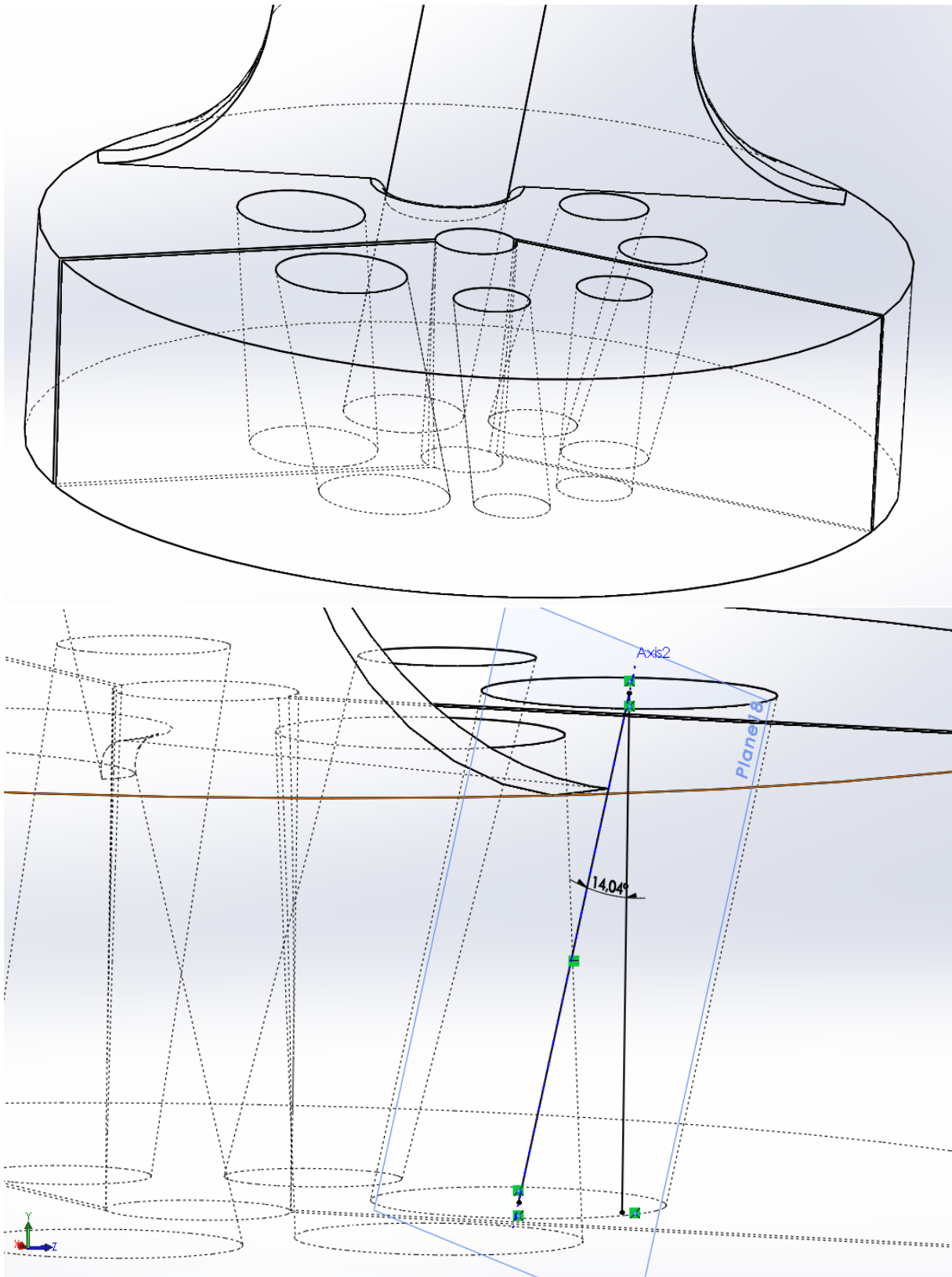


Figure 64: Angle dimensions of the holes in the lid.

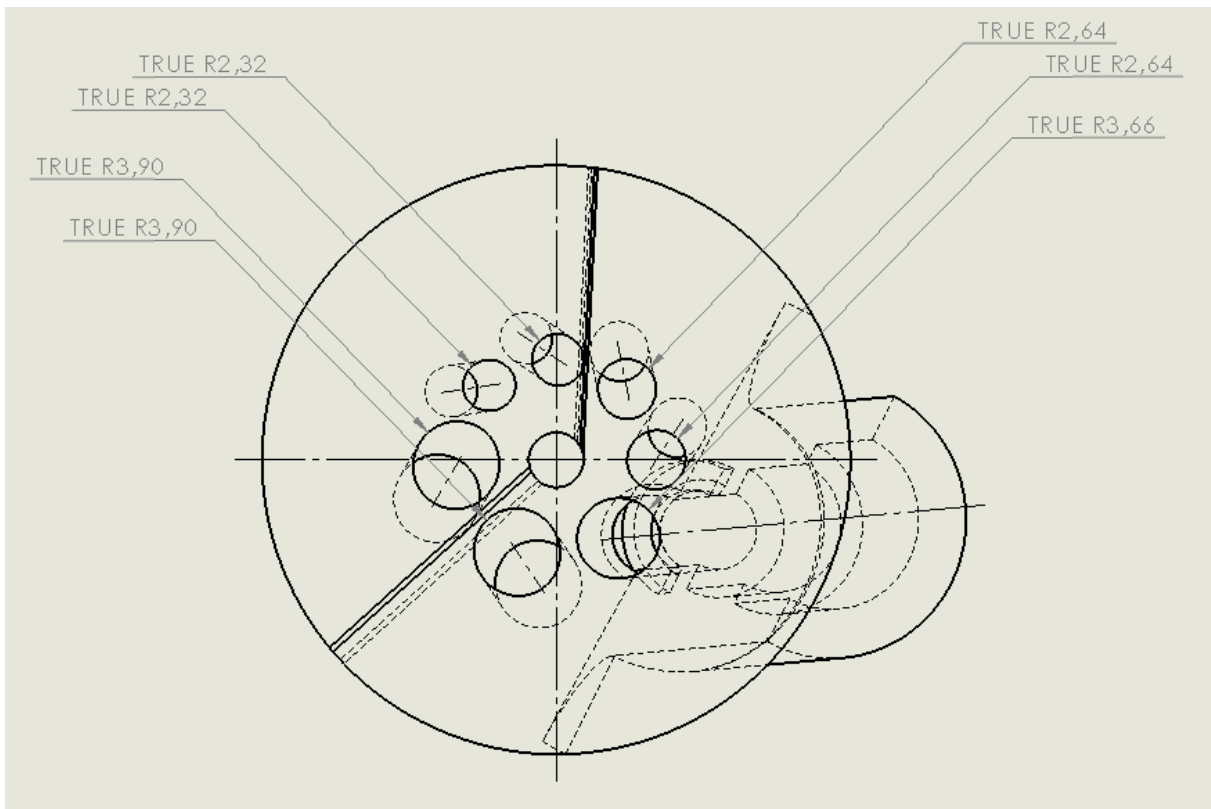
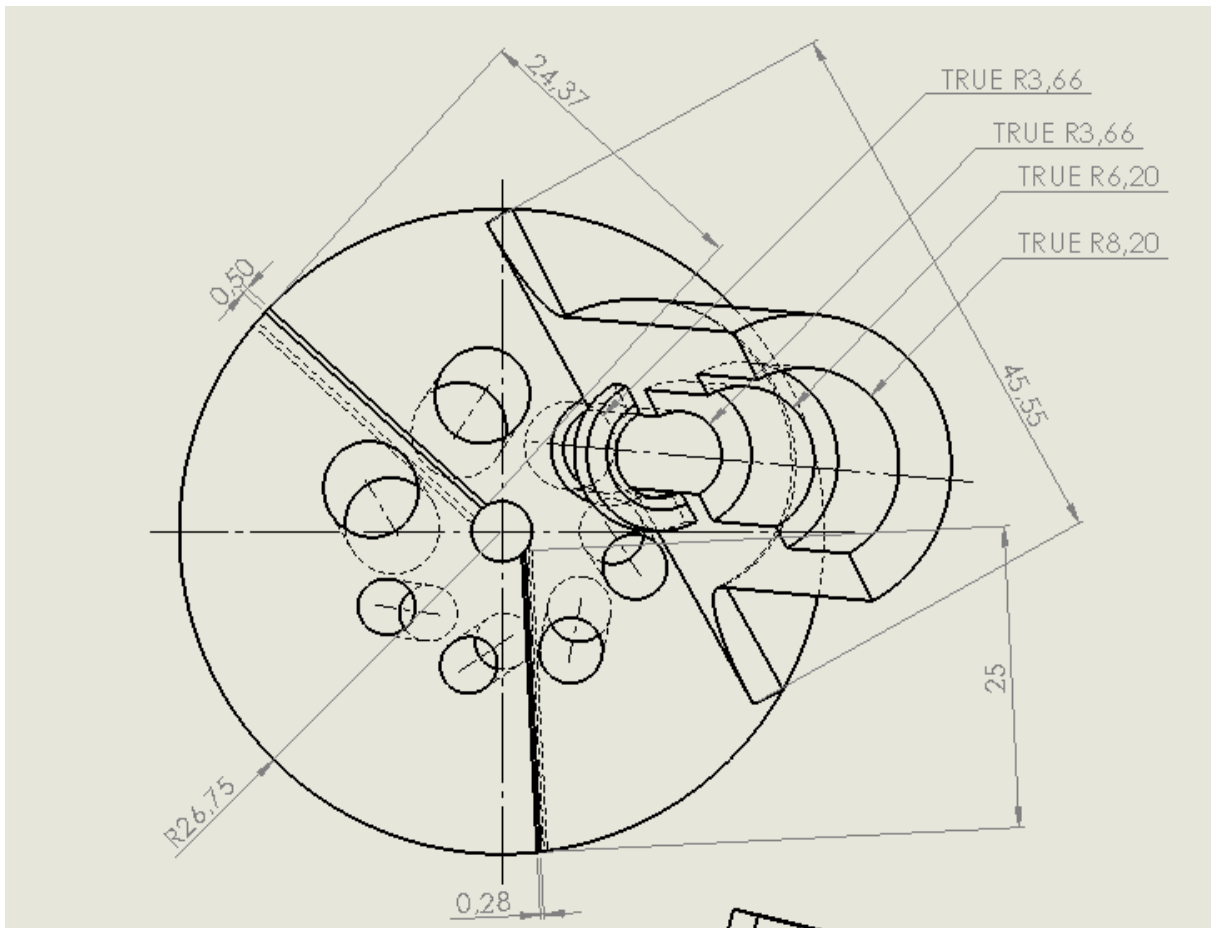


Figure 65: Dimensions [mm] lid.

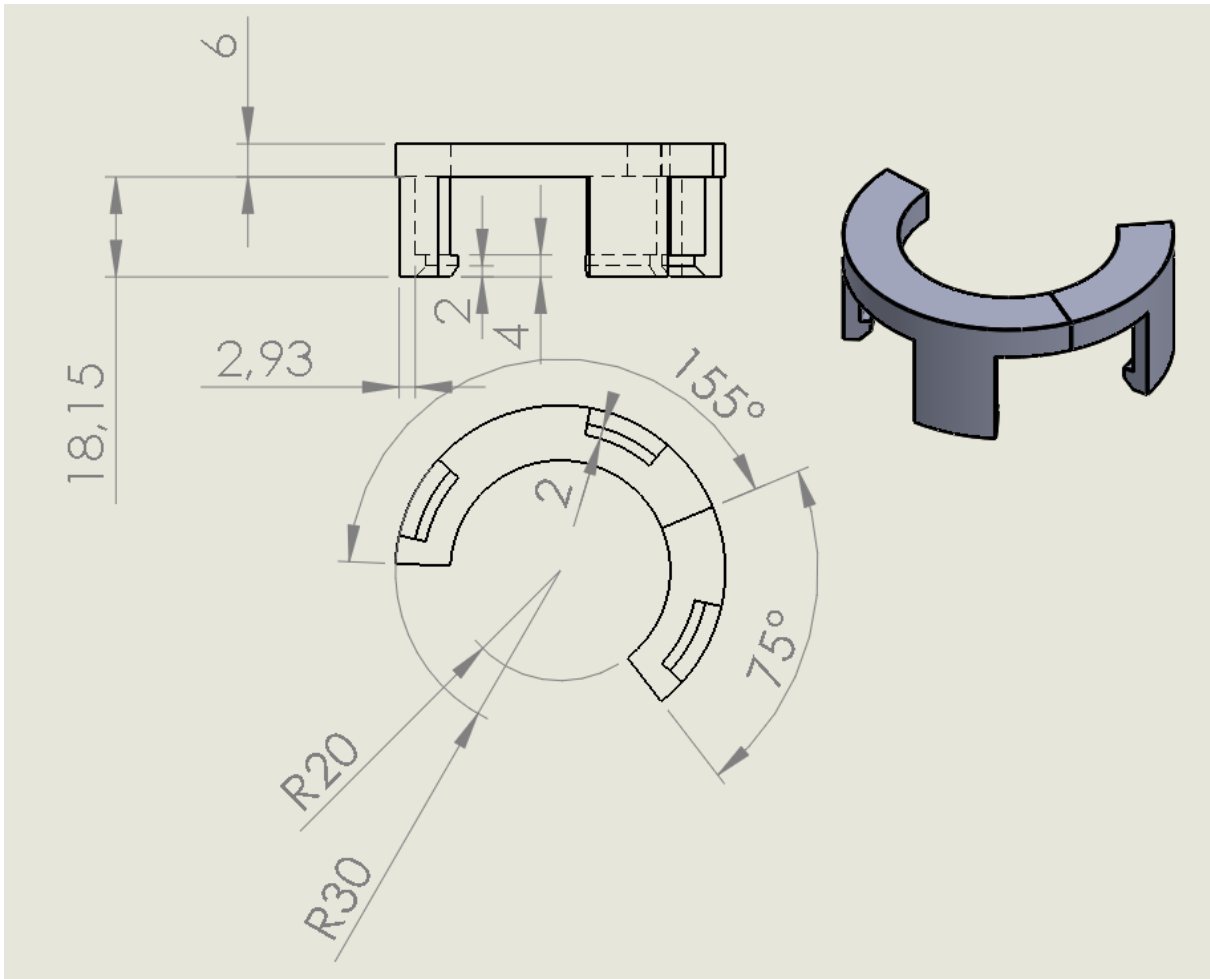
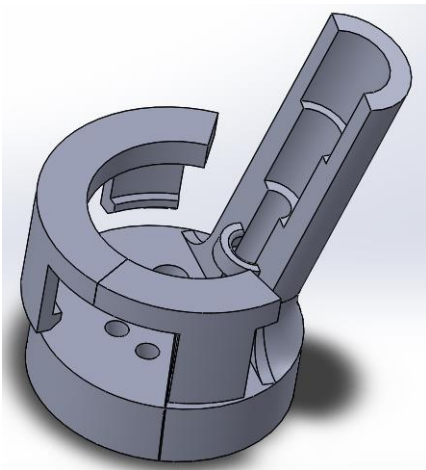


Figure 66: Dimensions [mm] top lid.



Appendix F

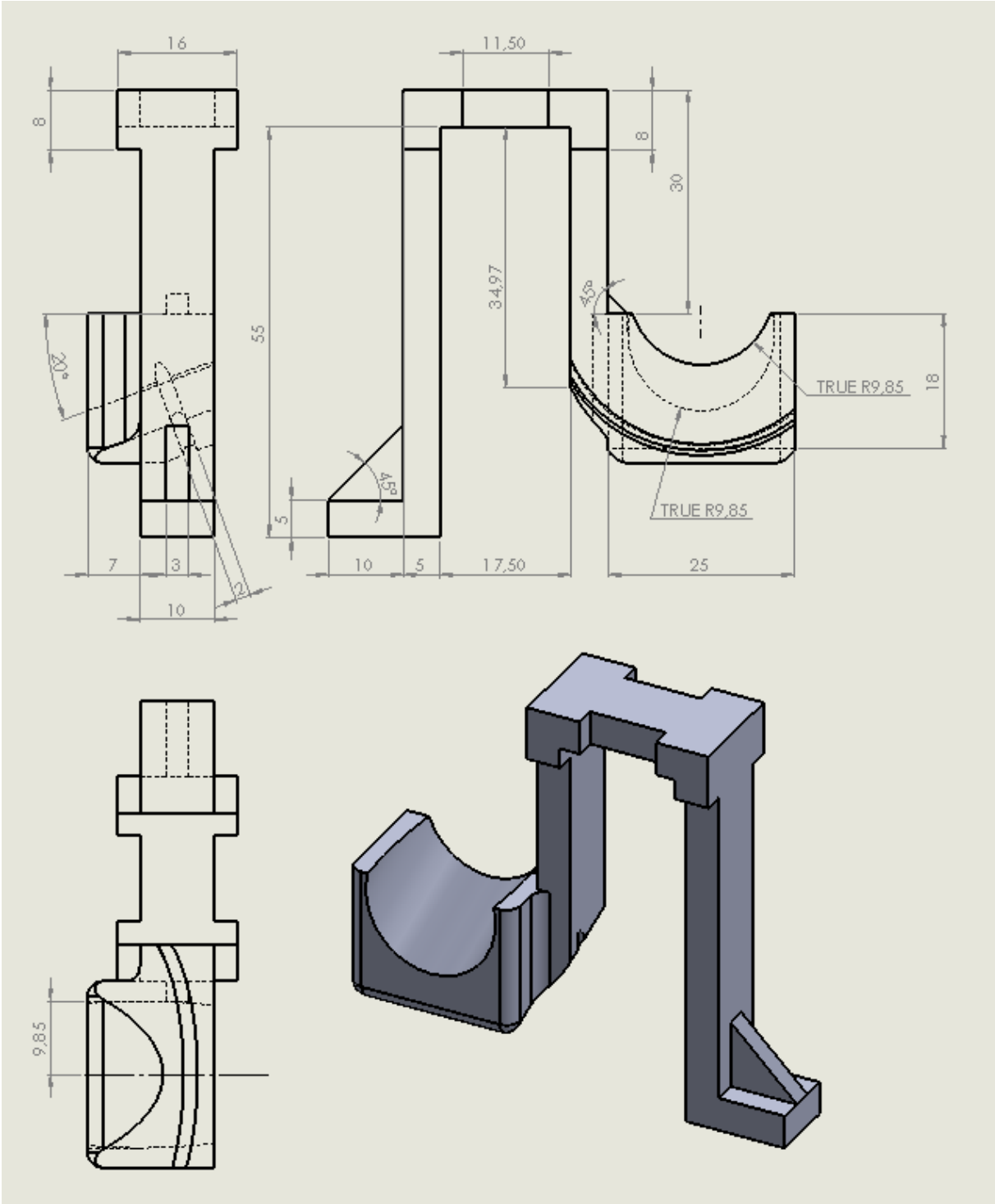


Figure 67: Dimensions [mm] short holder.

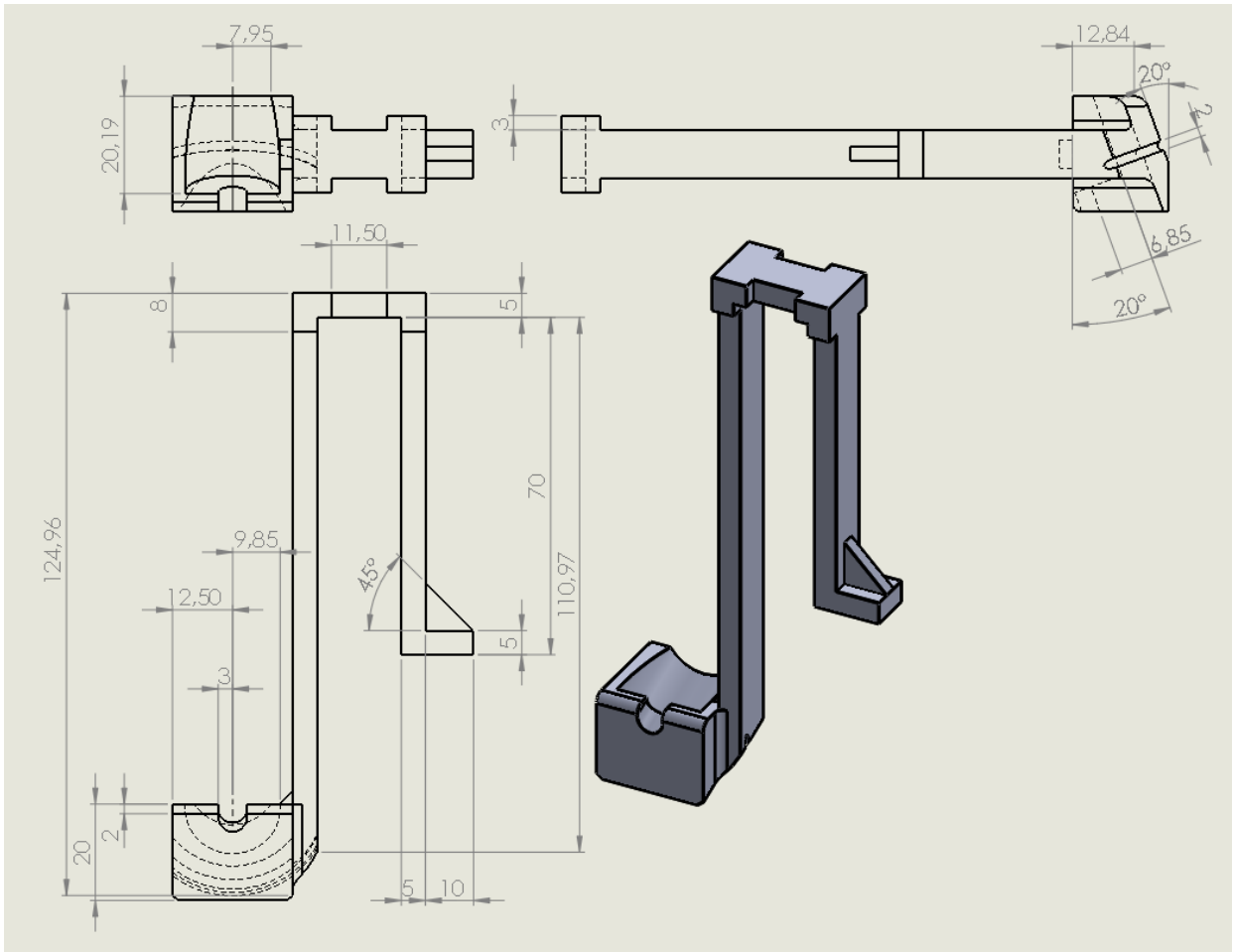


Figure 68: Dimensions [mm] long holder.

## Appendix G

# Technical Specifications The Compact Titrator G20

<b>Potentiometric sensor input</b>	Measuring range	± 2000 mV
	Resolution	0.1 mV
	Error limit	0.2 mV
<b>Polarized sensor input</b>	Measuring range I <sub>pol</sub> / U <sub>pol</sub>	0 ... 2000 mV / 0 ... 200 µA
	Resolution I <sub>pol</sub> / U <sub>pol</sub>	0.1 mV / 0.1 µA
	Error limit I <sub>pol</sub> / U <sub>pol</sub>	2 mV / 0.2 µA
	Current source range I <sub>pol</sub> / U <sub>pol</sub>	0–24 µA AC / 0–2000 mV AC
	Current source resolution I <sub>pol</sub> / U <sub>pol</sub>	0.1 µA / 0.1 mV
<b>PT1000 temperature sensor</b>	Measuring range	-20...130 °C
	Resolution	0.1 °C
	Error limit	0.2 °C
<b>Burette drive</b>	Burette resolution	1/20'000 of the burette volume
	Burette resolution (20mL burette)	1 µL
	Error limit	0.2% of the burette volume
	Resolver resolution	0.0625% of the burette volume
	Fill and eject time	20 s
<b>Titration dimensions</b>	Width x depth x height	210 x 333 x 320 mm
	Weight	4.2 kg
	Screen	QVGA 5.7" color TFT
	Resolution	320 x 240 pixels

### Spesifikasjoner - DGi102-Mini

Kort beskrivelse	Plug & Play combined semi-micro glass pH electrode with a ceramic frit for aqueous media
Bruksområder	acid/base aqueous
Measurement range	pH 0-14
Temperature range	0-100 °C
Length	162.5 mm
Shaft diameter	6 mm
Material nummer	51109508



Appendix H

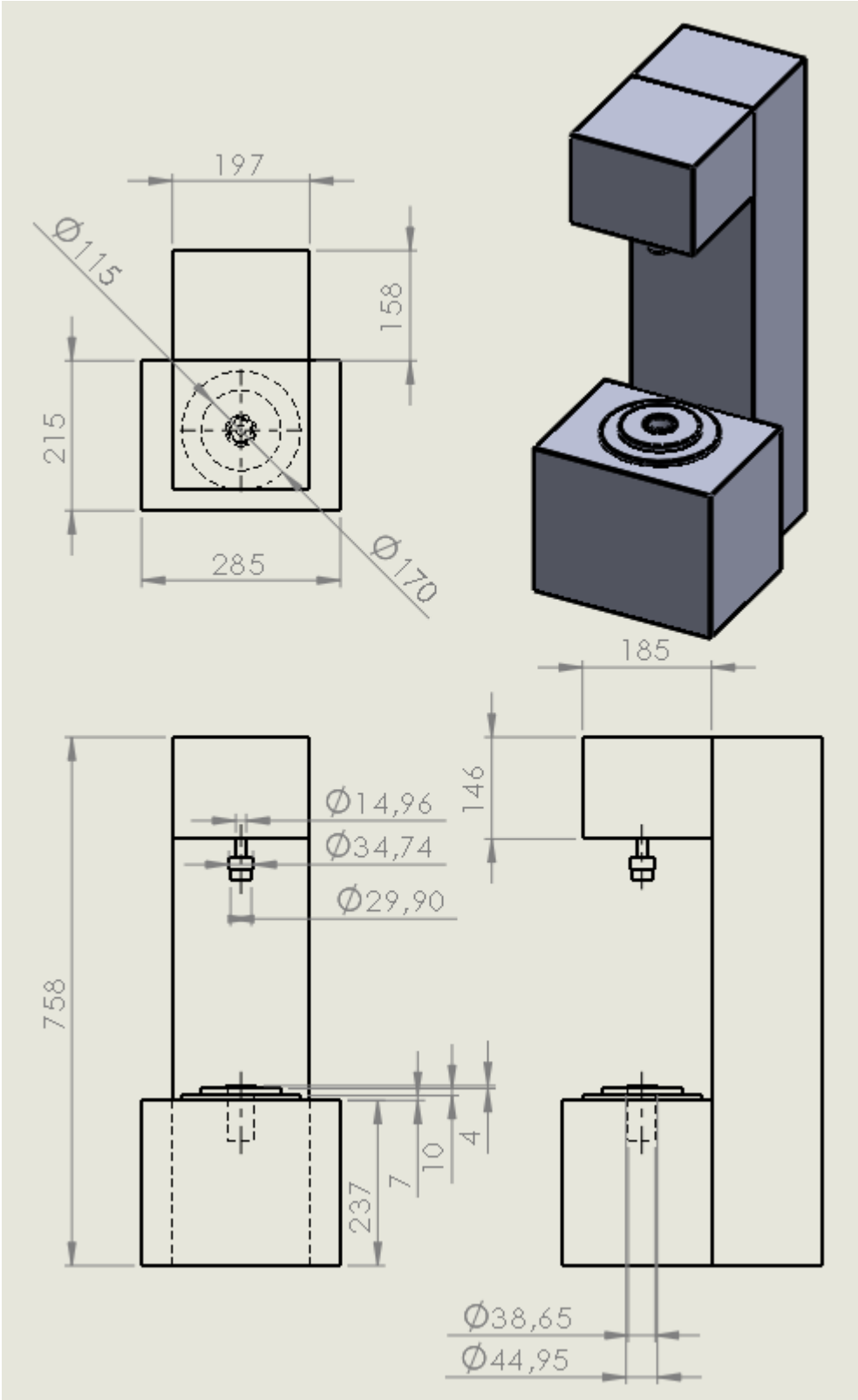


Figure 69: Dimensions rheometer UDS200 (Germany).

# Appendix I

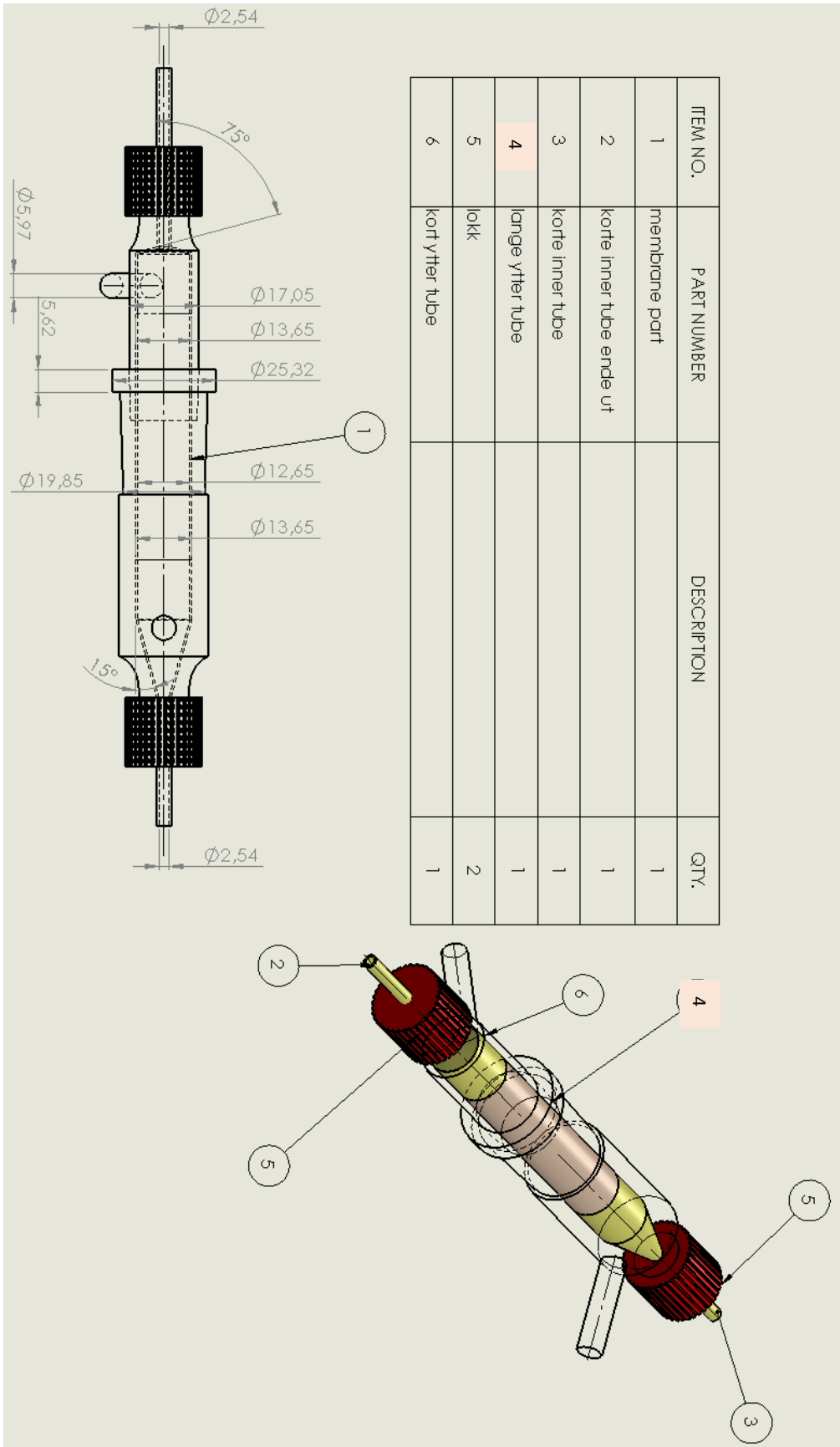
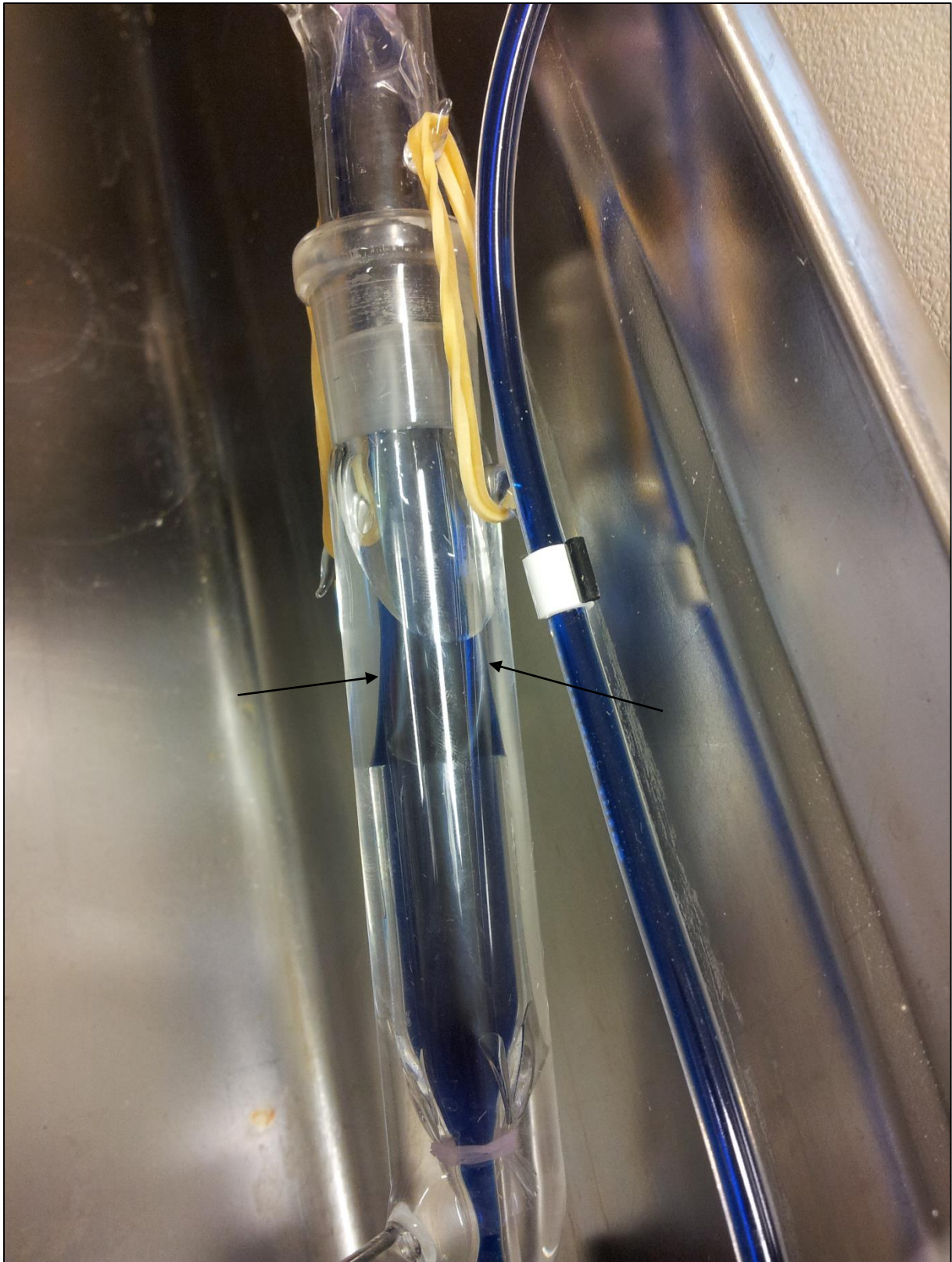


Figure 70: Dimensions [mm] of future idea for design of the small intestine device.

## Appendix J

A guide to setup the small intestine-device.

- ❖ Set up the peristaltic pump at wanted settings (flow rate, cassettes etc.)
- ❖ After cutting of the wanted membrane length, rinse it through water and pull the each end over its inner membrane tube. Put each inner membrane end through an outer buffer-tube end and tighten.
- ❖ Connect the right tube system to the peristaltic pump
  - Stomach – two tubes with i.d. 3.17 mm (black marking) connected together through the pump with both ends in the rheometer cup.
  - Buffer – two tubes with i.d. 2.54 mm (purple marking) connected together through the pump with one end in the buffer container and one end connected to the buffer-tube end at the lowest elevation. Then one single tube of the same type is connected to the other buffer-tube end and goes directly to the buffer container.
  - Small intestine – two tubes with i.d. 2.54 mm (purple marking) connected together through the pump with one end in the rheometer cup and the other end connected to the inner membrane end at the lowest elevation. Then one single tube of the same type is connected to the other inner membrane end and goes directly into the rheometer cup.
- ❖ When starting the inner membrane and buffer circuits – start filling the membrane full first before starting the buffer circuit. This is to make sure that the membrane not folds together inside the tube (Figure 71), challenging the diffusion. However – during the primary tests, the membrane ones folded together ones the fluid reach its end point and the pressure through the tube changed.
- ❖ Emptying the inner membrane and buffer circuits
  - Empty the buffer circuit first. The membrane will easier slip of the tube when it is immersed in buffer volume, so emptying the buffer circuit first helps prevent this.



*Figure 71: the membrane easily folds when the pressure changes both inside and outside the membrane.*

# Appendix K

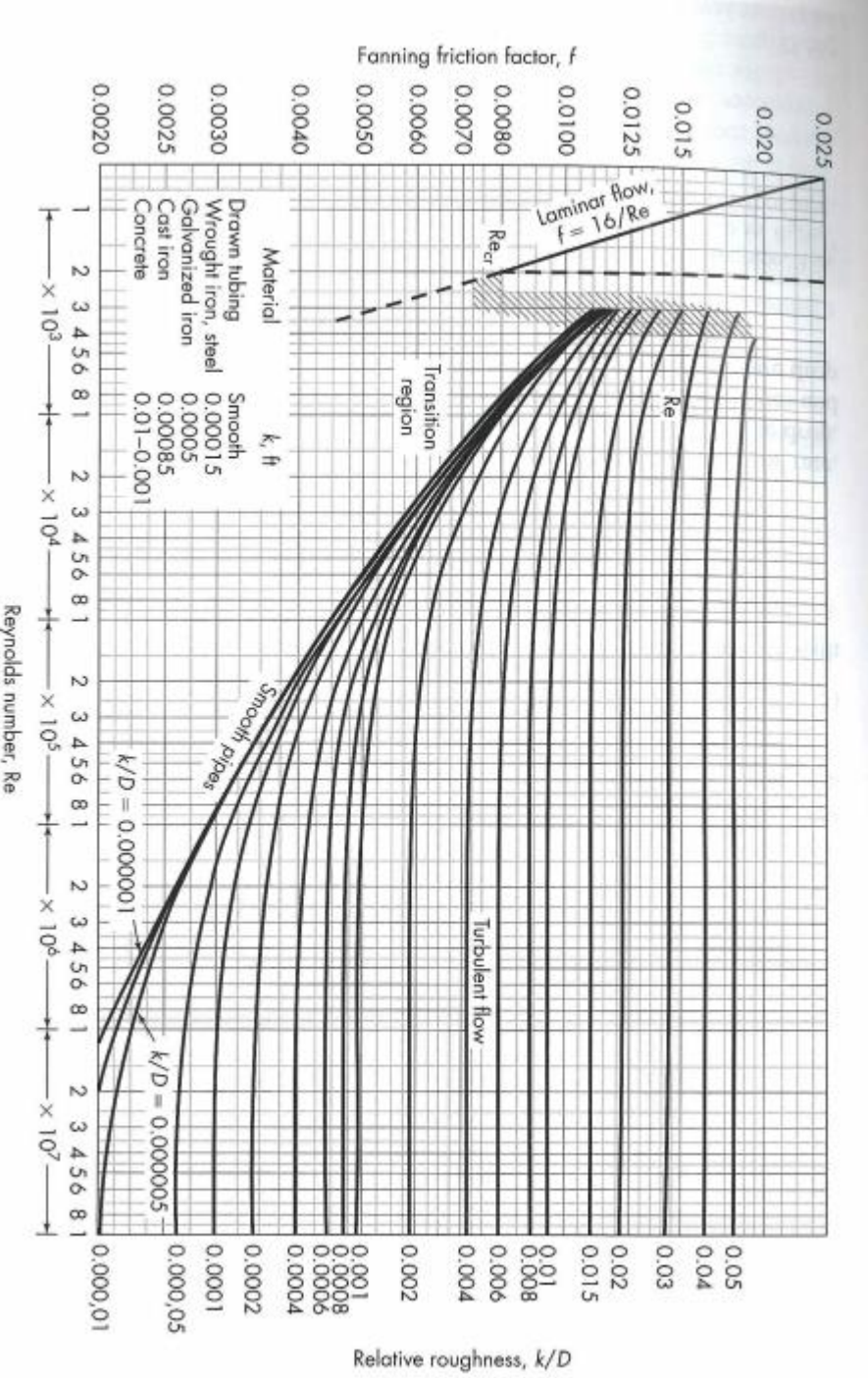


Figure 72: Friction factor plot for circular pipes (McCabe et al. 2005).

## Appendix L

Table 37: Properties of some fluids (Fellows, 2009).

**Table 1.8** Properties of fluids

	Thermal conductivity ( $\text{W m}^{-1} \text{ } ^\circ\text{K}^{-1}$ )	Specific heat ( $\text{kJ kg}^{-1} \text{ } ^\circ\text{K}^{-1}$ )	Density ( $\text{kg m}^{-3}$ )	Dynamic viscosity ( $\text{N s m}^{-2}$ )	Temperature ( $^\circ\text{C}$ )
Air	0.024	1.005	1.29	$1.73 \times 10^{-5}$	0
	0.031	1.005	0.94	$2.21 \times 10^{-5}$	100
Carbon dioxide	0.015	0.80	1.98		0
Oxygen		0.92		$1.48 \times 10^{-3}$	20
Nitrogen	0.024	1.05	1.30		0
Refrigerant 12	0.0083	0.92			
Water	0.57	4.21	1000	$1.79 \times 10^{-3}$	0
	0.68	4.21	958	$0.28 \times 10^{-3}$	100
Sucrose solution (60%)				$6.02 \times 10^{-2}$	20
Sucrose solution (20%)	0.54	3.8	1070	$1.92 \times 10^{-3}$	20
Sodium chloride solution (22%)	0.54	3.4	1240	$2.7 \times 10^{-3}$	2
Acetic acid	0.17	2.2	1050	$1.2 \times 10^{-3}$	20
Ethanol	0.18	2.3	790	$1.2 \times 10^{-3}$	20
Rape-seed oil			900	$1.18 \times 10^{-1}$	20
Maize oil		1.73			20
Olive oil	0.168			$8.4 \times 10^{-2}$	29
Sunflower oil		1.93			20
Whole milk	0.56	3.9	1030	$2.12 \times 10^{-3}$	20
				$2.8 \times 10^{-3}$	10
Skim milk			1040	$1.4 \times 10^{-3}$	25
Cream (20% fat)			1010	$6.2 \times 10^{-3}$	3
Locust bean gum (1% solution)				$1.5 \times 10^{-2}$	
Xanthan gum (1% solution)			1000		

## Appendix M

Table 38: Consistency coefficients and flow behaviour indices for power law fluids (Smith 2011).

	$K$	$n$
Skim milk concentrate	0.02–4.28	0.72–0.92
Yoghurt	0.3–1.4	0.55–0.65
Egg white	0.12–0.19	0.56–0.6
Apple sauce	7–37	0.17–0.4
Various jams	5–25	0.55–0.7
Apricot puree	5–300	0.27–0.53
10% solids peach puree	4.5	0.34
Guava	2.6–11	0.38–0.68
Tomato paste	7–83	0.09–0.36
Tomato puree	204–406	0.22–0.34

## Appendix N

Table 39: Villus dimensions, density, and area as a function of intestinal position in mice on a meat diet (Diamond et al. 1984).

Distance from pyloric sphincter (cm)	Meat mice				
	0	14	28	42	56
Villus length ( $\mu\text{m}$ )	$302 \pm 18$	$363 \pm 30$	$208 \pm 8$	$183 \pm 9$	$193 \pm 11$
Villus width ( $\mu\text{m}$ )	$138 \pm 7$	$121 \pm 8$	$119 \pm 5$	$106 \pm 3$	$93 \pm 2$
Villus height ( $\mu\text{m}$ )	$524 \pm 19$	$386 \pm 63$	$314 \pm 9$	$226 \pm 11$	$203 \pm 16$
Villus density (number/ $\text{mm}^2$ )	$18 \pm 1$	$23 \pm 1$	$33 \pm 4$	$38 \pm 5$	$33 \pm 2$
Nominal area ( $\text{cm}^2/\text{cm length}$ )	$0.92 \pm 0.02$	$1.00 \pm 0.05$	$0.97 \pm 0.08$	$0.85 \pm 0.06$	$0.71 \pm 0.05$
Villus area = $M_a$ ( $\text{cm}^2/\text{cm length}$ )	$5.5 \pm 0.4$	$6.1 \pm 0.7$	$4.7 \pm 0.3$	$3.2 \pm 0.2$	$2.2 \pm 0.1$
Villus area = $R_a$ ( $\text{cm}^2/\text{cm}^2$ nominal area)	$6.0 \pm 0.6$	$5.9 \pm 0.6$	$5.0 \pm 0.5$	$3.9 \pm 0.5$	$3.1 \pm 0.3$



# Appendix O

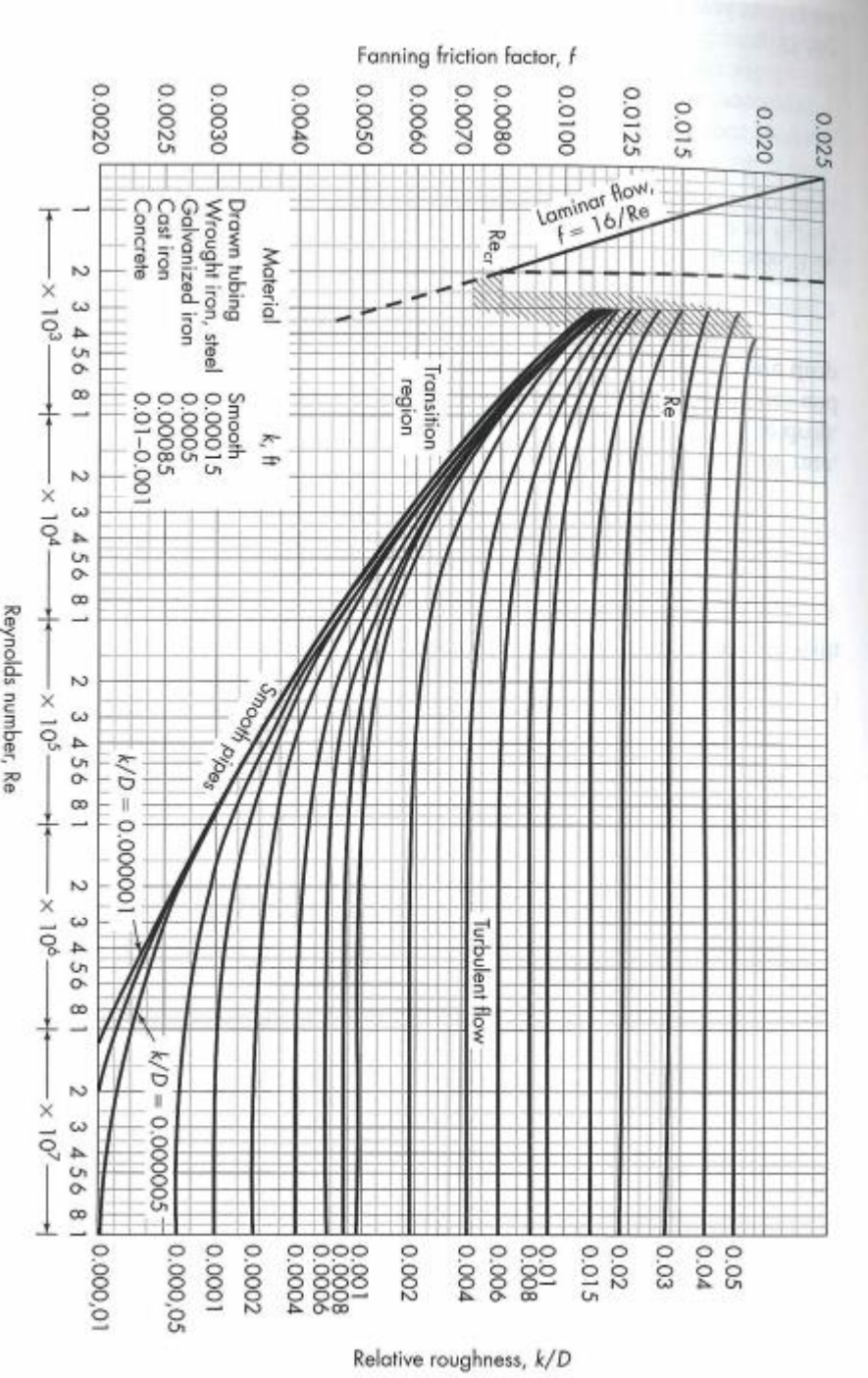


Figure 73: Friction factor plot for circular pipes (McCabe et al. 2005).

Appendix P

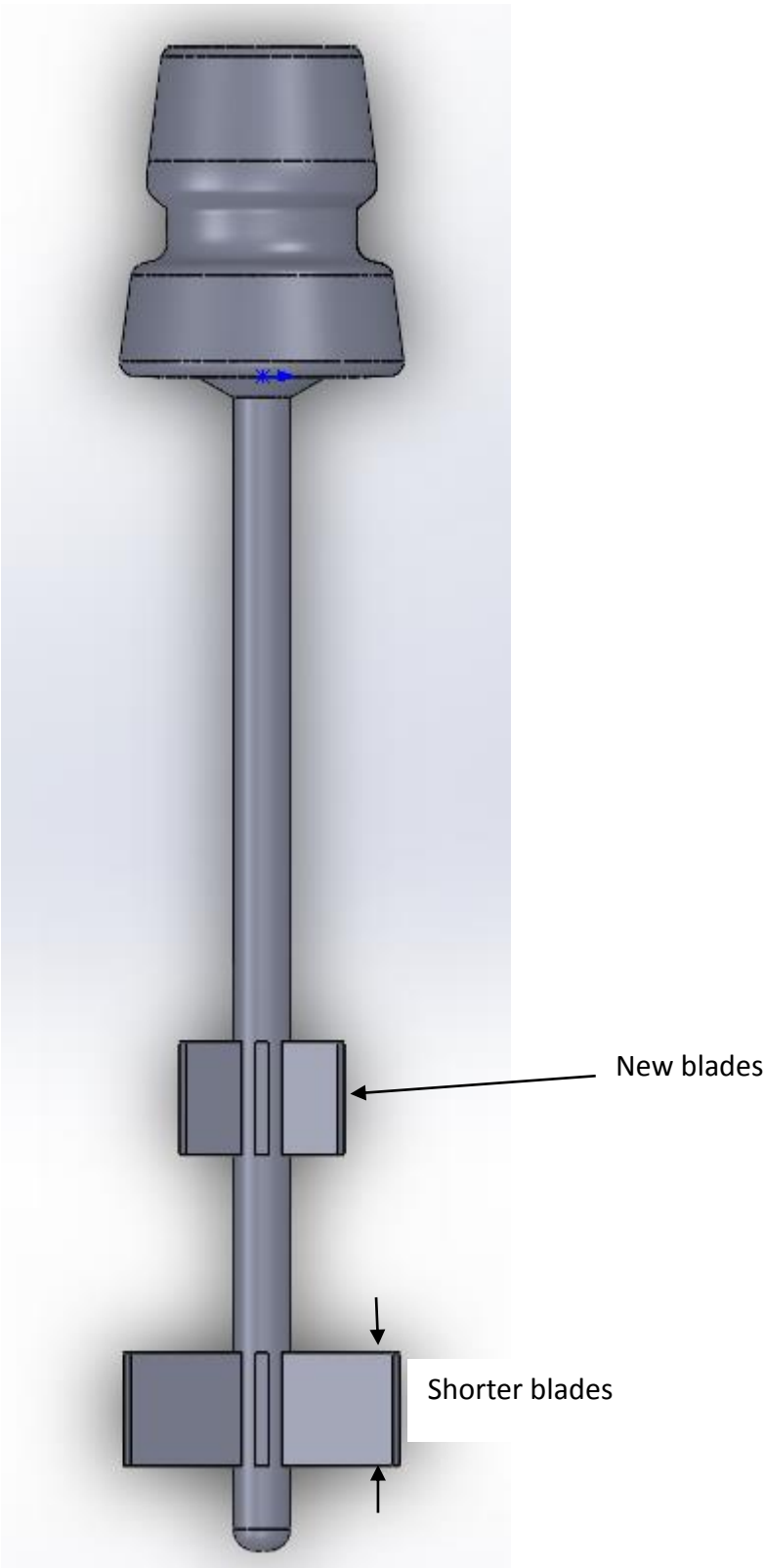


Figure 74: A simple sketch of an idea for a new probe propeller.



Norwegian University  
of Life Sciences

Postboks 5003  
NO-1432 Ås, Norway  
+47 67 23 00 00  
[www.nmbu.no](http://www.nmbu.no)